2016

Part I: Photochemical Generation of Cyclohexyne from a Hydrocarbon Precursor Part II: A Triptycenyl Flower

Daniel Maurer

Part I: Photochemical Generation of Cyclohexyne from a Hydrocarbon Precursor
Part II: A Triptycenyl Flower

by

Daniel Maurer

Submitted to the Department of Chemistry
in partial fulfillment of the requirements for the degree of

Bachelor of Arts in Chemistry with Honors

at

Colby College

Submitted May 2016

Mentor .....
Dasan M. Thamattoor
Professor of Chemistry

Reader .....
Nicholas Boekelheide
Assistant Professor of Chemistry

Part I: Photochemical Generation of Cyclohexyne from a Hydrocarbon Precursor
Part II: A Triptycenyl Flower

by

Daniel Maurer

Approved:

Mentor
Dasan M. Thamattoor
Professor of Chemistry

Date

Reader
Nicholas Boekelheide
Assistant Professor of Chemistry

Date

Vitae

Daniel Patrick Maurer was born in Burnsville, Minnesota in 1993. After graduating from The Blake School in 2012, he entered Colby College in Waterville, Maine to study chemistry with a concentration in biochemistry. At Colby, he began working in Professor Thamattoor's research laboratory his freshman year and enjoyed working as a tutor and teaching assistant for chemistry. Also interested in biochemical and biomedical engineering, he applied and was accepted to the Dartmouth dual degree program. After studying at Dartmouth College his junior year, he returned to Colby for his senior year and was inducted into Phi Beta Kappa in the spring. He will graduate on May 22, 2016 with a Bachelor of Arts in chemistry - biochemistry. In the following year, he will return to Dartmouth to complete the dual degree program and graduate in June, 2017 with a Bachelor of Engineering degree. In the future, he is planning on applying to MD-PhD programs to study medicinal chemistry.

Acknowledgments

I truly cannot express enough thanks for all of those who have supported me throughout my time at Colby. Advice and guidance given by my mentor, Dasan M. Thamattoor, has been invaluable. His passion and all-around kindness are inspiring and will continue to impact me throughout my life. He is full of answers to my never ending questions, and never ceased to teach or help me at odd hours.

The entire chemistry department faculty have instilled a deep and fundamental sense of curiosity within me. My curiosity drove me to ask many questions of my peers, and I am grateful for their love of learning and discussion. My experience at Colby has been a fantastic one, and was largely shaped by the faculty and peers within the chemistry department. They have all imparted a great deal of knowledge onto me, and for that I am thankful.

Of course, my thirst for knowledge could not have begun to be quenched without the unconditional love and support of my parents, David and Debra Maurer, throughout my entire life. For their sacrifices in the name of my education and their unwavering encouragement, I am forever grateful.

I would also like to thank the National Science Foundation (CHE - 1300937) for funding the work presented in this thesis.

Thank you.

Contents

List of Figures

Part I: Photochemical Generation of Cyclohexyne from a Hydrocarbon Precursor

Abstract

Photolysis of phenanthrene-based methylenecyclopropane derivatives have previously been shown to generate alkylidenecarbenes, which readily rearrange to form alkynes. In this work, we show that photolysis of an analogous cyclic alkylidenecarbene precursor at ambient temperature forms cyclohexyne via the putative cyclopentylidenecarbene, and can be trapped by dienes via a Diels-Alder reaction. Cyclohexyne and other strained cycloalkynes are of much interest to theoreticians and experimentalists alike. Results of coupled-cluster and DFT calculations on the potential energy surface of cyclopentylidenecarbene and the corresponding strained cyclohexyne are also presented. The photochemical generation of cyclopentylidenecarbene, and thus cyclohexyne, from a hydrocarbon precursor that is readily synthesized and conveniently handled is a first, and will likely facilitate further structural studies using matrix isolation spectroscopy and kinetic investigations by ultrafast laser flash photolysis.

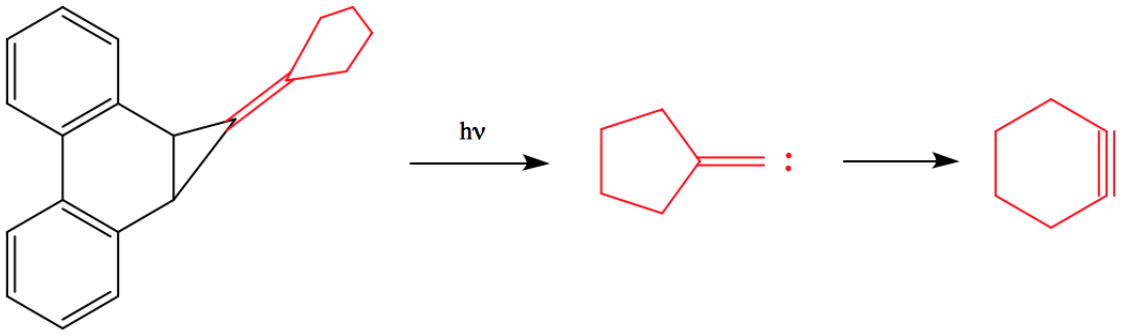

Introduction

1.1 A Brief Background and History of Carbene Chemistry

Carbenes are molecules containing a neutral, divalent carbon. For this reason, most carbenes are extremely reactive intermediates. Dumas and Regnault were the first to attempt to generate a carbene. In 1864, they tried to make the simplest carbene, methylene, by the dehydration of methanol.[1] In the early twentieth century, Staudinger converted alkenes to cyclopropyl rings using diazomethane to generate methylene.[2] In the mid 1900s, carbon-hydrogen bond insertions and cyclopropanation reactions were beginning to become more widely known. During this time, Doering and Hoffman showed the synthetic usefulness of dichlorocarbene.[3] In 1954, George Pimentel developed a technique called matrix isolation that allowed for the structure of reactive species, such as carbenes, to be observed.[4] In a quest to find a carbene stable at room temperature, Fischer characterized a tungsten carbonyl carbene complex, in which carbenes were stabilized by coordination to the metal.[5] In part for Fischer's discovery of a carbene stabilized by a metal, he was awarded the Nobel Prize in 1973. Fifteen years later in 1988, Bertrand isolated the first stable carbene without a metal, and shortly thereafter Arduengo isolated the first N-heterocyclic carbene and obtained its X-ray crystal structure.[6,7] Since the discovery of stable carbenes and the development of structural and kinetic characterization techniques, the field of carbene chemistry has grown rapidly. As of 2010, there are roughly three thousand papers published each year regarding carbenes, and this number is only growing. There is a plethora of applications for carbenes including synthesis, transition metal catalysis, stabilizing reactive species, and medical applications. Now, carbene chemistry is found in research laboratories across the world.

Although stable carbenes are known, the vast majority are extremely reactive intermediates. Carbenes have been proposed as intermediates in mechanistic steps in laboratory syntheses as well as in nature. Until recently, it has been difficult to study carbenes due to short life times, typically on the order of nanoseconds.[8] For these reasons, carbenes have both

intrigued and challenged many chemists, particularly in the past few decades. As Bertrand put it in a lecture on carbenes - twenty years ago, carbene chemistry was fundamental research, a curiosity, and now carbene chemistry is found everywhere.

1.2 Electronic Structure of Carbenes and Alkylidenecarbenes

Carbenes have a neutral, divalent carbon that is necessarily electron deficient. The most common type of carbene is the disubstituted (saturated) carbene. The carbene carbon is approximately sp^2 hybridized and has a geometry with two substituents and two nonbonding electrons. The sp^2 hybridization, by definition, leaves a p orbital unhybridized. The sp^2 and p orbitals and two nonbonding electrons leads to two categories of spin states, the singlet and the triplet (Figure 1.1).

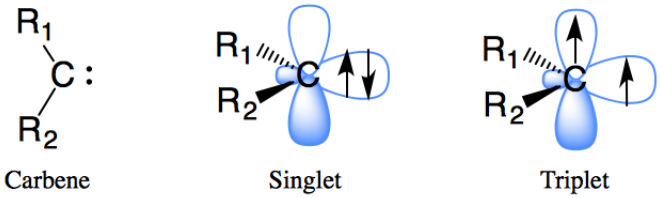

Figure 1.1. Singlet and triplet electronic configurations of saturated carbenes.

The multiplicity of the spin states are given by 2S+1 where S is the total spin. The carbene with spin paired electrons in Figure 1.1 has a total spin of zero, resulting in the multiplicity as a singlet. Similarly, the carbene with two unpaired electrons and parallel spins has a total spin of 1, resulting in the multiplicity as a triplet. Carbenes are generally more stable in their triplet states, but they can be stablized as a singlet by electron donation from substituents into the empty p orbital.

The research presented in this study regards alkylidenecarbenes, which differ from the aforementioned carbenes in that they are monosubstituted, or unsaturated (Figure 1.2). The carbene carbon at the end of a carbon-carbon double bond, is approximately sp hybridized with a linear geometry. The sp orbital has half s-character as opposed to one third s-

character in the sp^2 hybrid orbital. In comparison to the saturated carbene, the electrons on the carbene carbon in an alkylidenecarbene are held much closer to the nucleus, resulting in a much more stable singlet state. Calculations typically show that the lone pair of electrons is in an orbital with mostly s-character and only 36.5% p-character.[9,11] Thus, the singlet state is energetically favored by 30-60 kcal/mol, and the reactivity of an alkylidenecarbene can be modeled from the singlet state.[8]

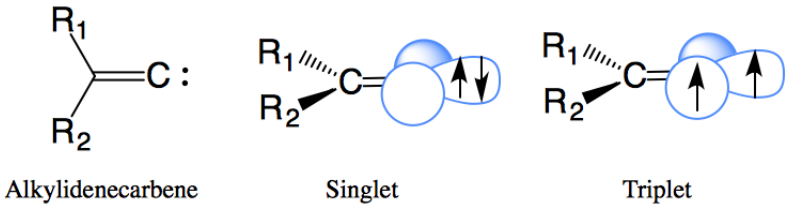

Figure 1.2. Singlet and triplet electronic configurations of unsaturated carbenes.

1.3 Generation of Alkylidenecarbenes

Alkylidenecarbenes can be generated in situ by α-elimination, but carbenes are often generated by photochemical and/or pyrochemical means. These methods are the focus for this study since structural studies using matrix isolation necessitate photochemical or pyrochemical generation methods. As with saturated carbenes, nitrogen extrusion from diazo compounds is one of the most widely used methods.[9] The loss of nitrogen gas is a large thermodynamic driving force for the generation of the carbene (Scheme 1.3). Two related methods have been reported to synthesize 1-diazoalkenes **1** from aldehydes and ketones, which can be used to generate the corresponding alkylidenecarbene **2** by either irradiation or heat.[9] However, these methods often generate the corresponding alkylidenecarbene in situ, and many alkylidenecarbenes are not accessible through these synthetic routes.

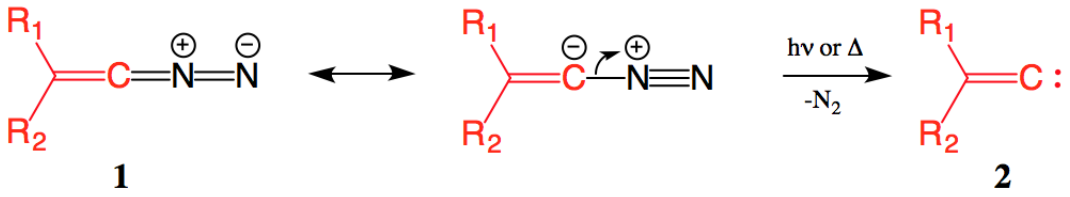

Scheme 1.3. Generation of alkylidenecarbenes from 1-diazoalkenes.

These diazo compounds are used due to the ease of carbene generation, but its drawbacks are difficulty in synthesis and handling, carcinogenicity, and potential explosiveness. Additionally, Platz demonstrated that products attributed to the formation of carbenes from nitrogenous precursors often actually come from a photochemically excited state of the precursor itself.[10] In otherwords, even if it is possible to synthesize a nitrogenous precursor, it may not even generate the intended carbene.

An example of a pyrochemical method is the use of derivatives of Meldrum's acid **3** (Scheme 1.4). The pyrolysis eliminates acetone and carbon dioxide to result in a ketene, which can then extrude carbon monoxide to generate the alkylidenecarbene **2**. In order to generate **2**, the Meldrum's acid derivative **3** needs to be heated between 450 to 600 °C.[12]

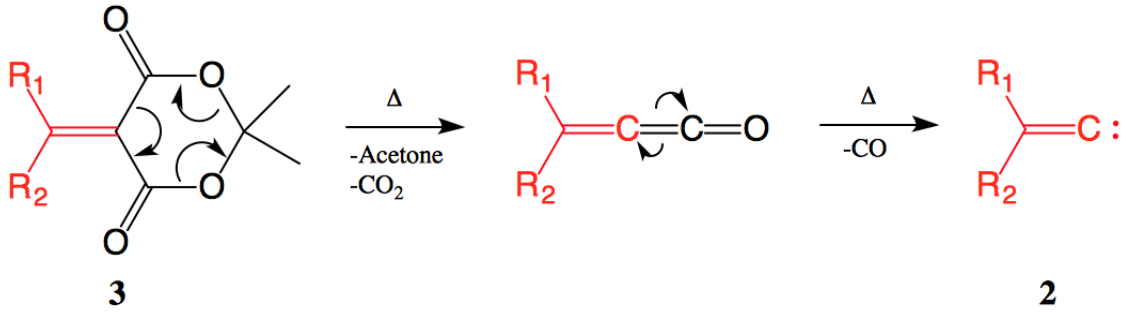

Scheme 1.4. Generation of alkylidenecarbenes from derivatives of Meldrum's acid.

While the pyrolysis of **3** is effective in its generation of carbenes, it has limitations to the studies that can be performed. Specific pathways may not be able to be determined because at such high temperatures, the carbene and its product(s) may be in equilibrium. Furthermore, it is more difficult to trap reactive species when using pyrolysis as opposed to

photolysis.[12]

A third method, is to use ring strain and aromaticity as the thermodynamic driving force for the generation of alkylidene carbenes, which was first demonstrated in 1965 by generating methylene (Scheme 1.5a $R_1 = R_2 = H$).[13] After a 25 year hiatus, the same method was used to generate dichlorocarbene (Scheme 1.5a $R_1 = R_2 = Cl$).[14] Since then, many labs have been incorporating different substituents in order to generate the corresponding carbenes.[31] Moore and Vidaurri-Martinez were able to use this method to generate an unsaturated carbene (Scheme 1.5b).[15]

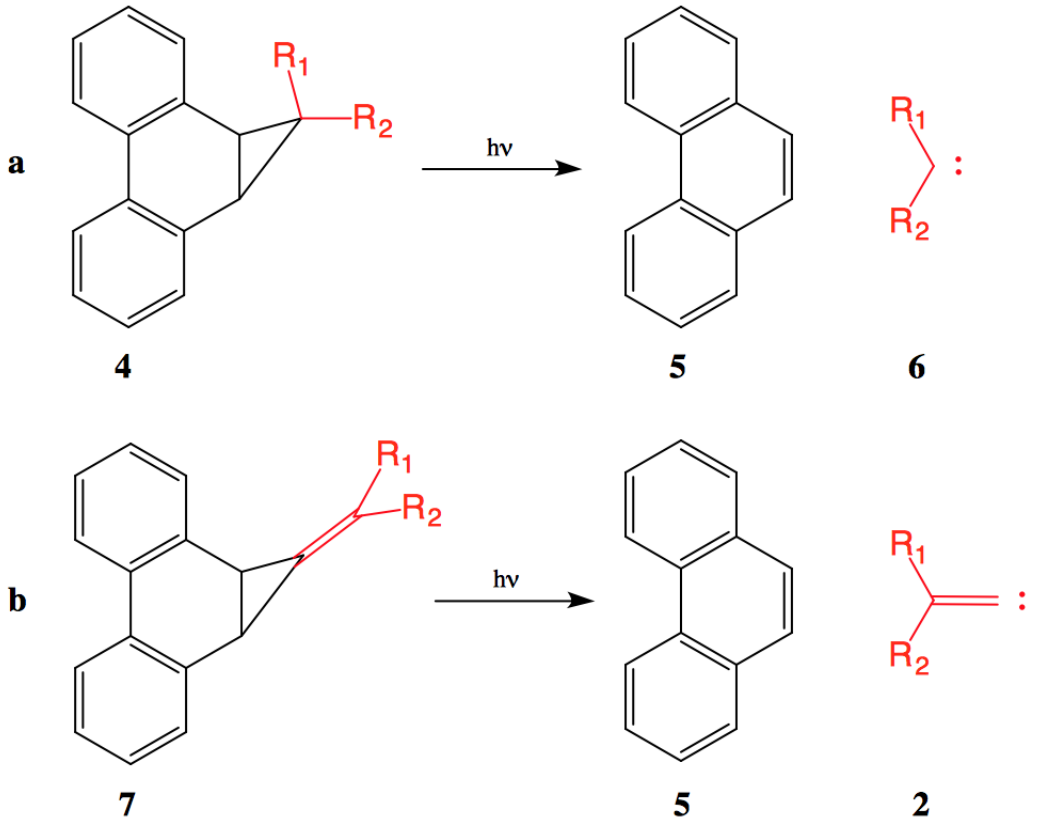

Scheme 1.5. Generation of alkylidenecarbenes from a hydrocarbon precursor.

The strain of the cyclopropyl ring in precursors **4** and **7** aid in the formation of phenanthrene **5** and the corresponding carbene. Additionally, there is a large thermodynamic driving force for the conversion of **4** or **7**, which has two isolated aromatic rings (resonance energy = ~72 kcal/mol), to phenanthrene **5** (resonance energy = ~92 kcal/mol), which has

a fused three-ring aromatic system. These hydrocarbon precursors are safer and easier to work with as well as have a longer shelf-life. There is another hydrocarbon system that is an indan-based system (Figure 1.6), which allows for an easier generation of carbenes and aids in matrix isolation since it is smaller and easer to deposit on the window.

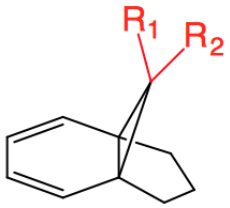

Figure 1.6. An indan-based hydrocarbon carbene precursor.

However, the phenanthrene-based system allows for a much easier synthesis, and therefore this study will be using the phenanthrene-based system to investigate alkylidenecarbenes.

1.4 Reactivity of Alkylidenecarbenes

The most common reactions of alkylidenecarbenes fall into three categories. The first is cyclopropanation of alkenes (Scheme 1.7). Singlet carbenes, such as alkylidenecarbenes, are electrophilic due to the empty p orbital, and nucleophilic due to the lone pair. For this reason, singlet carbenes can add across double bonds to form a cyclopropyl ring.

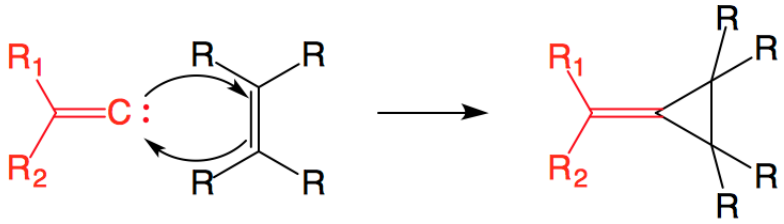

Scheme 1.7. Cyclopropanation of an alkene with an alkylidenecarbene.

Alkylidenecarbenes are often used in 1,5 C-H or O-H bond insertions (Scheme 1.8).[9] These insertions occur through a transition state where the empty p orbital of the carbene interacts with the electrons in the C-H or O-H σ bonds.[9]

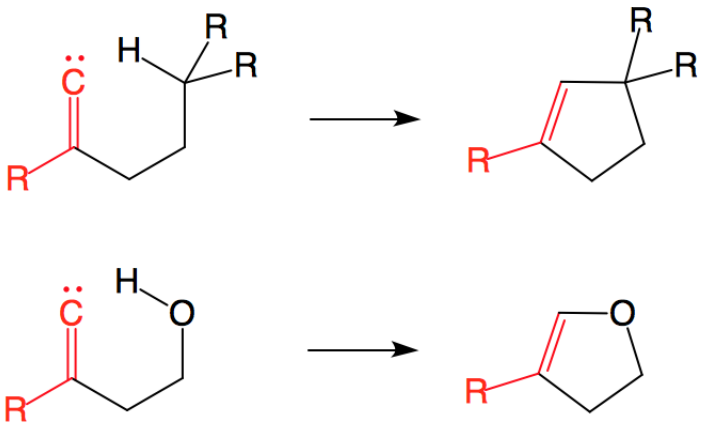

Scheme 1.8. 1,5 C-H and O-H bond insertions.

Another reaction alkylidenecarbenes often undergo is the alkylidenecarbene - alkyne rearrangement (Scheme 1.9).[16] One group on the carbon bonded to the carbene carbon migrates to the carbene carbon, and the lone pair from the carbene carbon forms a π bond resulting in a triple bond. The 1,2-shift is an intramolecular reaction, so it often occurs much faster than cyclopropanation with an alkene or dimerization, which are intermolecular reactions. Note that as shown in Scheme 1.9, the C-R bonds are aligned with the empty p orbital of the carbene carbon. This is what allows for the migration of a substituent to the carbene carbon.

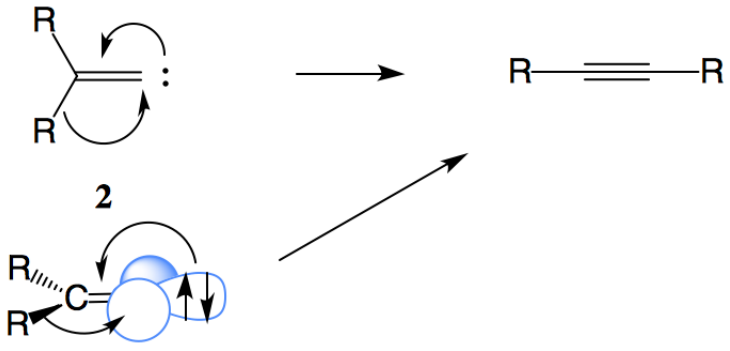

Scheme 1.9. Alkylidenecarbene - alkyne rearrangement.

In 2012, Moore et al. generated benzylidenecarbene **8** using a phenanthrene-based precursor.[15] A carbon-13 labeling study determined that the hydrogen shifted faster than the

phenyl ring, which agreed with their calculations (Scheme 1.10).[15]

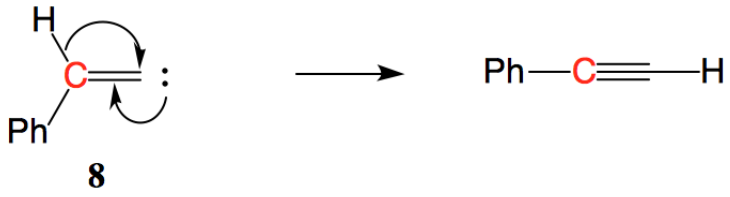

Scheme 1.10. Benzylidenecarbene - phenylacetylene rearrangement.[15]

If instead of having two separate groups on the alkylidenecarbene **2**, the two groups are connected in a ring, the rearrangement will form a cycloalkyne if it is thermodynamically favorable and not kinetically protected, which is dependent on the amount of ring strain due to the constrained angle being significantly less than the 180° of sp hybridized carbons. If the ring size of the carbene is five, cyclopentylidenecarbene **9** will rearrange to cyclohexyne **10** (Scheme 1.11).[18,19]

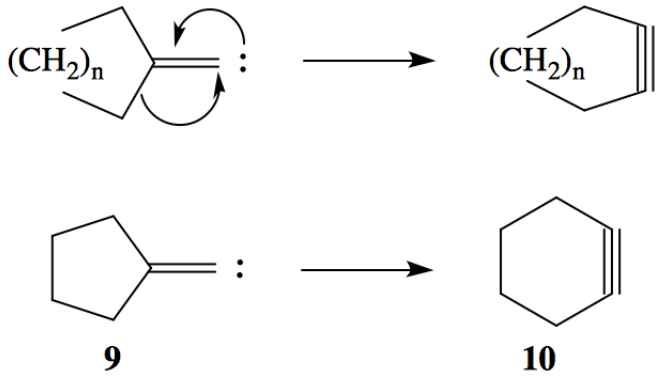

Scheme 1.11. Ring expansion of cyclopentylidenecarbene **9** to form cyclohexyne **10**.

Previous methods of generating **9** required the use of additional reagents or high temperatures (750-800 °C).[17–19] At these high temperatures, the authors note that "the 'real' yield must be much higher than 2% because much of it is removed as benzene, butatriene, and ethylene at these temperatures," which indicates the necessity to use a photolytic precursor.[17]

Experiments have demonstrated that other disubstituted alkylidenecarbenes, namely dimethylvinylidencarbene, cyclohexylidenecarbene, and adamantylidenecarbene, do not under go the alkylidenecarbene - alkyne rearrangement (Scheme 1.12).[20–22]

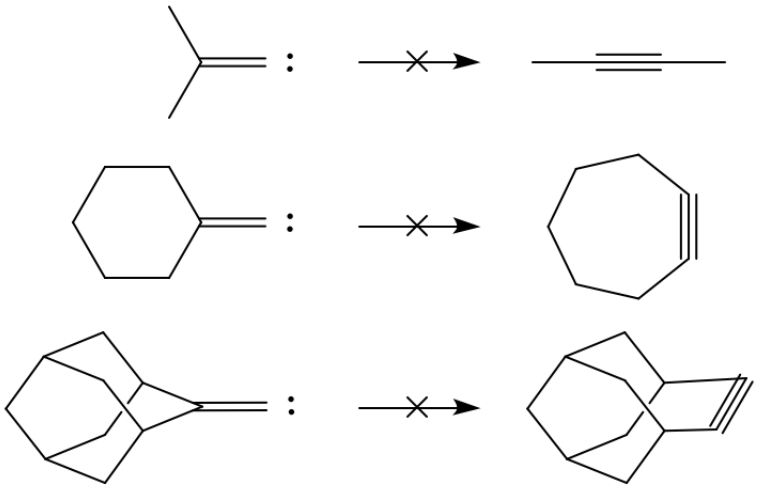

Scheme 1.12. Alkylidenecarbene - alkyne rearrangement of dimethylvinylidenecarbene, cyclohexylidenecarbene, and adamantylidenecarbene does not occur.[20–22]

Since the rearragnement of **9** to **10** is known[18], the synthesis and characterization of cyclohexyne **10** from cyclopentylidenecarbene **9** generated photochemically from a phenanthrene-based precursor **5** is the goal of this study.

1.5 Generation of Cyclohexyne

Cyclohexyne can be made by methods other than the rearrangement of cyclopentylidene carbene **9** (Scheme 1.13).[19,23–25] The alternate methods begin with a six-membered ring and elminate groups to form the triple bond. The method most often used, particularly in synthetic reactions, is β-elimination (Scheme 1.13a).[23] While quite useful in synthetic reactions, photochemical or pyrochemical methods are needed for structural studies using matrix isolation and photochemical methods are required for kinetics studies.

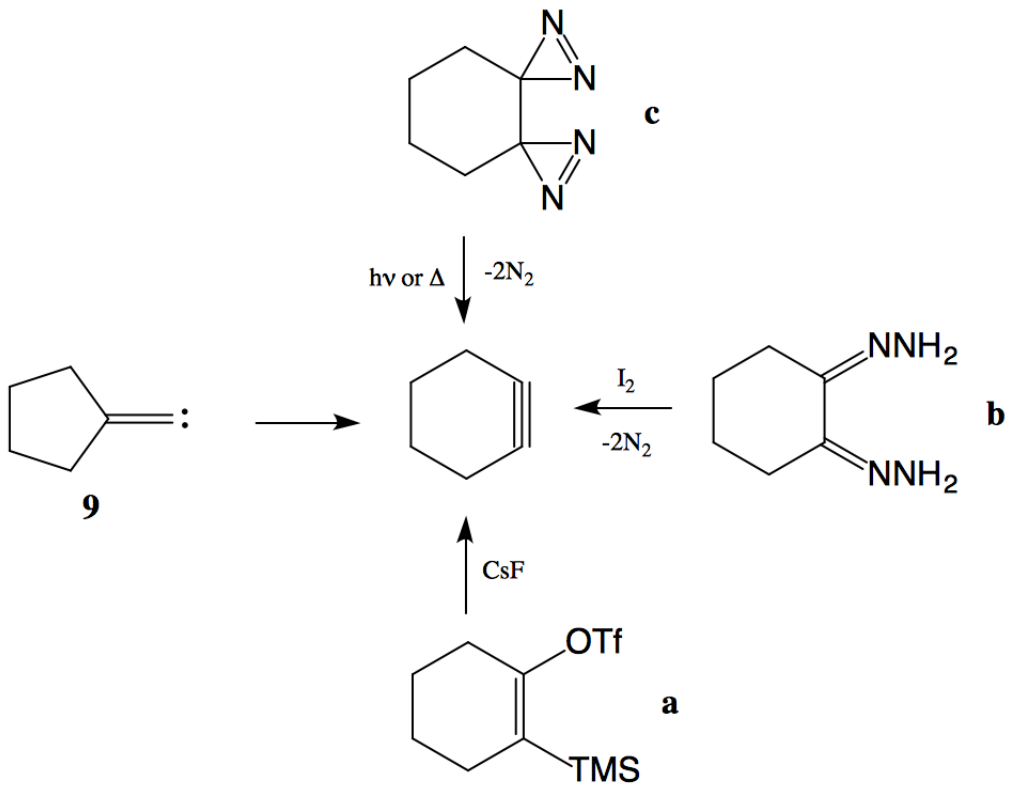

Scheme 1.13. Methods of generating cyclohexyne (a) β-elimination[23] (b) oxidation and nitrogen extrusion[24] (c) nitrogen extrusion.[25]

Nitrogen extrusion has been used via two different methods. 1,2-hydrazone subsituted cyclohexane can be first oxidized with iodine, which can then release nitrogen gas to form cyclohexyne (Scheme 1.13b).[24] However, as mentioned previously, such reagents cannot be added when using matrix isolation and flash photolysis techniques. The other nitrogen extrusion method is the only example in the literature of the photochemical generation of cyclohexyne. This method involves synthesizing a 1,2-bisdiazirine substituted cyclohexane, which upon photolysis or pyrolysis will release two equivalents of nitrogen gas to form cyclohexyne (Scheme 1.13c).[25] However, diazirine compounds are difficult to synthesize and quite dangerous to work with. Additionally, it does not allow for the study of the cyclopentylidenecarbene - cyclohexyne rearrangement. It would be of great benefit for structural studies to use a precursor that is readily synthesized and handled and forms **9** upon photolysis. One example of the generation of cyclopentylidenecarbene is through the pyrolysis of a Meldrum's

acid derivative at high temperatures.[12] Previous calculations have found that cyclohexyne is 19.0 kcal/mol more stable than cyclopentylidenecarbene.[12] However, at the high temperatures required for pyrolysis, cyclopentylidenecarbene and cyclohexyne may very well be in equilibrium. Additionally, the reverse Diels-Alder reaction of cyclohexyne to form ethylene and butatriene is activated by heat. Tseng et al. were unsuccessful in trapping cyclohexyne through the generation of cyclopentylidenecarbene via pyrolysis. Thus, in order to study the structure of cyclohexyne and its formation from cyclopentylidenecarbene, the use of a phenanthrene-based photochemical precursor is preferred (Scheme 1.14).

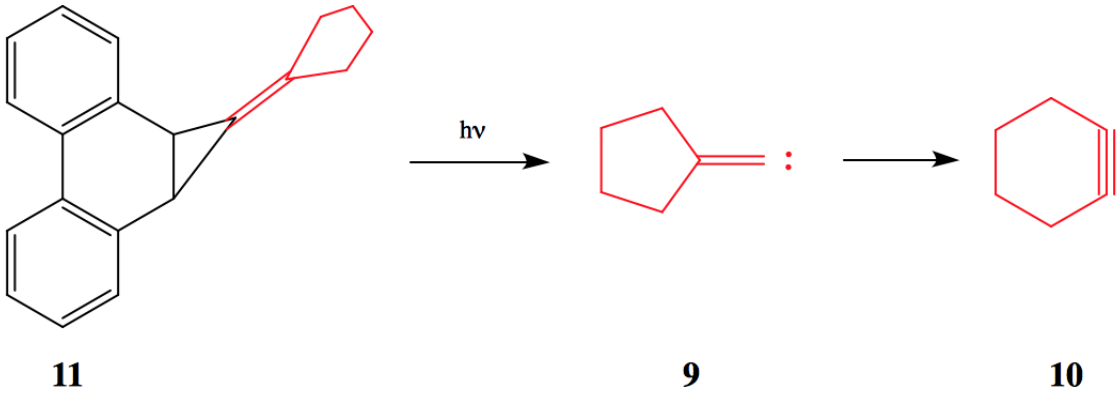

Scheme 1.14. Generation of cyclohexyne **10** from a phenanthrene-based precursor **11** via cyclopentylidenecarbene **9**.

1.6 Reactivity of Cyclohexyne

The reactivity of cyclohexyne has been studied since the 1960s when Wittig published a paper on the dimerization, trimerization, and tetramerization of cyclohexyne (Schemes 1.15-1.17).[26] The highly strained cyclohexyne will first dimerize (Scheme 1.15).[26] Then, another cyclohexyne can add via a Diels-Alder mechanism where the alkyne acts as a dienophile (Scheme 1.16).[26] Two dimers can combine, or two cyclohexynes can combine with a dimer to form the tetramer (Scheme 1.17).[26]

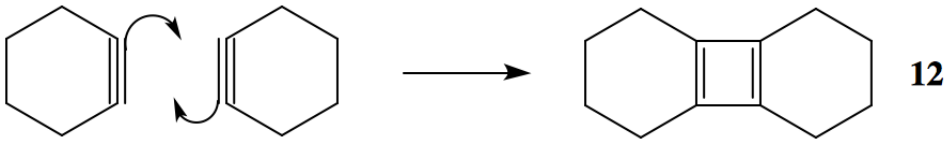

Scheme 1.15. Cyclohexyne dimerization.[26]

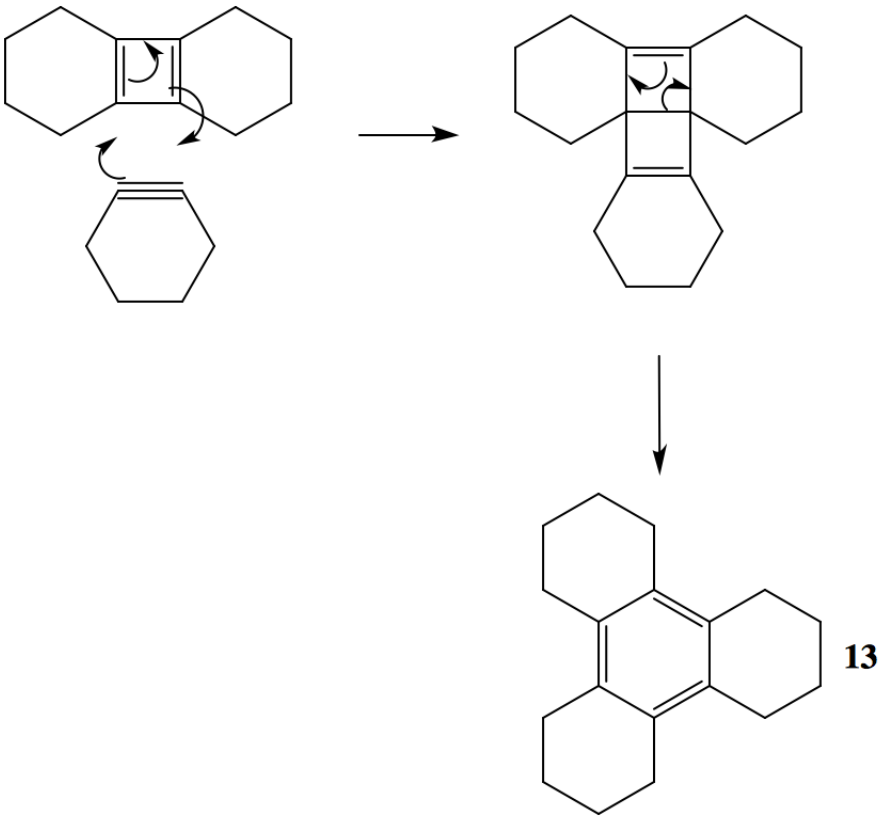

Scheme 1.16. Cyclohexyne trimerization.[26]

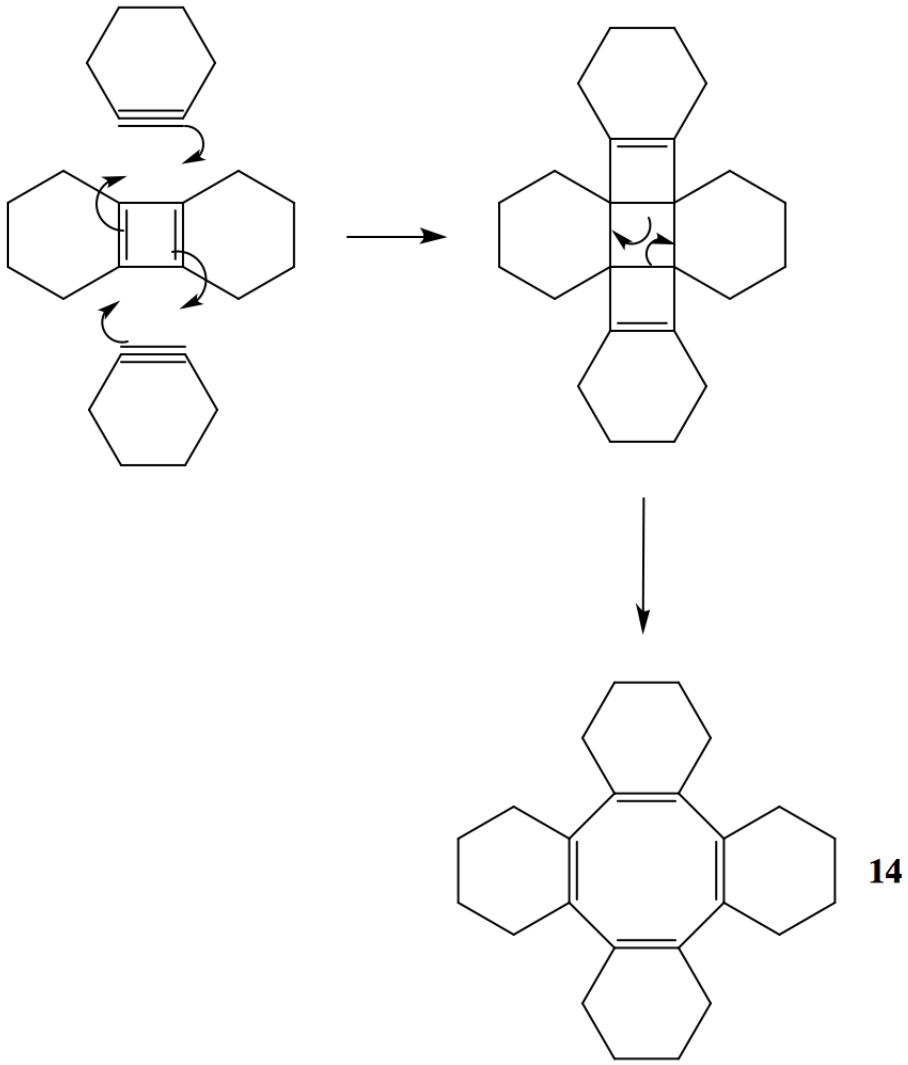

Scheme 1.17. Cyclohexyne tetramerization.[26]

By observing the formation of the dimer, trimer, and tetramer, the generation of cyclohexyne can be confirmed. The fact that cyclohexyne is a dienophile can be used to trap cyclohexyne using dienes. The two that are most commonly used in the trapping of cyclohexyne are 1,3-diphenylisobenzofuran **18** and tetraphenylcyclopentadienone (tetracyclone) **17** (Scheme 1.18).[24,25,27]

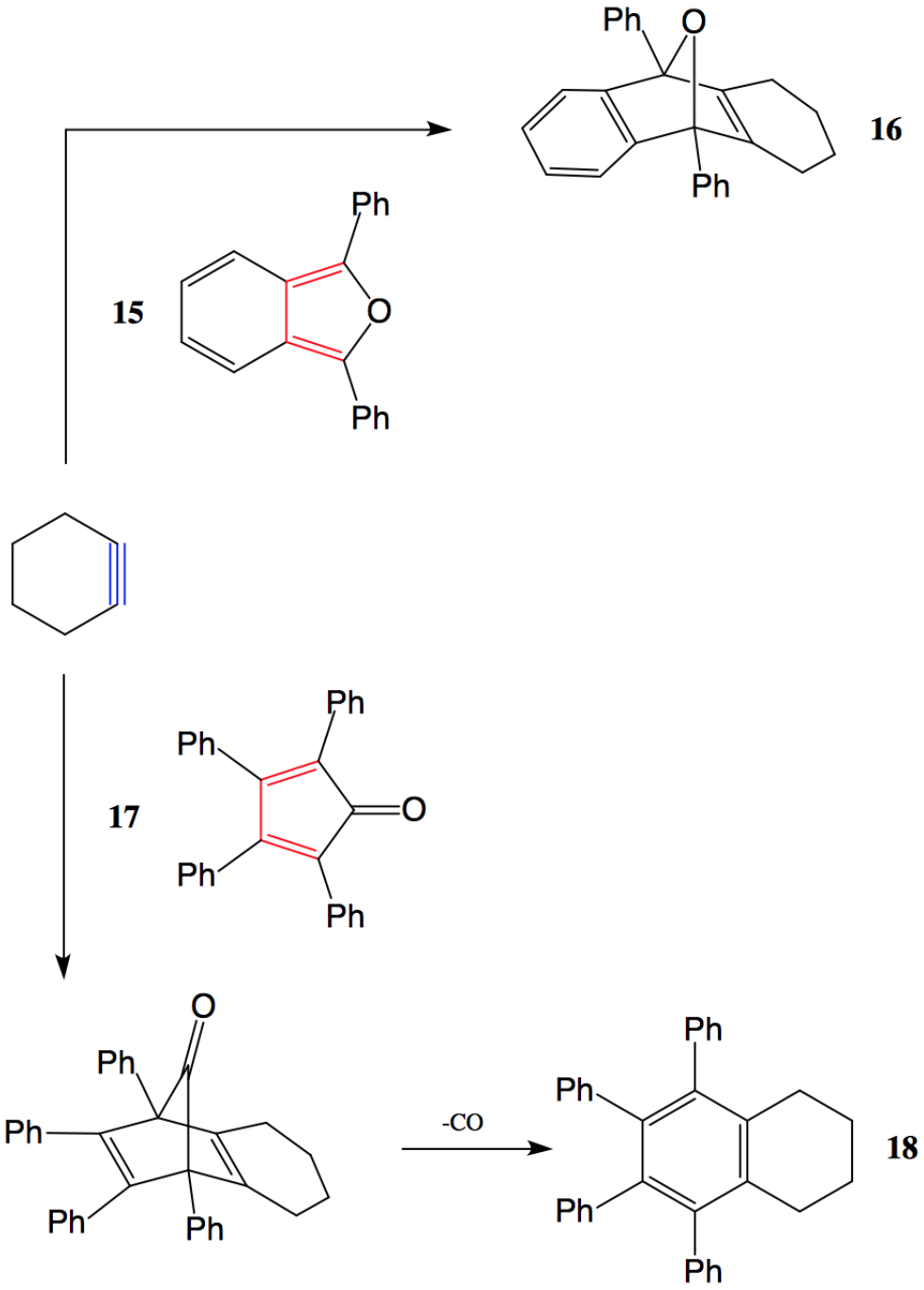

Scheme 1.18. Diels-Alder adducts from the trapping of cyclohexyne with 1,3-diphenylisobenzofuran and tetracyclone.[24,25,27]

The Diels-Alder reaction of cyclohexyne and **15** gives an aromatic adduct, which is a driving force for the reaction. Similarly, the addition of cyclohexyne to **17** and the loss of

carbon monoxide gives an aromatic adduct.

The reactivity of cyclohexyne has recently been gaining traction as a synthetic tool. Recently, Houk and Gark demonstrated that cyclohexyne can be used to create bicyclic heterocyclic scaffolds that are used in many compounds including drugs and natural products.[23] Additionally, Gampe and Carreira have reviewed how cyclohexyne can be used for efficient syntheses of natural products such as guanacastapenes.[28,29]

1.7 A More Efficient Synthesis of Phenanthrene-Based Precursors

The synthesis of methylenecyclopropanes, such as **11**, is not trivial. The synthetic route will be briefly discussed in this introduction as it pertains to the project goals, but it will be more thoroughly discussed in the next section. Moore et al. synthesized **21** via the addition of dibromocarbene to phenanthrene[30], substitution, and finally β-elimination (Scheme 1.19).[15]

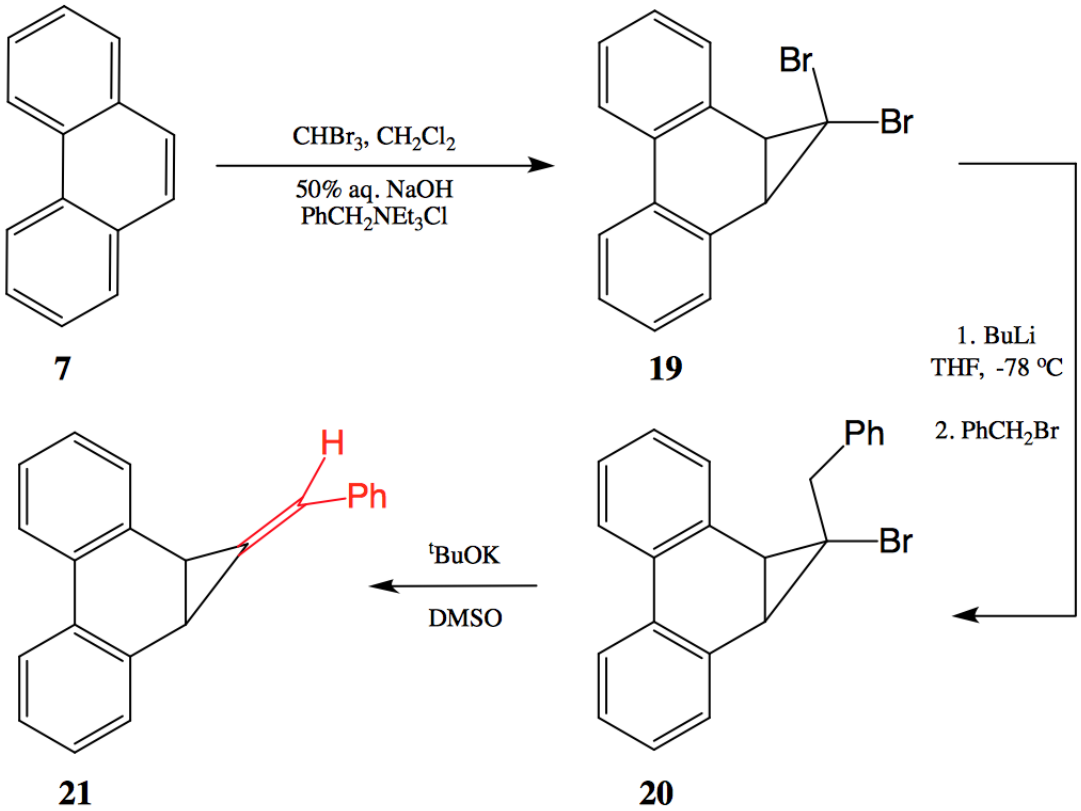

Scheme 1.19. Method for synthesizing monosubstituted methylenecyclopropanes.[15]

Previous efforts were unsuccessful in synthesizing disubstituted vinylidene precursors by methods similar to Moore et al. Recently, Hardikar et al. synthesized a disubstituted vinylidene phenanthrene-based precursor via a reaction developed by Petasis et al. that involved using a titanium reagent and undergoing a Wittig-type mechanism.[20,32] Unfortunately, the method by Hardikar et al. produced low yields that is additionally limited by purification. Therefore, in this study, a different approach will be attempted. Takeda et al. published a modification to the Petasis procedure that eliminates a step in the overall synthetic route.[34]

1.8 Ring Expansion Calculations Are Outdated

The previous calculations done on cyclopentylidenecarbene **9** and its rearrangement into cyclohexyne **10** was in 1995 by MCSCF(4,4)/6-31G* and MP4/6-31G*//MP2/6-31G*.[35] The results show a kinetic barrier of 11-24 kcal/mol, an estimation with a large error. It seems apparent that similar calculations should be done at a higher level of theory, using more modern computational techniques.

Results and Discussion

2.1 Synthetic Considerations in the Preparation of Phenanthrene-Based Precursors

The phenanthrene-based precursor **11** was synthesized by two methods in order to study the photochemical generation of cyclopentylidenecarbene **9** and subsequent rearrangement to cyclohexyne **10**. The first step in all routes was the cyclopropanation by the addition of a dihalocarbene to phenanthrene as shown in Scheme 2.1 and 2.5. This was achieved by α-elimination (the removal of the acidic proton on chloroform or bromoform to create the relatively stable trihalogenated carbanion) followed by the loss of a halogen. The dihalocarbene selectively adds across the 9,10 bond in phenanthrene for two reasons. The first is that the 9,10 bond has the most double bond character compared to all the other bonds in phenanthrene. The second is that the addition to the 9,10 bond results in two separate aromatic rings (resonance energy = $\sim$72 kcal/mol), which is more thermodynamically more favorable than a fused napthalene ring (resonance energy = $\sim$61 kcal/mol), which would be formed by the addition at a different position. The added benzyltriethyl ammonium chloride acts as a phase transfer catalyst (PTC) to transfer the aqueous hydroxide ion to the organic phase where it can then deprotonate the haloform, forming the trihalogenated carbanion. After loss of the halogen, the PTC can bring the halide ion to the aqueous phase where it can be replaced by another hydroxide ion, completing the catalytic cycle.

After difficulty using the synthetic route set forth by Moore et al. (Scheme 1.19) to synthesize fully substituted vinylidenecarbene precursors, Hardikar et al. synthesized a phenanthrene-based precursor via a different route (Scheme 2.1).[20]

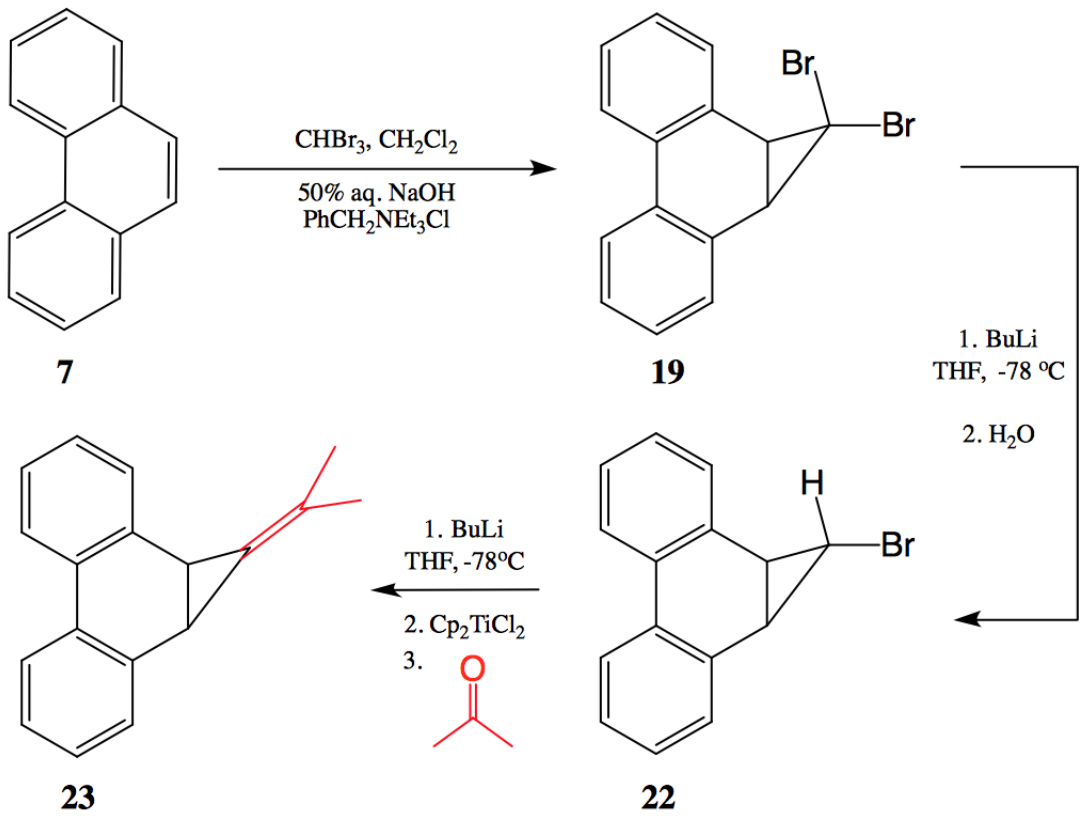

Scheme 2.1. A method for synthesizing disubstituted vinylidenecarbene precursors using a modified Petasis procedure.[20,32]

After the addition of the dibromocarbene to phenanthrene[30], dehalogenation via the addition of butyllithium, and subsequent quenching yielded the monobromo derivative **22**.[31] The confirmation of an *exo* monobromo derivative **22** is evident from the coupling constant between the two types of protons attached to the cyclopropyl ring (Figure 2.2). In the synthesized **22**, the proton in question was experimentally shown to have a coupling constant of $J = 4.3$ Hz, providing evidence that the protons are trans with respect to the cyclopropyl ring.[31] If it were to be *endo*, a copuling constant near $J = 9.2$ Hz would be observed, based on density functional calculations.[31]

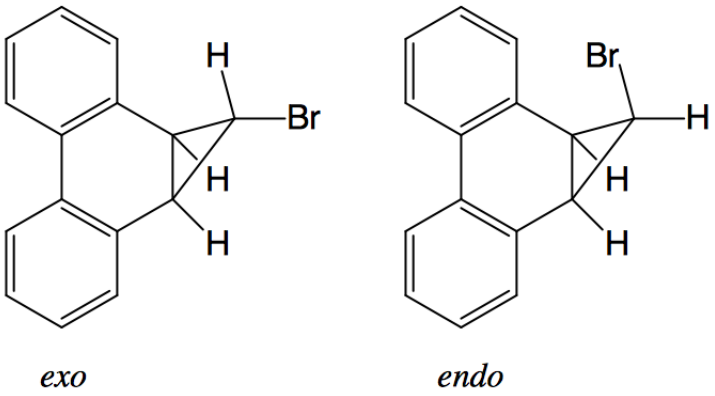

Figure 2.2. *exo* and *endo* derivatives of **22**.

Then, adapting a procedure reported by Petasis et al., the precursor for dimethylvinylidenecarbene **23** was obtained.[20,32] The reaction appears to be a Wittig-type reaction except the starting material is a monohalogenated carbon instead of an ylide. Indeed, Scheme 2.3 shows this Wittig-type mechanism after the formation of a sp^2 hybridized carbon complexed to titanocene. A resonance structure for this complex would show that it is an ylide. Initially, the titanium coordinates two cyclopropyl anions, which are formed after the addition of butyllithium to the monobromo derivative **22**. Proximity allows one of the two anions to deprotonate the other, forming the starting material for the Wittig-type reaction as well as the dihydrogen derivative **24**.

While the latter method opens for the possibility of a wide variety of ketones to be added to make the corresponding metheylenecyclopropane, there is a significant drawback. The Wittig-type mechanism of the Petasis procedure necessitates two equivalents of **22** to be added, half of which is converted into the dihydrogen derivative **24** (Scheme 2.3).

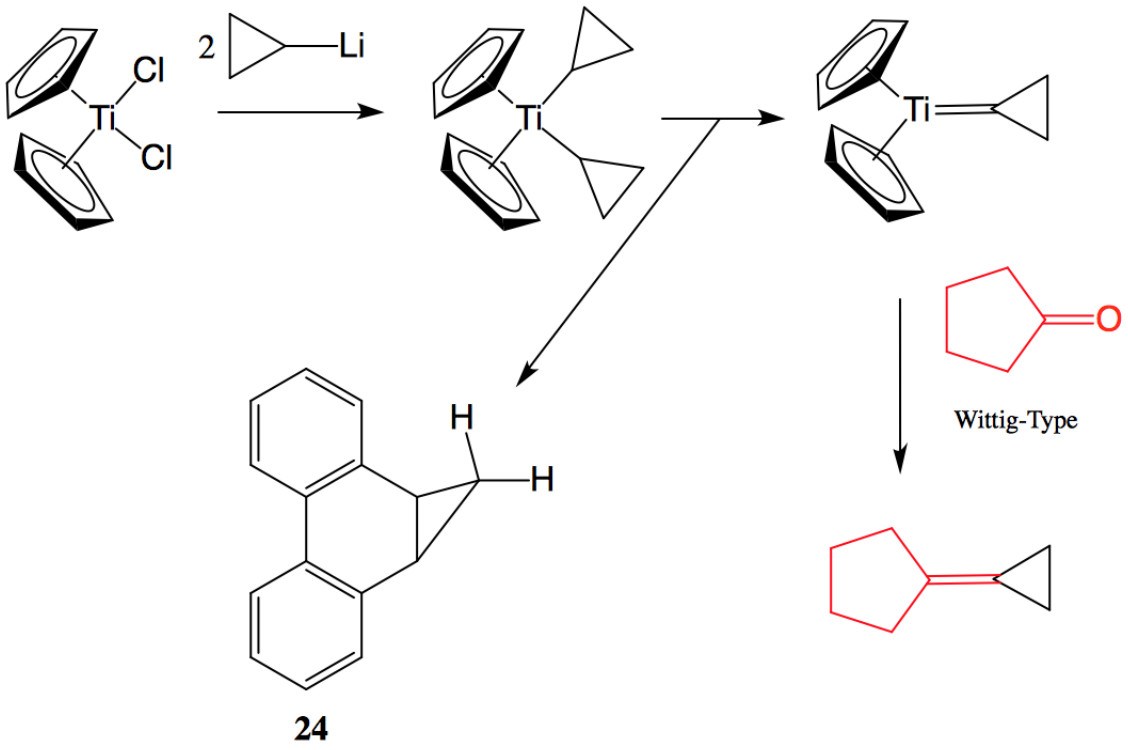

Scheme 2.3. Petasis mechanism resulting in half conversion to the dihydrogen species **24**.

The maximum yield with respect to the amount of **22** is then 50%. Furthermore, unlike in the reactions Petasis performed, **24** is not volatile, and has be removed through purification methods. Since both **24** and the desired compound **11** are hydrocarbons, the polarities are very similar making column chromatography methods inefficient. Also, there are roughly equivalent amounts of **24** and **11**, which makes recrystallization difficult.

Matsubara et al. reported the olefination of *gem*-dibromoalkanes with ketones using Samarium / Samarium Iodide and a chromium catalyst.[36] The scheme shown in Scheme 2.4a was promising as it did not necessarily indicate the formation of the dihydrogen derivative **24**, which would make purification efforts easier, eliminate a synthetic step, and result in a larger overall yield. The question was then if it would apply to the larger systems. The reaction shown in Scheme 2.4b was attempted several times. Although the GC/MS analysis of the reaction mixture did indicate the presence of the desired product **11**, and no presence of **24**, there was little to negligible yield of the product. By far, the main product was the

monobromo derivative **22**.

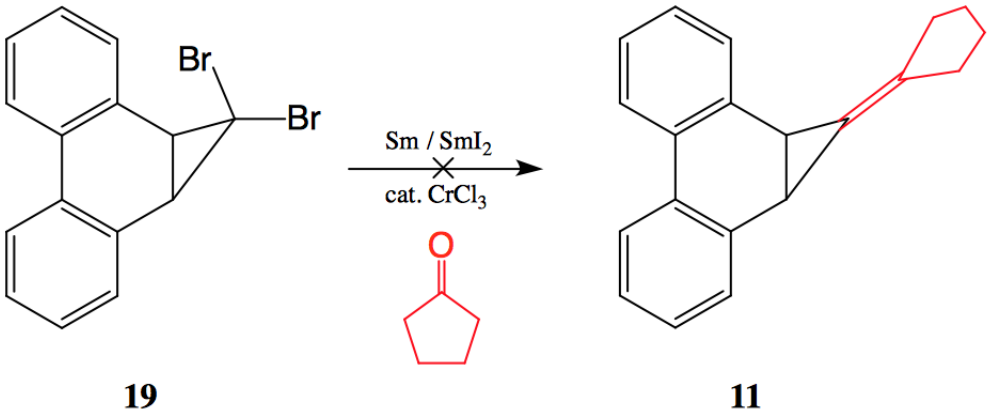

Scheme 2.4. Olefination attempt of a *gem*-dibromocyclopropane.

Many other reactions were attempted using cyclopentanone or iodocyclopentane, but the protons at the α position relative to the carbonyl or halogen proved to be too acidic. Thus, whenever an anion was formed on the cyclopropyl ring, it simply deprotonated one of the acidic protons to arrive at a protonated version (either **22** or **24**) of the starting material. After frustration with the purification process and the inefficiency of the chromium catalyzed olefination, another literature search presented a modification to Petasis procedure published by Takeda et al., which eliminates a synthetic step. Scheme 2.5 shows this one step procedure from **25**[33] to **11** by first reducing titanium with triethylphosphite and oxidizing magnesium, and then the subsequent addition of a ketone or aldehyde.[34]

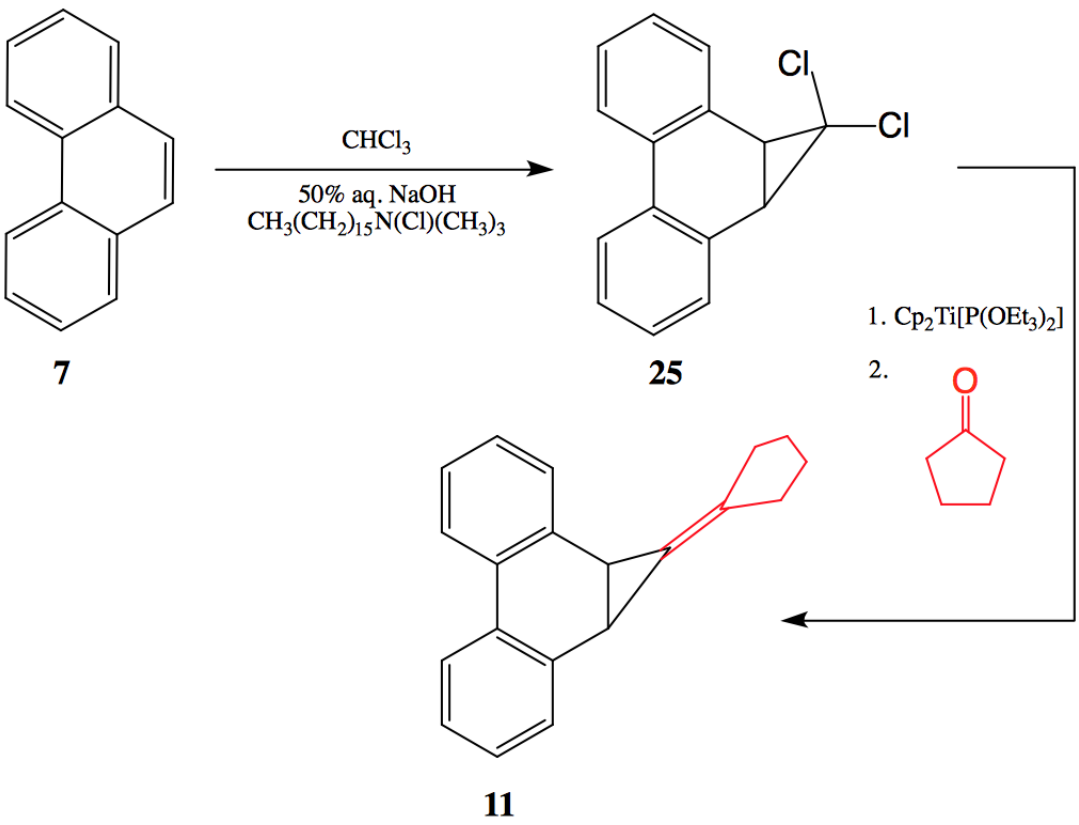

Scheme 2.5. A new method for synthesizing disubstituted vinylidenecarbene precursors using a modified Takeda procedure.[34]

Although this reaction worked and it is more efficient and cheap, it still required significant purification efforts. The yields of the final step to synthesize **11** were roughly similar (28% for Petasis, 22% for Takeda on similar scales). However, the adapted Takeda procedure was significantly easier and safer to run. Whereas the Petasis procedure required the addition of an organolithium reagent, cooling the solution to -78 °C, and refluxing overnight, the Takeda procedure required none of these and proceeded well at room temperature. Petasis was able to store the titanocene complexed with two cyclopropyl anions without decompositions for several months at -20 °C.[32] However, all efforts to isolate the active intermediate from with one cyclopropyl complexed to titanocene were unsuccessful.[32,34] If that active intermediate could be isolated, it could be stockpiled to allow for a one step synthesis with similar ease to that of an ordinary Wittig reaction.

Despite which method was used, the precursor **11** was successfully synthesized and characterized including a crystal structure (Figure 2.6). The ^{1}H NMR spectrum showed the expected four signals in the alkyl region around 2 ppm due to the different chemical environments on opposite sides of the cyclopentyl ring. Furthermore, the singlet near 3 ppm showed promise to be used as a way to monitor photolysis experiments by ^{1}H NMR. The clean GC spectrum and mass ratio of $m/z = 258$ confirmed the purity of **11** after column chromatography and recrystallization from hexanes or ethanol.

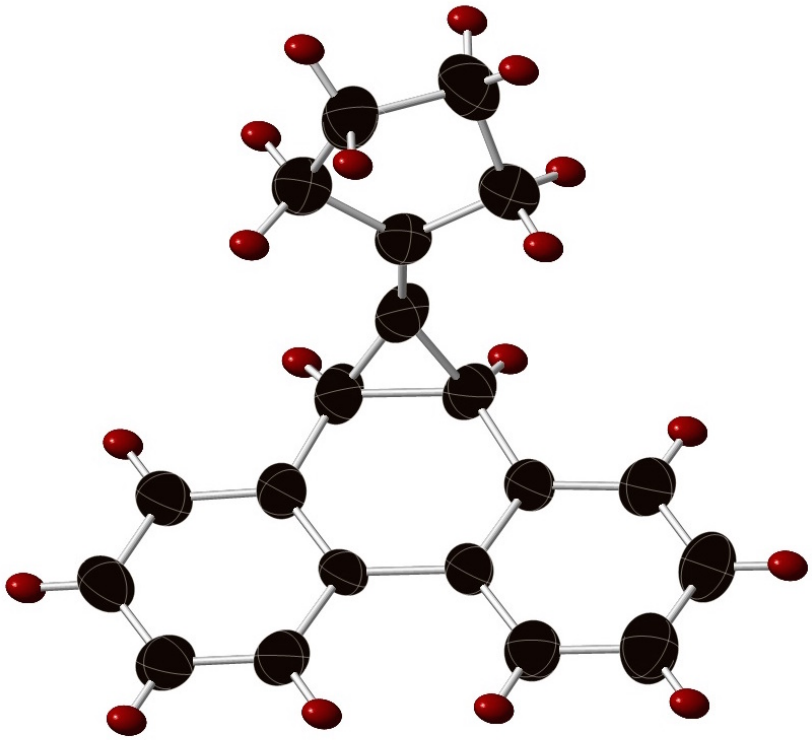

Figure 2.6. X-ray crystal structure of precursor **11**.

2.2 Photolysis and Trapping Experiments

Precursor **11** underwent photolysis at ~350 nm to produce cyclopentylidenecarbene **9** and subsequently cyclohexyne **10**. The formation of **10** was determined by three photolysis reactions. The first was a photolysis of **11** by itself dissolved in either benzene or benzene-

d6. The second and third were photolyses with two different trapping agents (**15** and **17**) added as discussed in the Introduction. The photolyses were monitored every 1-2 hours by ^{1}H NMR initially, and subsequent trials were monitored by GC/MS. The signal from the ^{1}H NMR around 3 ppm corresponds to the protons at the base of the cyclopropyl ring (Figure 2.2). This signal is well separated from the other signals before and after photolysis and provided a means of monitoring the photolysis. Once the signal no longer decreased, the photolysis was stopped, analyzed by GC/MS, and purified. As well as the production of **10**, another byproduct **26** was produced. The overall photolysis scheme is shown in Scheme 2.7.

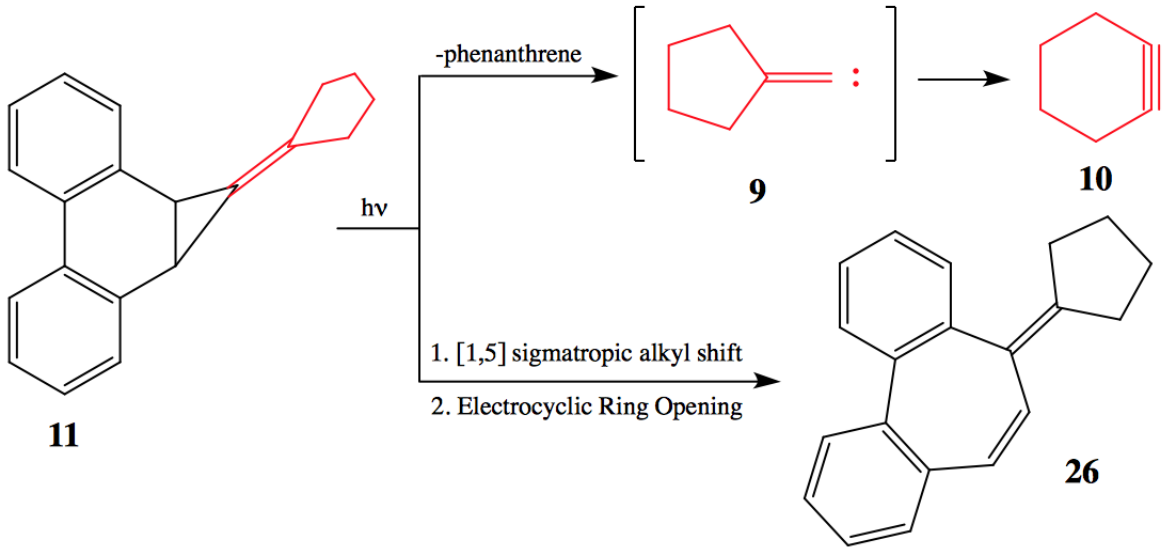

Scheme 2.7. The two major photolysis products **10** and **26**.

2.2.1 Neat Photolysis

During the photolysis, an additional byproduct was formed with the same mass as the original precursor **11**, but a slightly different retention time, indicating an isomer was formed. Hardikar et al. also found an isomer during the photolysis of the dimethylvinylidenecarbene precursor.[20] The formation of the isomer is explained by an antarafacial [1,5] sigmatropic alkyl shift followed by an electrocyclic ring opening (Scheme 2.8).[20,37] Precedence for this rearrangement was observed in an indan-based disubstituted vinylidene system.[37]

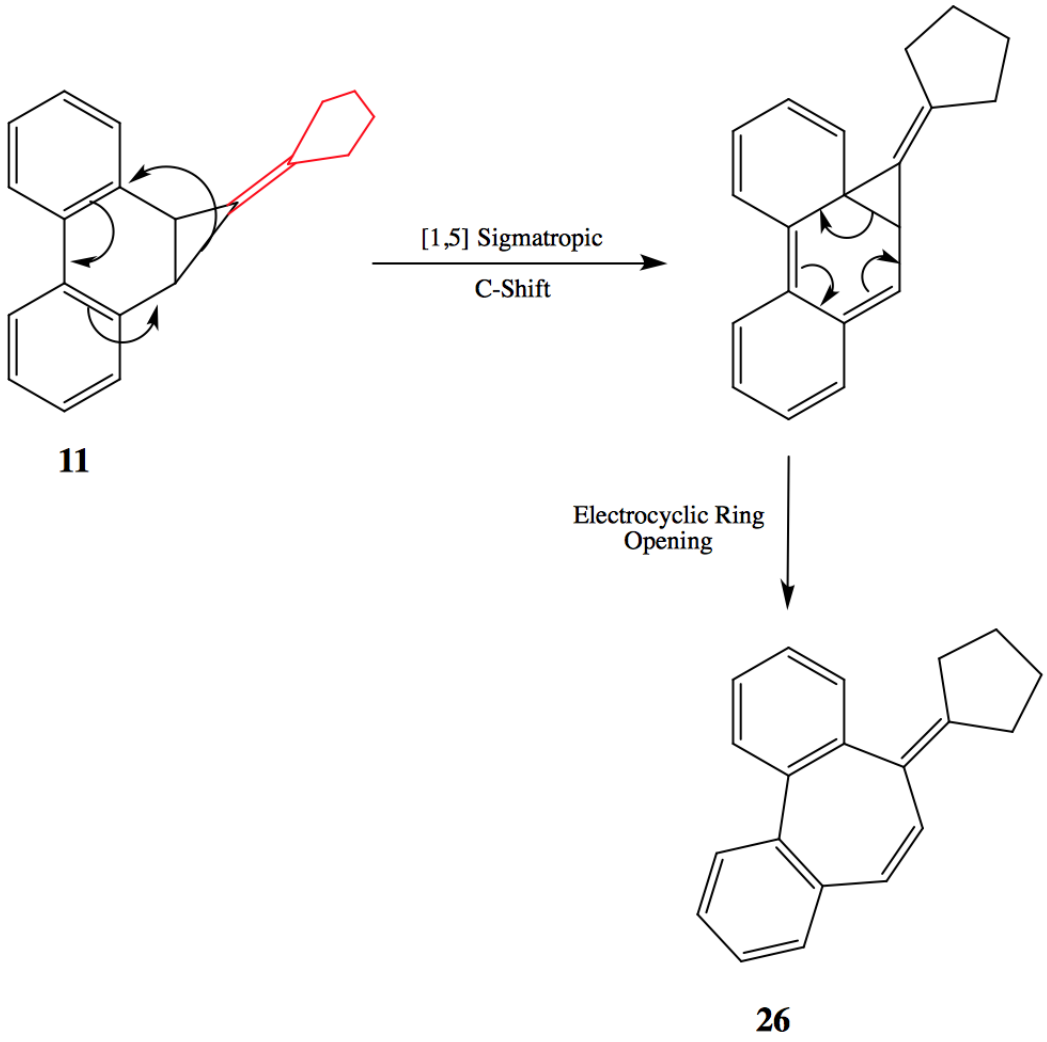

Scheme 2.8. Mechanism of the photochemical production of isomer **26**.

The ^{1}H NMR of 8 hours of the neat photolysis (Figure 2.9) shows two main conclusions. The first is that the precursor **11** is photolabile as expected. The singlet labeled **a** shows the signal around 3 ppm disappearing at the same time the signal labeled **b** appears. Signal **b** exactly matches that of the protons at the 9 and 10 positions on phenanthrene. Since the original precursor diminished and phenanthrene formed, that necessarily means that cyclopentylidenecarbene **9** was formed. During the photolysis, signals **a**, **b**, and **c** appeared simultaneously. Signal **c** is within the typical alkene region, indicating a product has alkenyl protons. Further photolysis after the precursor was completely gone resulted in the appear-

ance of a new signal **d** at 4.2 ppm, indicating a change to a product and not the precursor. The alkyl region was difficult to interpret since there are many products that could be formed that would bear signals in that region such as the cyclopentylidene dimer and/or trimer, the cyclohexyne dimer, trimer, and/or tetramer, and the isomer.

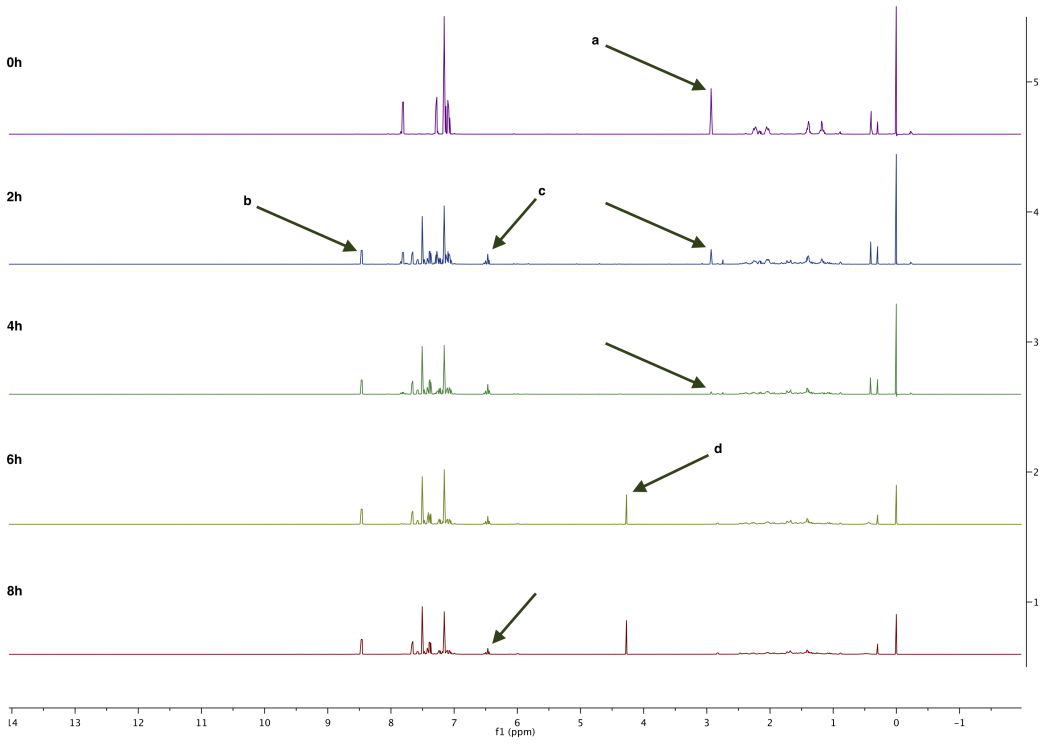

Figure 2.9. Neat photolysis of precursor **11** over 8 h: (a) precursor **11** (b) phenanthrene **5** (c) isomer **26** (d) oxidized isomer.

After 8 hours of the photolysis, another GC/MS trace was acquired. The post-photolysis GC/MS data (Figure 2.10) gave an initial indication that cyclohexyne was formed. From the introduction, Schemes 1.15-1.17 summarize the dimerization, trimerization, and tetramerization of cyclohexyne. The post-photolysis GC/MS showed compounds with an m/z ratio of 160, 240, and 320 potentially corresponding to the dimer, trimer, and tetramer respectively. Since the dimer was never able to be purified, it could indeed be a dimer of the cyclopentylidenecarbene. However, a database comparison showed it was likely the octahydrobiphenylene (dimer). Additionally, the trimer was isolated, albeit in low yield, and a

comparison to a standard of the dodecahydrotriphenylene (trimer) confirmed its formation. The presence of the trimer most likely indicates that the dimer was of cyclohexyne **10** and not its corresponding carbene **9**. Additionally, at the end of the photolysis, the major product between the dimer, trimer, and tetramer was the tetramer with a mass of 320. With a later retention time, a very small amount of a compound with an m/z of 338 was apparent. This most likely corresponds to the addition of cyclopentylidenecarbene to the original precursor[38], indicating that cyclopentylidenecarbene was first formed and then quickly and intramolecularly rearranged to cyclohexyne.

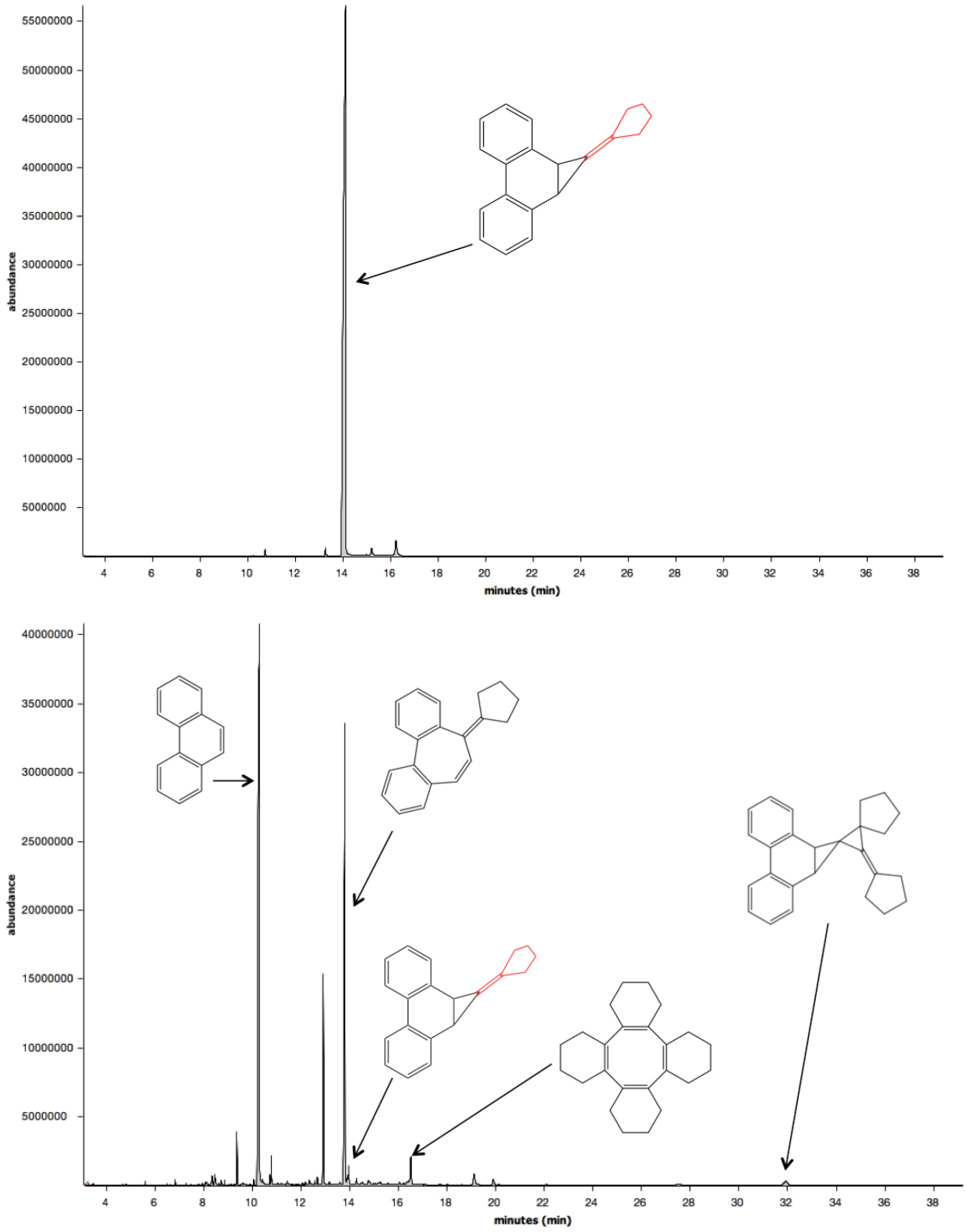

Figure 2.10. Neat photolysis of precursor **11**: (top) precursor **11** pre-photolysis (bottom) after 8h of photolysis

The major peak, other than phenanthrene, was the byproduct with the same mass as the original precursor **11**, but a slightly different retention time. After purification by column chromatography, the isomer was isolated. Unfortunately, the isomer was a clear oil, so a crystal structure was not obtained. Unknowingly, the isomer was left open to the atmosphere and became oxidized overtime and the GC/MS then indicated two compounds. The oxidized compound had a mass of 274, which is one oxygen atom heavier than the original isomer. Subsequent photolyses stored the rearranged product under argon to prevent oxidation, and could then be fully characterized including ^{1}H and ^{13}C NMR, IR, and high resolution mass spectrometry. Signals in the alkene region integrated to 2H. Now looking back at Figure 2.9, the peak appearing at 4.2 ppm makes sense. Epoxides often appear in the 3-5 ppm region. Signal **d** then corresponds to the oxidized product. Notably, signal **d** increases as all of the **c** signals decrease. Since the effect of oxidation lowered all signals in the alkene region equivalently, it indicates that the double bond being oxidized housed both of the protons found in the alkene region. This information, along with the characterization, concludes that the isomer was that shown in **26**. Subsequent photolyses were purified using preparative TLC to obtain an adequate sample for analysis (37% yield).

The strategy for further confirmation was to synthesize a standard of **26**. The plan for its synthesis is shown in Scheme 2.11. The first retrosynthetic step is a standard Wittig reation. The second retrosynthetic step is a Suzuki coupling followed by an aldol condensation, which has been reported to undergo both in one step.[39,40]

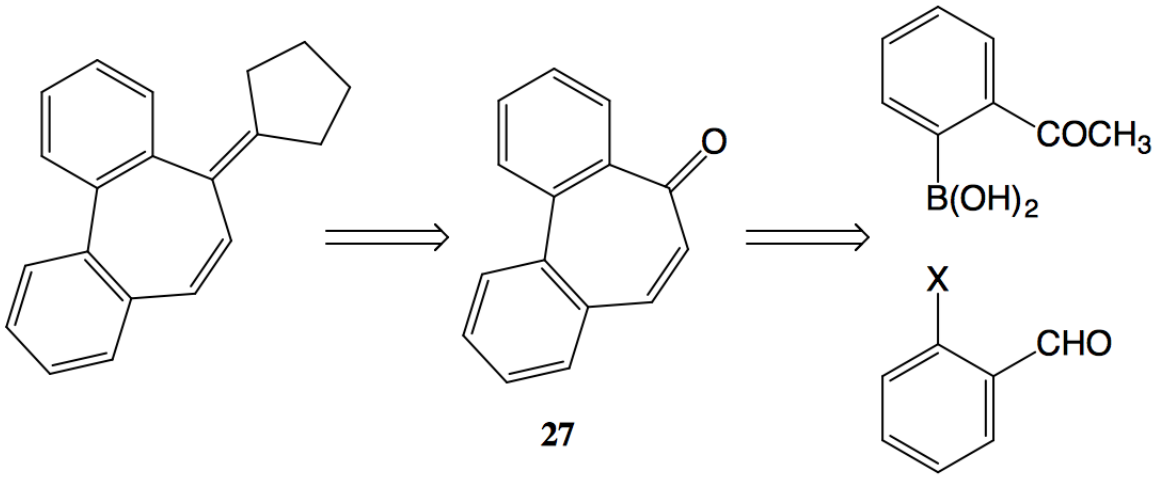

Scheme 2.11. Retrosynthetic strategy for isomer **26**.[39,40]

The synthesis of ketone **27** was successful via the Suzuki coupling with palladium tetrakis(triphenylphosphine) and the subsequent aldol condensation.[39,40] However, for unknown reasons, the Wittig reaction did not proceed at all. Nevertheless, the IR, GC/MS, and NMR data are convincing to determine the structure of the isomer **26**.

2.2.2 Photolysis with Trapping Agents

The trapping reactions were monitored by GC/MS. The formation of the trapped product was very clear, as shown by the gas chromatograms in Figures 2.12 and 2.13. The photolyses with trapping agents took much longer since the UV light could be absorbed by the reagents, causing less photolysis of the precursor per unit of time. This was particularly true for the tetracyclone trap, which took 40 hours for completion. Previous syntheses of cyclohexyne have trapped cyclohexyne using 1,3-diphenylisobenzofuran **15**[18,19,25] or tetracyclone **17**[24]. However, previous production of cyclopentylidenecarbene trapped as cyclohexyne has been by α-elimination.[18]

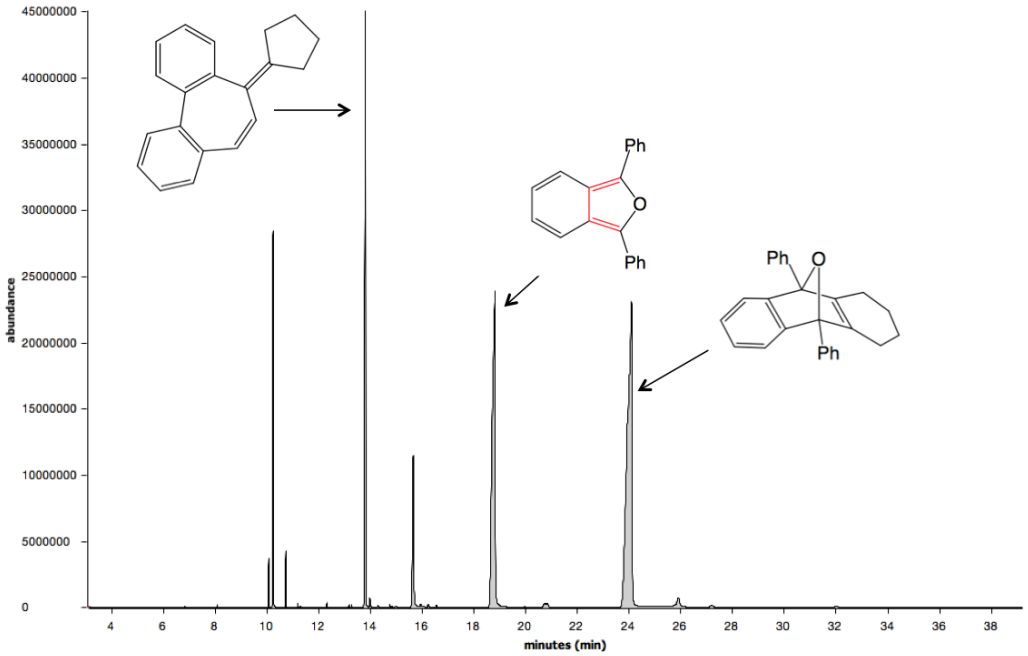

Figure 2.12. Post-photolysis gas chromatogram using 1,3-diphenylisobenzofuran **15** as a trapping agent.

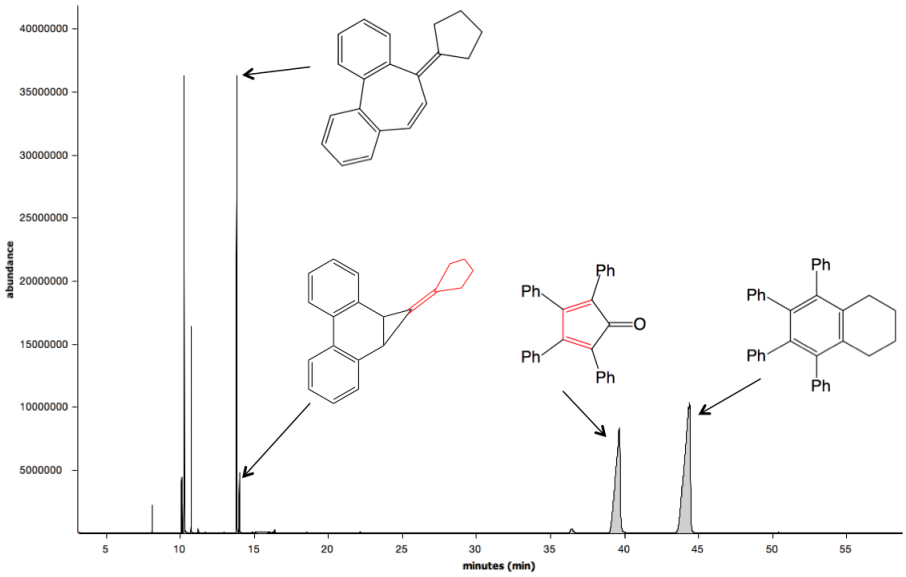

Figure 2.13. Post-photolysis gas chromatogram using tetracyclone **17** as a trapping agent.

Here, we present the first ever successful trapping of cyclohexyne from cyclopentylidenecarbene using a photolabile precursor. Furthermore, until now, crystal structures for the trapped products have not been reported (Figure 2.14). These structures show concretely

that it is the addition of cyclohexyne rather than an addition of cyclopentylidenecarbene.

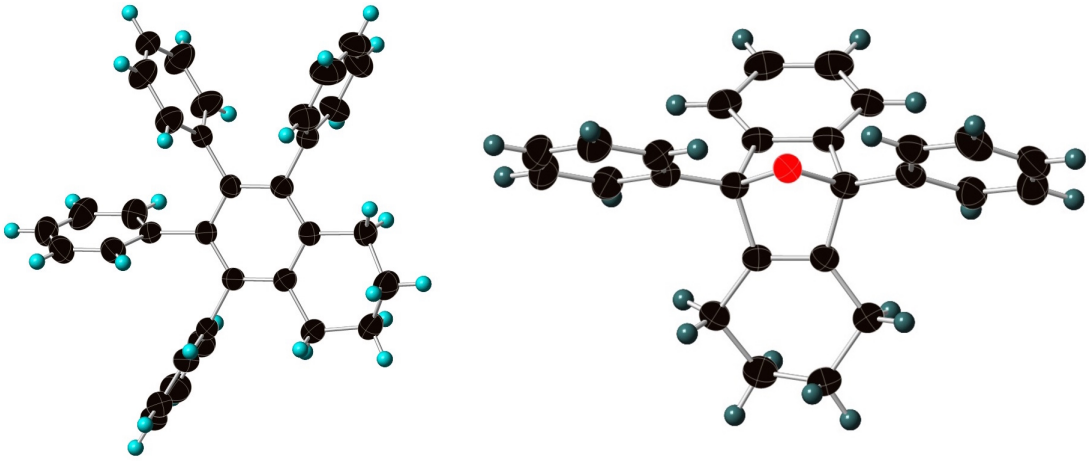

Figure 2.14. X-ray crystal structure of trapped products **16** and **18**.

2.3 Results of Computational Studies

Cyclopentylidenecarbene **9** and its conversion into cyclohexyne **10** was studied at the CCSD(T)/cc-pVTZ//B3LYP/6-31+G* level (Figure 2.15). The geometry was optimized using density functional theory followed by a more accurate single point energy using coupled cluster methods. The coupled cluster methods better model the electron interactions by using an exponential operator that incorporates single, double, and triple excited states. The singlet was found to be more stable than the triplet by 45.6 kcal/mol, and thus the reactivity is determined by the singlet, as expected. The cyclohexyne optimized to a C_2 symmetry and was found to be more stable by 11.6 kcal/mol relative to the singlet cyclopentylidenecarbene. The transition state between the singlet **9** and the C_2 **10** was found to be 11.5 kcal/mol higher in energy relative to the singlet **9** with an imaginary frequency of ν=-375 cm^{-1}.

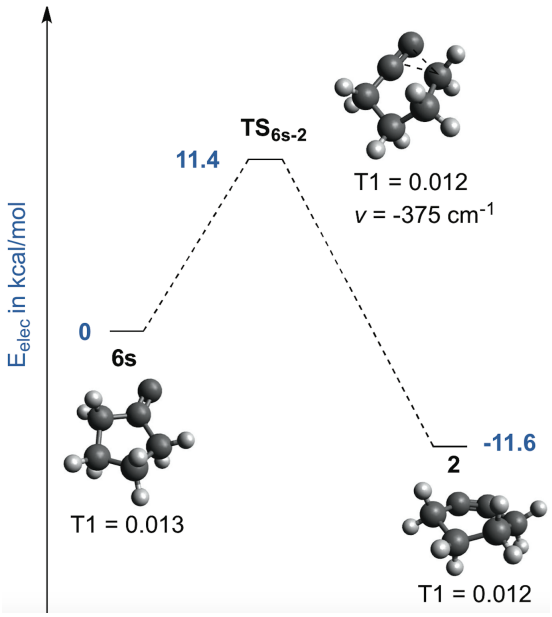

Figure 2.15. Singlet cyclopentylidenecarbene to C_2 cyclohexyne energetics at CCSD(T)/cc-pVTZ//B3LYP/6-31+G*.

The IR frequency of the C-C triple bond in cyclohexyne was calculated to appear at 2200.31 cm^{-1}. This calculation seems to refute Wentrup's debated claim to have observed cyclohexyne by IR with a peak ∼2100 cm^{-1}.[17] Additionally, an IRC calculation confirmed the transition state. It is interesting to note here that cyclohexylidenecarbene, although has a barrier of only 2.4 kcal/mol higher calculated at the same level of theory, does not rearrange to cycloheptyne.[21] Additionally, the rearrangement of dimethylvinylidenecarbene to butyne has a barrier of 11.7 kcal/mol, only 0.1 kcal/mol higher than the barrier in the present study.[20] Thus, whether the rearrangement is observed seems to be due to additional factors other than the kinetic barrier and thermodynamic drive. While dimethylvinylidenecarbene and cyclopentylidenecarbene have essentially the same kinetic barrier, only cyclopentylidenecarbene rearranges. There are other additional processes that these carbenes could favor or disfavor such as dimerization, cyclopropanation, or C-H bond insertion. These reactions are mostly kinetically controlled and thus, the fastest reaction will determine the major product.

2.4 Matrix Isolation

Matrix isolation was performed on precursor **11**, which was sublimed under high vacuum onto an argon matrix at 8 K. Flash photolysis at 308 nm with a frequency at 10 Hz for 30 minutes was performed and the IR spectrum was taken. The difference between precursor **11** and the photolysed precursor showed peaks corresponding to phenanthrene and a very small peak at 2100 cm^{-1} with an absorbance of 0.05. While this frequency matches well with Wentrup's previous claim of peaks at 2090 and 2105 cm^{-1}, his claims are highly controversial, and further experiments detailed in the next section will be needed to determine the IR spectrum of cyclohexyne.[17] The extremely low absorption noted above can be attributed to violating a selection rule of vibrational spectroscopy. The symmetry of cyclohexyne does not allow for a change in dipole moment in the stretching of the alkyne.

2.5 Concluding Remarks and Future Work

A quicker, easier, and safer synthetic route to phenanthrene-based alkylidenecarbene precursors was developed using an adapted procedure from Takeda et al. that reduces titanocene dichloride before undergoing a Wittig-type reaction with a given ketone. The photolysis of precursor **11** formed the putative cyclopentylidenecarbene and rearranged to the corresponding cyclohexyne, which could di, tri, and tetramerize or be trapped by the dienes 1,3-diphenylisobenzofuran or tetracyclone (Scheme 2.16). The precursor and trapped adducts were fully characterized by GC/MS, NMR, IR, and X-Ray Crystallography. A byproduct also noted by Hardikar et al. was identified as the precursor undergoing a sigmatropic shift followed by an electrocyclic ring expansion.

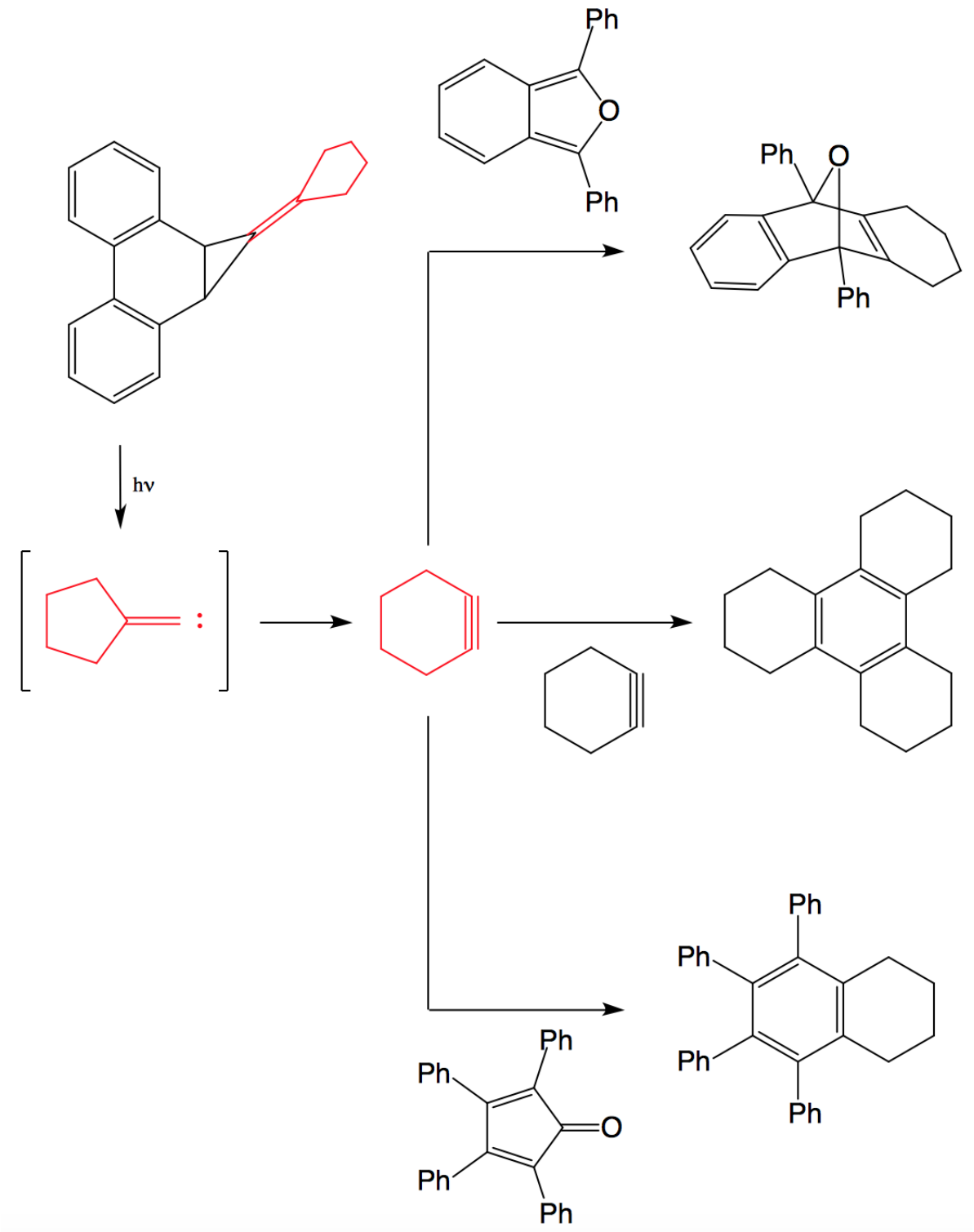

Scheme 2.16. Photolysis of precursor **11** generates cyclohexyne that can be trapped by itself or dienes.

Computational studies at CCSD(T)/cc-pVTZ//B3LYP/6-31+G* showed the singlet **9** rearranges to cyclohexyne **10** through a transition state that is 11.4 kcal/mol higher in energy relative to the carbene.

Precursor **11** is advantageous to studying cyclopentylidenecarbene and cyclohexyne for several reasons. 1) The precursor can be readily prepared in two steps in quantities that allow for multiple studies. 2) The precursor **11** is stable and conveniently handled as opposed to bisdiazo and bisdiazirine compounds. 3) The photochemical generation of cyclopentylidenecarbene, instead of other methods that involve the need of additional reagents or high temperatures, allows for kinetic studies using time-resolved laser flash photolysis and structural studies using matrix isolation spectroscopy. Additionally, our lab is currently testing the rearrangement of cyclobutylidenecarbene into cyclopentyne by similar methods. One can also imagine using this method to generate and study heterocyclicalkynes and other caged cycloalkynes. Finally, adding cyclopentanone with a ^{13}C label at the base of the carbonyl will form cyclohexyne with an asymmetrical triple bond, which will give a stronger absorbance in the IR spectrum.

Experimental Procedures

3.1 General Remarks

Tetrahydrofuran was dried by passage through two columns (2 ft x 4 in) of activated alumina. All other solvents and reagents were used as obtained from commercial sources. Other than the synthesis of 1,1-dihalo-1a,9b-dihydro-1H-cyclopropa[l]phenanthrenes, all reactions were carried out under an argon atmosphere in oven dried glassware. Flash chromatography was performed on pre-packed silica gel columns (70-230 mesh). NMR spectra were recorded at 500 MHz for ^{1}H and 125 MHz for ^{13}C in $CDCl_3$. The shifts are reported in δ ppm and referenced to either tetramethylsilane (TMS) or the residual proton signal from the solvent. GC/MS data were obtained with a capillary gas chromatograph interfaced with a quadrupole, triple-axis mass selective detector operating in electron impact (EI) mode. Exact masses were found using time of flight mass spectrometry (TOF-MS) equipped with a direct analysis in real time (DART) ion source in positive ionization mode (DART-TOF-MS).

3.2 1,1-dibromo-1a,9b-dihydro-1H-cyclopropa[l]phenanthrene (19)[30]

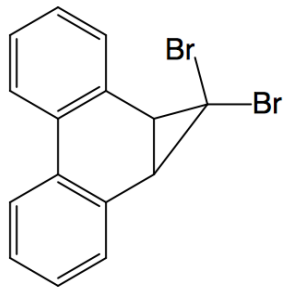

To a stirring mixture of phenanthrene (35.6 g, 200 mmol), benzyltriethylammonium chloride (0.54 g, 2.4 mmol), bromoform (40 mL, 115.6 g, 460 mmol), dichloromethane (40 mL), and ethanol (1 mL), was added 50% aq. sodium hydroxide (80 mL) in small portions over 10 min. After stirring at r.t. for 4 days, the thick, dark brown mixture was poured into a separatory funnel after being rinsed with dichloromethane (100 mL) and water (100 mL). The aqueous layer was extracted with dichloromethane (2 x 50 mL). The organic layer was subsequently washed with 2 M hydrochloric acid (2 x 100 mL), water (2 x 100 mL), and brine (1 x 100 mL). The remaining residue after evaporation of the solvent was recrystallized from chloroform and charcoal to give **19** as a white solid (25.97 g,

74 mmol, 37%). mp: 110-111 C; ^{1}H NMR: δ 8.00 (dd, J = 7.9, 1.3 Hz, 2H), 7.49 (dd, J = 7.4, 1.5 Hz, 2H), 7.40 (td, J = 7.5, 1.5 Hz, 2H), 7.33 (td, J = 7.5, 1.5 Hz, 2H), 3.5 (s, 2H); ^{13}C NMR δ 135.4, 131.7, 131.2, 130.9, 129.2, 128.3, 128.3, 128.1, 127.7, 123.0, 37.4, 30.9.

3.3 *exo*-1-bromo-1a,9b-dihydro-1H-cyclopropa[l]phenanthrene (22)[31]

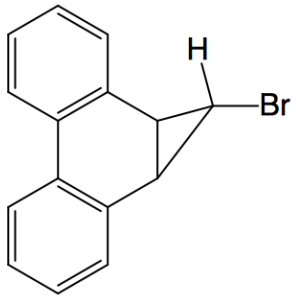

Tert-butyllithium (37 mL, 1.7 M in pentanes, 62.9 mmol) was added drop-wise by syringe to a magnetically stirred solution of **19** (10.51 g, 30 mmol) in anhydrous THF (150 mL) at -75 °C. Stirring was continued at this temperature for another 45 min after completion of addition, and the resulting dark green solution was quenched with water. The reaction mixture was then allowed to slowly warm to room temperature, and transferred to a separatory funnel with the aid of water (100 mL) and ether (100 mL). The organic and aqueous layers were separated, and the latter was extracted with ether (2 x 60 mL). The combined organic layers were subsequently washed with water (2 x 60 mL) and brine (1 x 60 mL). After evaporation of the solvent, the crude material was recrystallized from hexanes to give **22** as a white solid (3.8 g, 14 mmol, 46.7%). mp 114-116 °C; ^{1}H NMR: δ 7.95-7.93 (m, 2H), 7.50-7.47 (m, 2H), 7.32-7.26 (m, 4H), 3.01 (d, J = 3.2 Hz, 2H), 2.41 (t, J = 3.2 Hz, 1H); ^{13}C NMR δ 131.9, 129.7, 129.3, 128.1, 127.3, 123.3, 29.9, 27.7; FTIR (ATR) ν 3069, 3032, 1485, 1445, 1195, 978, cm^{-1}; LRMS (EI) m/z 272 (M^{+} + 2), 270 (M^{+}), 191.

3.4 1,1-dichloro-1a,9b-dihydro-1H-cyclopropa[l]phenanthrene (25)[33]

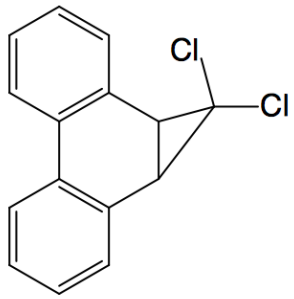

To a stirring mixture of phenanthrene (30 g, 0.17 mol), cetyltrimethylammonium chloride (0.4432 g, 1.4 mmol), chloroform (50 mL, g, mol), was added 50% aq. sodium hydroxide in small portions over 10 min. After stirring at 50 °C for 24 h, 10% sulfuric acid was added until the pH of the mixture was ∼3. The resulting mixture was extracted with ethyl acetate (200 mL) and subsequently washed with water (300 mL) and brine (200 mL) and dried over sodium sulfate. After evaporation of the solvent, the crude material was recrystallized from 95% ethanol to give **25** as an off white solid (8.42 g, 32 mmol, 18.8%). mp: 136.3-137.0 °C. ^{1}H NMR: δ 8.01 (dd, J = 7.8, 1.2 Hz, 2H), 7.48 (dd, J = 7.4, 1.5 Hz, 2H), 7.39 (td, J = 7.7, 1.7 Hz, 2H), 7.33 (td, J = 7.6, 1.4 Hz, 2H), 3.5 (s, 2H); LRMS (EI) m/z 262 ($M^+ + 2$), 260 (M^+), 225, 190, 178.

3.5 1-cyclopentylidene-1a,9b-dihydro-1H-cyclopropa[l]phenanthrene (11)

3.5.1 Method A[32]

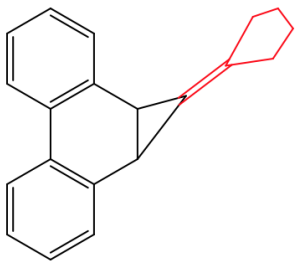

Tert-butyllithium (13 mL, 1.7 M in pentanes, 22.1 mmol) was added dropwise by syringe to a solution of **22** in anhydrous THF (50 mL) at -72 °C. After completion of the addition, the reaction mixture turned dark green and was stirred for 40 min before adding bis(cyclopentadienyl)titanium(IV) dichloride (1.1 g, 4.4 mmol). The reaction was stirred for 5 min and then warmed to 0 °C and stirred for 90 min. Cyclopentanone (2.0 mL, 22.6 mmol) was then added to the dark red-brown solution. After stirring for 5 min, the reaction mixture was heated to 55 °C for 15 h. The resulting orange reaction mixture was purified directly by flash chromatography on silica gel (hexanes) to obtain **11** (357 mg, 1.4 mmol, 28%) as a white solid after recrystallization from hexanes.

3.5.2 Method B[34]

Triethyl phosphite (10.6 mL, 10.2 g, 60 mmol) was added to a solution of crushed magnesium turnings (0.8 g, 33 mmol), powdered 4 Å molecular sieves (1.5 g), and bis(cyclopentadienyl)titanium(IV) dichloride (7.5 g, 6 mmol) stirring at r.t. Within 20 minutes the reaction mixture turned dark green and eventually dark brown. After stirring for an additional 3 h, **25** (2.6 g, 10 mmol) dissolved in THF (40 mL) was added to the reaction mixture, which turned dark green. Cyclopentanone (0.5 mL, 0.475 g, 5 mmol) was added after 20 min of stirring. After an additional 1 h of stirring, the reaction mixture was diluted with ethyl acetate (30 mL) and filtered through a pad of Celite. The solvent was removed from the orange mixture by reduced pressure and was purified by flash chromatography on silica gel (hexanes) to give **11** (200 mg, 0.78 mmol, 15.6%) as a white solid after recrystallization from ethanol. mp: 112-114 °C; ^{1}H NMR: δ 7.92 (d, J = 6.9 Hz, 2H), 7.36 (d, J = 6.4 Hz, 2H), 7.21 (d, J = 5.5 Hz, 4H), 3.07 (s, 2H), 2.29 (q, J = 7.5 Hz, 2H), 2.06 (q, J = 6.9, 6.1 Hz, 2H), 1.59 (dt, J = 12.9, 6.6 Hz, 2H), 1.48 (dt, J = 12.9, 6.6 Hz, 2); ^{13}C NMR: δ 133.9, 133.0, 129.2, 128.8, 127.5, 125.7, 123.2, 114.7, 30.9, 26.4, 22.3; FTIR (ATR): ν 3061, 2980, 1431, 768, 728 cm^{-1}; LRMS (EI): m/z 258 (M^{+}), 230, 215, 178.

3.6 5H-dibenzo[a,c][7]annulen-5-one (27)[39,40]

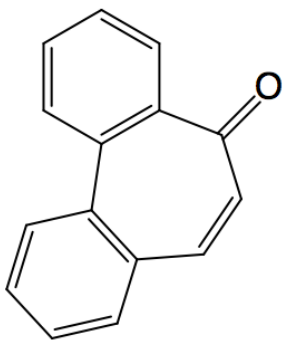

Argon was vigorously bubbled through a stirring solution of (2-acetylphenyl)boronic acid (1.00 g, 6.1 mmol), 2-bromobenzaldehyde (0.6 mL, 0.951 g, 5.1 mmol), cesium carbonate (1.78 g, 5.5 mmol) in toluene (20 mL) and ethanol (10 mL) for 15 min in a pressure flask. After tetrakis(triphenylphosphine)palladium(0) (796 mg, 0.7 mmol) was added, the pressure flask was sealed and heated to 100 °C for 24 h before diluting with ethyl acetate (20 mL), filtering through Celite. The crude reaction mixture was purified by flash chromatography on silica gel (hexanes $\longrightarrow$ 3% ethyl acetate) to give **27** as a white solid (107.8 mg, 0.52 mmol, 10.4%). ^{1}H NMR: δ 7.98 (dd,

J = 7.8, 1.8 Hz, 1H), 7.95-7.86 (m, 2H), 7.68 (td, J = 7.7, 1.7 Hz, 1H), 7.62-7.45 (m, 4H), 7.36 (d, J = 12.2 Hz, 1H), 6.68 (d, J = 12.2 Hz, 1H); ^{13}C NMR: δ 192.6, 139.9, 137.0, 133.0, 131.5, 131.3, 130.2, 130.2, 129.4, 128.5, 128.2; LRMS (EI): m/z 206 (M^+), 178, 152.

3.7 General Remarks for Photolysis Experiments

The photolysis reactions were carried out in glass vials or NMR tubes using a Rayonet photochemical reactor equipped with 16 12-inch 8 W lamps with output centered at $\sim$ 350 nm (range $\sim$ 315 to 400 nm).

3.8 9,10-diphenyl-1,2,3,4,9,10-hexahydro-9,10-epoxyanthracene (16)

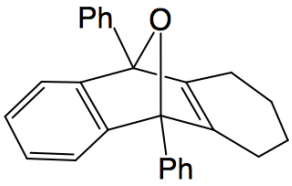

The precursor **11** (100 mg, 0.4 mmol) and 1,3-diphenylisobenzofuran **15** were photolysed in anhydrous benzene-d6 for 21 h. The course of the photochemical reaction was monitored by GC/MS. After the precursor **11** had been completely photolysed, the reaction mixture was chromatographed over silica gel with hexanes as the eluent to give the known adduct **16**[19,25,26] (91 mg, 0.26 mmol, 65%). ^{1}H NMR: δ 7.74-7.71 (m, 4H), 7.53-7.48 (m, 4H), 7.41 (tt, J = 6.8, 1.4 Hz, 2H), 7.22-7.19 (m, 2H), 6.96 (dd, J = 5.3, 3.0 Hz, 2H), 2.26 (dddd, J = 14.8, 10.5, 6.2, 3.6 Hz, 2H), 2.05 (dddd, J = 14.8, 10.5, 6.2, 3.6 Hz, 2H), 1.59 (ddddd, J = 11.3, 9.3, 6.5, 4.5, 2.3 Hz, 2H), 1.44 (ddddd, J = 11.3, 9.3, 6.5, 4.5, 2.3 Hz, 2H); ^{13}C NMR: δ 151.8, 150.1, 135.4, 128.4, 127.8, 127.7, 126.3, 124.6, 92.3, 23.4, 22.4; LRMS (EI): m/z 350 (M^+), 332, 245, 105.

3.9 5,6,7,8-tetraphenyl-1,2,3,4-tetrahydronaphthalene (18)

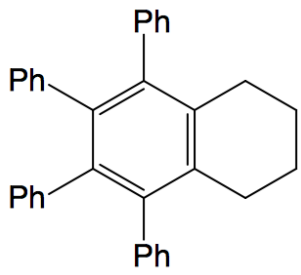

The precursor **11** (100 mg, 0.4 mmol) and tertracyclone **17** were photolysed in anhydrous benzene-d6 for 40 h. The course of the photochemical reaction was monitored by GC/MS. After the precursor **11** had been completely photolysed, the reaction mixture was chromatographed over silica gel with hexanes as the eluent to give the known adduct **18**[24,25] (75 mg, 0.17 mmol, 43%).^{1}H NMR: δ 7.17 (t, J = 7.5 Hz, 4H), 7.13-7.06 (m, 4H), 6.85-6.74 (m, 4H), 2.54 (ddd, J = 6.5, 4.2, 2.3 Hz, 4H), 1.73 (q, J = 3.5 Hz, 4H); ^{13}C NMR: δ 140.8, 138.4, 134.5, 131.3, 130.3, 127.4, 126.4, 125.9, 125.0, 107.7, 107.5, 29.7, 23.1; LRMS (EI): m/z 436 (M^{+}), 393, 359, 317.

3.10 5-cyclopentylidene-5H-dibenzo[a,c][7]annulene (26)

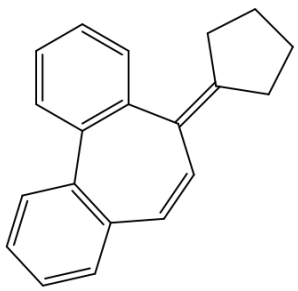

The precursor **11** (112 mg, 0.43 mmol) was photolysed in anhydrous benzene for 12 h. The course of the photochemical reaction was monitored by GC/MS. After the precursor **11** was completely photolysed, the reaction mixture was chromatographed over silica gel with hexanes as the eluent to give the isomer **26** as a clear oil (40 mg, 0.16mmol, 37%). ^{1}H NMR: δ 7.71-7.60 (m, 1H), 7.56-7.46 (m, 1H), 7.43-7.29 (m, 4H), 7.29-7.18 (m, 3H), 6.58-6.47 (m, 2H), 2.63-2.53 (m, 1H), 2.43 - 2.44 (m, 1H), 2.22-2.04 (m, 2H), 1.79-1.59 (m, 3H), 1.57-1.40 (m, 1H); ^{13}C NMR: δ 137.9, 136.5, 135.6, 130.4, 130.2, 129.3, 128.6, 128.2, 127.2, 126.8, 126.7, 31.8, 26.1. FTIR: ν 3058, 3014, 2953, 2867, 1481, 1436, 761, 731, 462 cm^{-1}HRMS (ESI-TOF) calc'd for $C_{20}H_{19}^{+}$ 259.1487, found 259.1482.

3.11 Dimer (12), Trimer (13), and Tetramer (14)

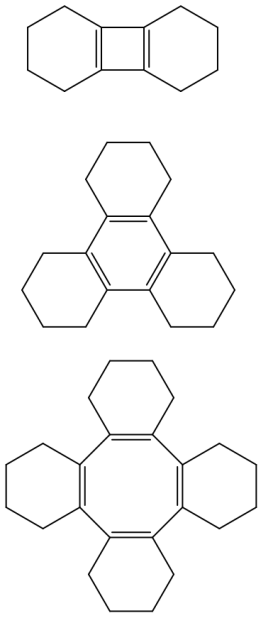

The precursor **11** (100 mg, 0.39 mmol) was photolysed in anhydrous benzene-d6 for 10 h. After the precursor **11** was completely photolysed (determined by GC/MS), the reaction mixture was chromatographed over silica gel with hexanes as the eluent to give the trimer **13** (11 mg, 0.046 mmol, 36%). However, the dimer and tetramer were not isolated, but matched a database search. The trimer **13** was confirmed by injecting a commercially available standard and observing the same retention time and fractioning pattern as the isolated **13** from the photolysis. LRMS (EI): m/z 240 (M^+), 225, 212, 198.

3.12 Computational Methods

All calculations were performed using Gaussin 09[41]. The geometries of **9**, **10**, and the transition state were optimized at B3LYP/6-31+G(d) followed by vibrational frequency calculations at the same level of theory. The single point energy calculations for **9**, **10**, and the transition state were calculated at CCSD(T)/cc-pVDZ.

3.13 X-ray Structure Determination

Single crystals of **11**, **16**, and **18** were prepared by the slow evaporation of hexanes or by recrystallization from hexanes. X-ray data were acquired at 173 K using a Bruker Smart Apex CCD diffractometer with graphite monochromated Mo Kα radiation ($\lambda = 0.71073$ Å). The data was processed with he Bruker Apex3 suite of programs[42] and the frames were integrated using the Bruker SAINT software[43] with a narrow-frame algorithm. The data was corrected for absorption effects using the multi-scan method SADABS[44]. Structure solution and refinement by least-squares on F^2 was done by using the Bruker SHELXTL

software package[45]. Nonhydrogen atoms were refined anisotropically and hydrogen atoms were calculated using a riding model. The .cif files were validated with the checkCIF/Platon facility using enCIFer[46].

Part II: A Triptycenyl Flower

Abstract

Aromaticity, a term still debated to this day, is a fundamental concept for chemists. Also under scrutiny is the idea that aromatic ring currents explain the diamagnetic anisotropic properties of aromatic compounds. Systematic approaches to evaluate the effect of magnetic shielding from aromatic ring currents have mainly focused on varying a substituent on an aromatic ring. This work synthesized bistriptycenyltoluene in order to study the through-space shielding effect. The synthetic method used is applicable to study the through-space shielding effect on a variety of substituents. In bistriptycenyl derivatives, the substituent is in the shielding region of four benzene rings (red) and the deshielding region of three benzene rings (blue). Furthermore, experimental chemical shifts are compared to computational findings based on the quantum mechanical procedures suggested by Rablen and Bally. Interestingly, the bistriptycenyltoluene also has the potential to demonstrate molecular gearing motions, and the synthetic route presented here can be used to prepare other molecular gears.

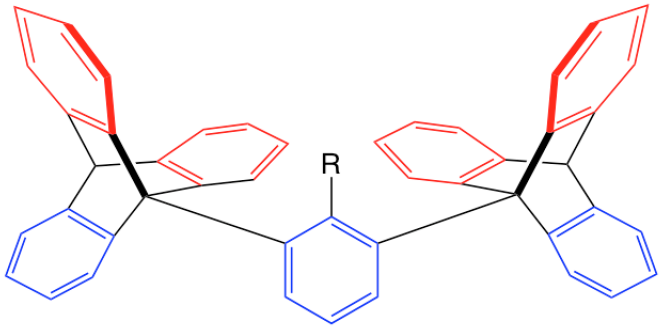

$R = CH_3$
Experimental (1.38 ppm)
Calculated GIAO/WP04/cc-pVDZ (1.473 ppm)

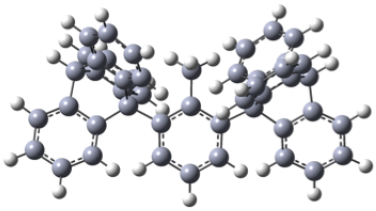

Side View

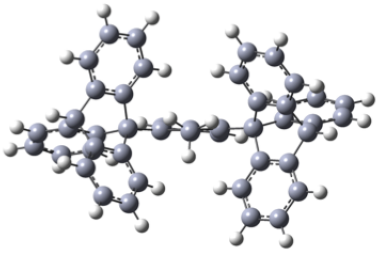

Top View

Introduction

1.1 Background on Aromatic Ring Currents

After Kekulé's discovery of the structure of benzene[47] (**28**), many began trying to explain its incredible stability. Most notably, Hückel developed the theory that describes the ability of electrons to move amongst aligned p obritals.[48–51] This naturally led to the construction of the general rules for aromaticity. If a molecule is cyclic, planar, fully conjugated, and has 4n+2 electrons in its conjugated system, it is aromatic and demonstrates remarkable stability. By far, the most common aromatic system is benzene **28** (Figure 1.1).

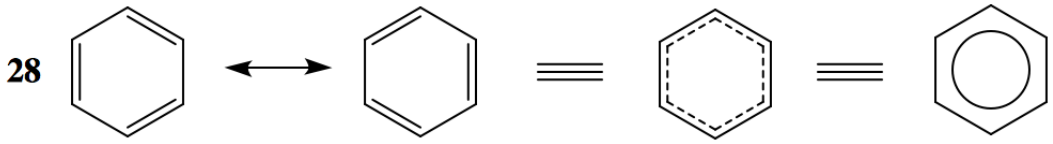

Figure 1.1. Structure of benzene.

To this day, there is still argument on what is meant by "aromaticity".[52,53] Some definitions involve the magnetic properties (diamagnetic anisotropy) attributed to aromatic systems. Pauling[54], Lonsdale[55], and London[56], believed that the diamagnetic anisotropy of benzene was due to an induced current in the presence of a magnetic field, called the ring current (Figure 1.2a). This "ring current" model has been disputed[53,57] and supported[58]. This theory not only fit well with Hückel's delocalization of electrons through p orbitals, but was also used by Pople to explain why the protons on benzene show a downfield shift relative to ethylene in a proton NMR spectrum (Figure 1.2b).[59]

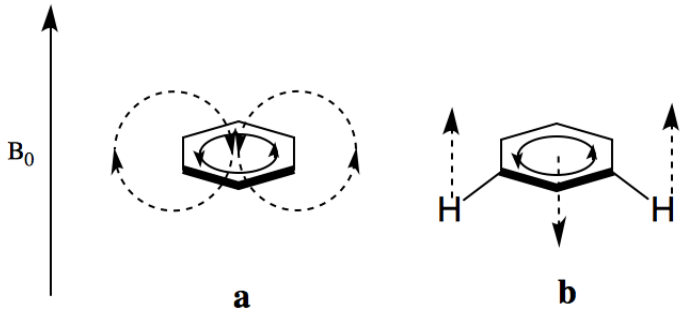

Figure 1.2. Ring current induced by an external magnetic field.

Essentially, the magnetic field outside the ring generated by the induced ring current acts in the same direction as the external magnetic field, so protons at the outskirts of rings are deshielded, and thus their corresponding proton NMR signals appear more downfield.

1.2 Experiments Demonstrating Upfield and Downfield Proton Chemical Shifts

Naturally, experimentalists began trying to synthesize compounds that project protons towards the center of the ring. An upfield (shielded) shift of these protons would support the ring current model. Indeed, when Pascal et al. synthesized **29** and Vögtle et al. synthesized **30**, the proton NMR signals were observed at -4.03 ppm and -4.08 ppm respectively (Figure 1.3).[60,61,65]

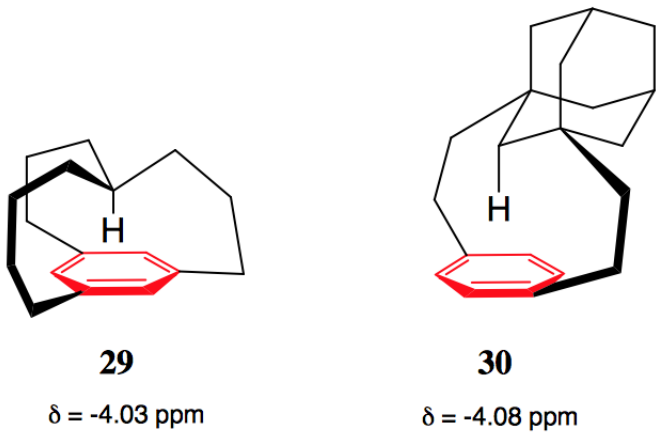

Figure 1.3. Compounds **29** and **30** exhibiting an extremely upfield shifted proton signals. Red rings are shielding the proton shown.[60,61,65]

While **29** and **30** hold the record for the lowest chemical shift, other compounds, such as **31** allow for a more comprehensive investigation of aromatic ring currents. Although Vinod and Hart synthesized **31** with the hope of making a molecular host, the molecule provides insight into aromatic ring currents.[62,63] The proton shown in Figure 1.4 is in the shielding zone of three benzene rings (red) and the deshielding zone of one benzene ring (blue).

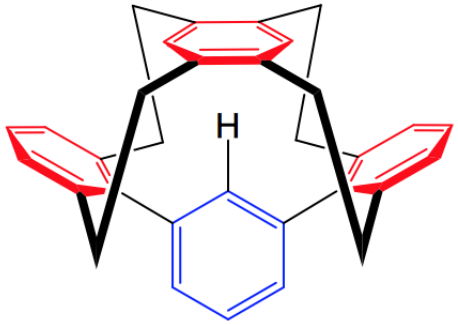

31

δ = 3.67 ppm

Figure 1.4. The proton in **31** is in the shielding zone of three benzene rings (red) and one benzene ring (blue).[62,63]

The magnetic fields from the induced ring currents result in a proton signal at 3.67 ppm, which has a significant upfield shift relative to benzene (∼7.3 ppm). The three deshielding rings, however, are not as close to the proton in question as in **29** and **30**. A compound such as **31** allows for the investigation of how both shielding and deshielding affect the chemical shift of the proton in question. Previously, Anson et al. systematically demonstrated how a substituent affects the shielding from a benzene ring.[64] This was accomplished by the synthesis of **32** with varying substituents at the ortho and para positions.

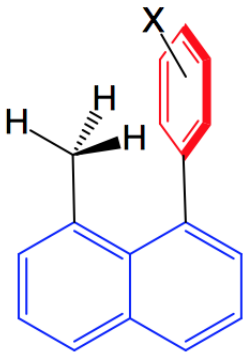

32

X = H, NH_2, OCH_3, CH_3, Cl, F, CN, CHO, and NO_2

Figure 1.5. Compound **32** was used to investigate the aromatic shielding effect of the substituted ring (red).[64]

1.3 Investigating the Aromatic Ring Current on Different Substituents

The literature, however, is particularly scant in demonstrating the shielding effects on different substituent groups. Most efforts thus far have focused solely on the methyl group. After a paper published in 2016 that synthesized **33** (Figure 1.6)[66] by a Suzuki coupling reaction, it was thought that **34**, a comparable compound with less strain, would be able to be synthesized (Figure 1.6).

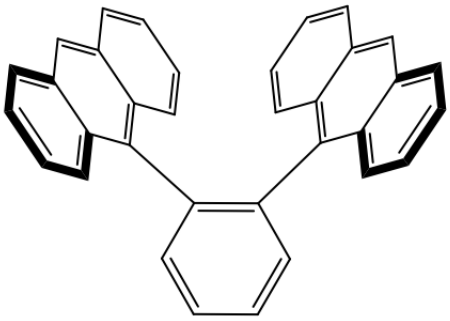

33

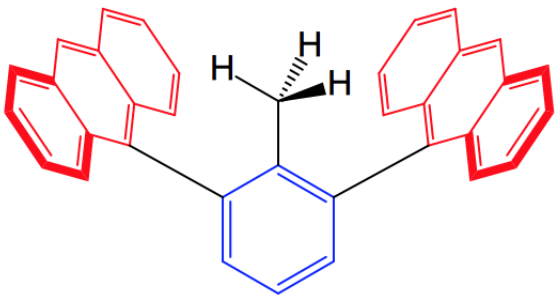

34

Scheme 1.6. Compound **34**, related to **33**[66], is expected to exhibit a downfield shift relative to toluene. Red rings are shielding and blue rings are deshielding.[66]

Surely, the anthracene substituents would shield the methyl protons, resulting in a upfield shifted signal. The question then becomes how would these polycyclic aromatic hydrocarbon substituents shield the methyl protons in comparison to phenyl groups both mono- and disubstituted. Proton NMR signals are reported for a variety of shielded toluenes shown in Figure 1.7.[67–69]

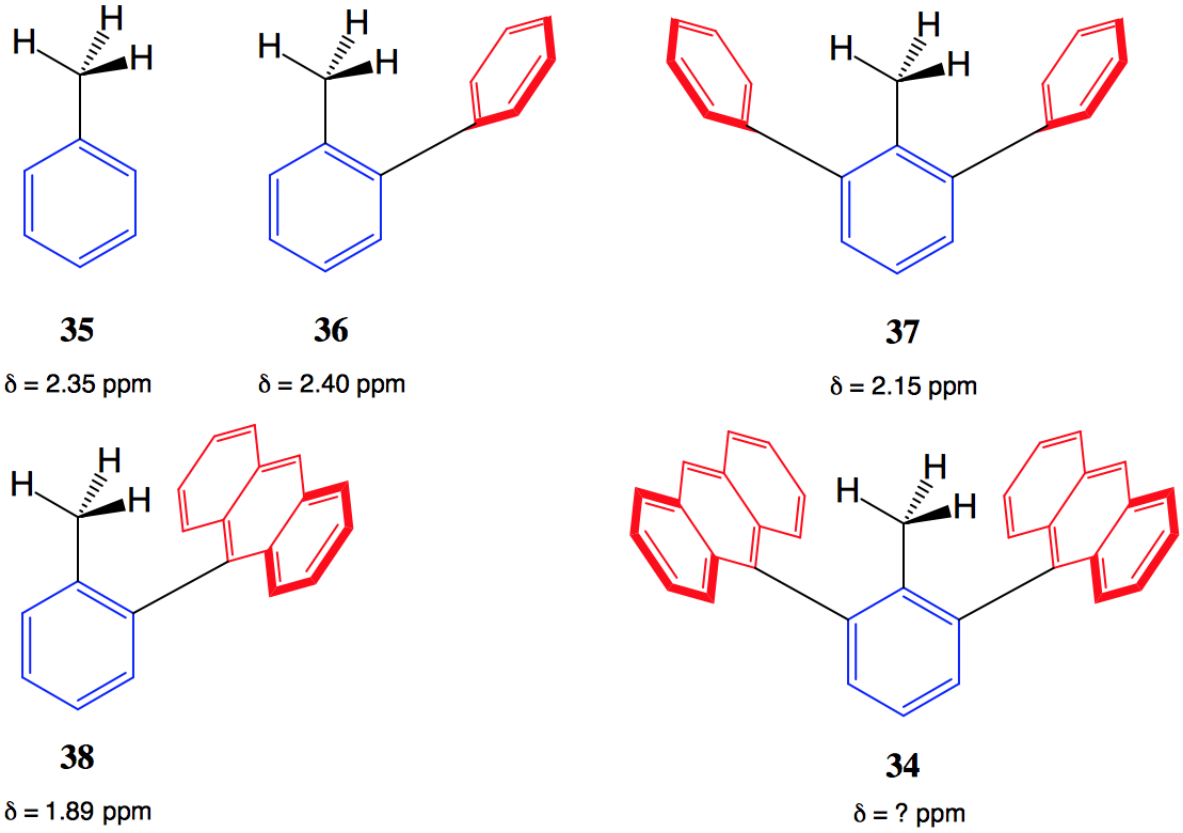

Figure 1.7. Compounds **34-38** exhibiting different proton signals due to aromatic substituents. Red rings are shielding and blue rings are deshielding.[67–69]

The 1,3-bisanthracenetoluene **34** has not yet been reported in the literature. Completing this series will give additional information about the shielding effects of anthracene substituents. However, that is not the main attractiveness of **34**. For a long time now, it has been known that a benzyne addition to anthracene via a Diels-Alder mechanism produces the major product (triptycene) with the addition to the center ring (Scheme 1.8).[70]

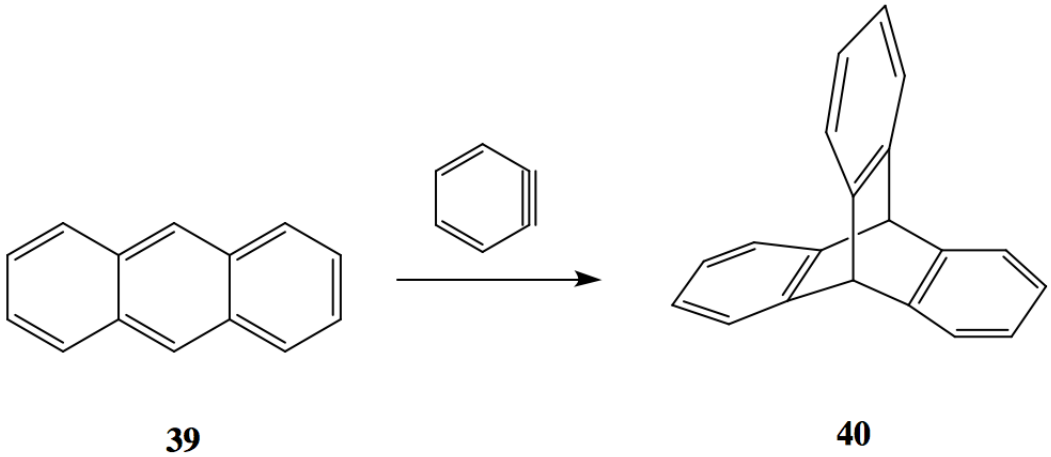

39 **40**

Figure 1.8. Synthesis of triptycene **40**.[70]

The addition of two equivalents of benzyne to **34** could potentially create two triptycene substituents surrounding the methyl group (Figure 1.9 R = CH_3). This bistriptycenyltoluene **41** would form a sort of flower around the methyl group. Four benzene rings will be closer to the methyl group and create a highly shielded region where the methyl group is located. However, now each triptycene will contain one benzene ring that contributes to the deshielding of the methyl group.

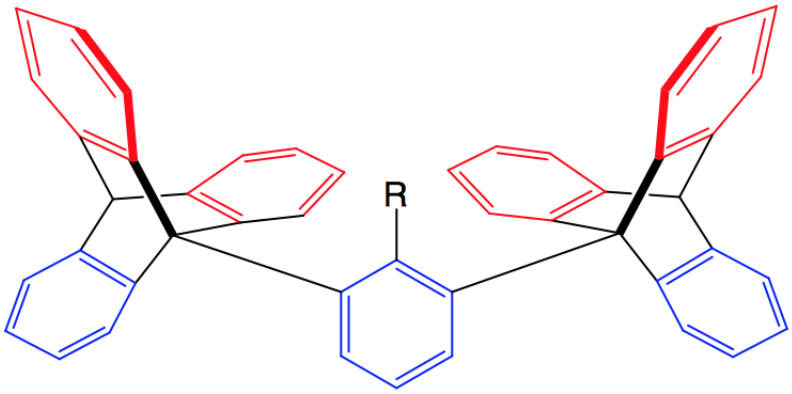

41

Figure 1.9. Bistriptycenyltoluene (R = CH_3).[67–69]

The synthesis of **41** is, barring sterically bulky R groups, rather independent of the

R group. This will allow for a series of different R groups to be placed in the middle of this triptycenyl flower: R = H, CH_3, BH_2, NH_2, ^{t}Bu, ^{i}Pr, OCH_3, OH, SH, PH_2, and a systematic approach of evaluating the shielding and deshielding effects of aromatic ring currents on protons covalently bonded to different elements. Particularly for alkyl protons, the progression from methyl to *tert*-butyl will allow the determination of the effect due to distance from the aromatic rings.

1.4 Molecular Gears

For many years, chemists have been fascinated by the possibility of creating molecular machines, and even individual molecules that acts in a mechanical fashion. The most popular method of creating these mechanical machines uses triptycene substituents as gears. There are two main types of gear systems: bevel gears (two gears at an angle, **42**[71] and **43**[72]) and spur gears (two gears in plane **44**[73]). Figure 1.10 shows only a select few of the triptycenyl molecular gears that have been made.[71–73]

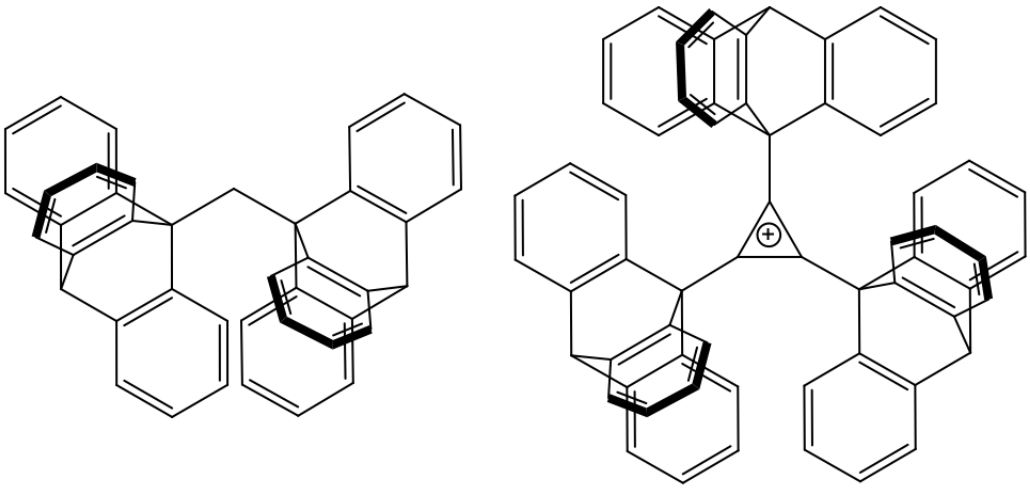

42 **43**

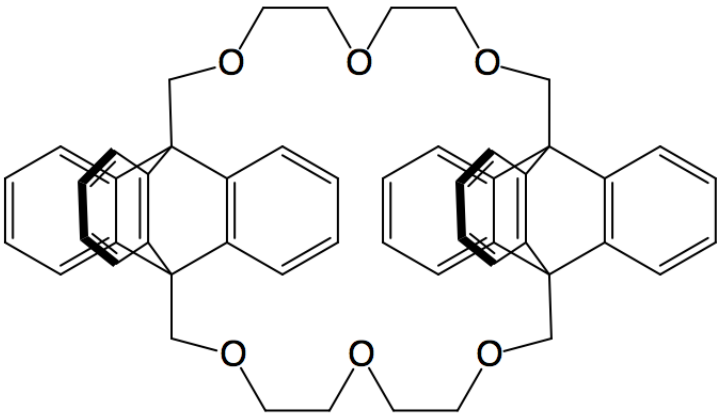

44

Figure 1.10. Selected examples of triptycenyl molecular gears.[71–73]

The bistriptycenyltoluene **41** has the potential to exhibit molecular gear motion, particularly in the case where R = *tert*-butyl. Furthermore, if **41** is synthesized, it could lead to a simple and straightforward synthesis for molecular gears.

Results and Discussion

2.1 Synthesis of a Triptycenyl Flower

Using adapted procedures[66,74,75] for a Suzuki coupling between an aryl halide and anthracene boronic acid, the bisanthracenyltoluene **34** was synthesized (Scheme 2.1). Using a commercially available 1,3-dibromotoluene and anthracen-9-ylboronic acid, the Suzuki coupling introduced two C-C bonds at the 1 and 3 positions.

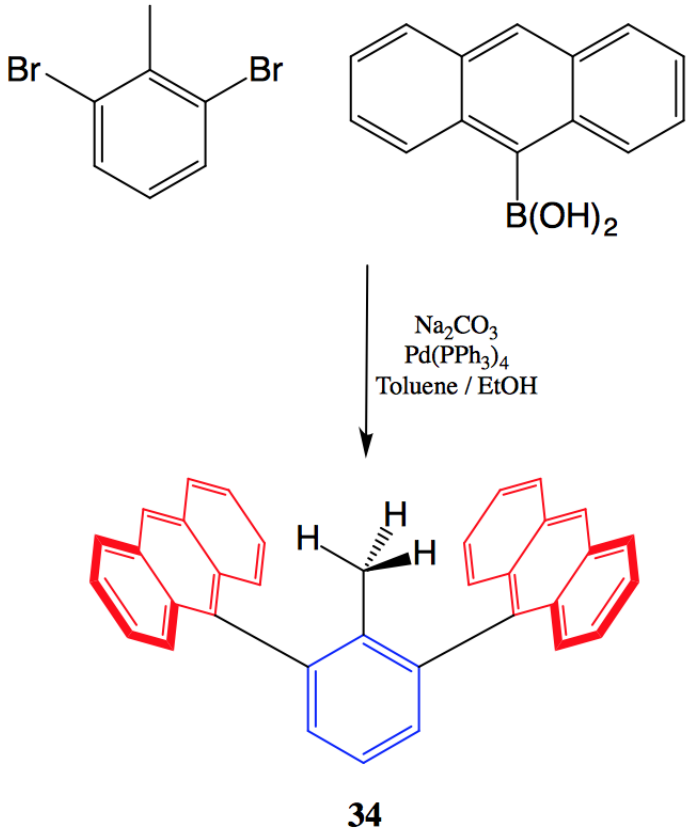

Scheme 2.1. Synthesis of bisanthracenyltoluene **34**.

The reaction proceeded as expected with a 12.5% yield. The crystal structure of **34** has not been reported until now and is depicted on the next page (Figure 2.2).

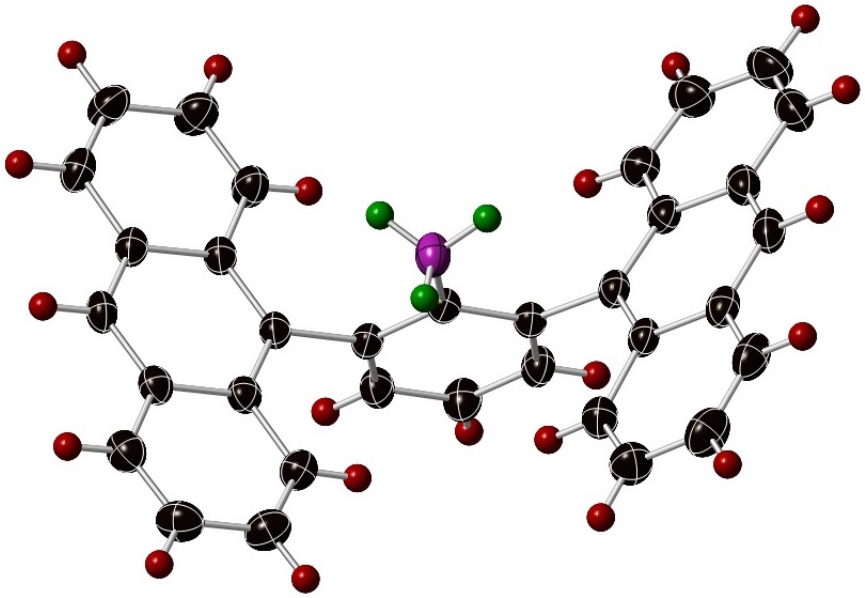

Figure 2.2. X-ray crystal structure of bisanthracenyltoluene **34**.

There are a variety of reagents used to add benzyne to anthracene rings. The benzene ring substituted with trimethylsilane and a triflate group across the 1 and 2 positions was used as a benzyne precursor because of its ease of use and reported high yields. The adapted procedure from Yoon et. al uses cesium fluoride, which upon dissociation the fluoride ion can attack the trimethylsilyl group for a β-elimination reaction with the triflate as an effective leaving group.[76] The benzyne is then generated in situ and can add to the anthracene substituents in a Diels-Alder fashion (Scheme 2.3).

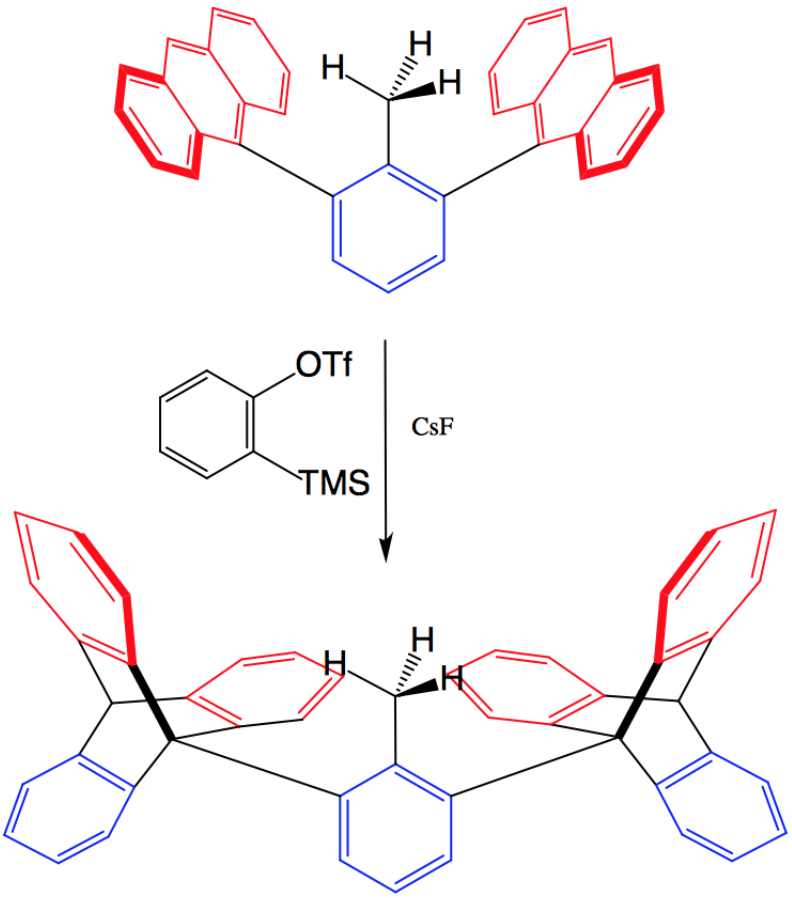

Scheme 2.3. Synthesis of bistriptycenyltoluene **41**.

The reaction proceeded with a 42% yield. Unfortunately, for both steps, the products were too large to monitor by GC/MS, and thus they were monitored by TLC. Also due to the low solubility of the products, a high ratio of dichloromethane to hexanes was used in the solvent system. Unfortunately, the crystals that have been grown thus far are very thin needles, and a crystal structure has not yet been obtained. However, an exact mass was obtained using high resolution mass spectrometry (calculated mass: 597.2582, found 597.2579).

2.2 ^{1}H NMR Spectroscopy

The ^{1}H NMR spectra were acquired in deuterated chloroform at 500 MHz. The methyl signal from toluene was found to be at 2.35 ppm from a residual signal in a ^{1}H NMR spectrum, and was used as a reference. The series of phenyl and anthracenyl substituted toluene derivatives are reproduced below for convenience (Figure 2.4).

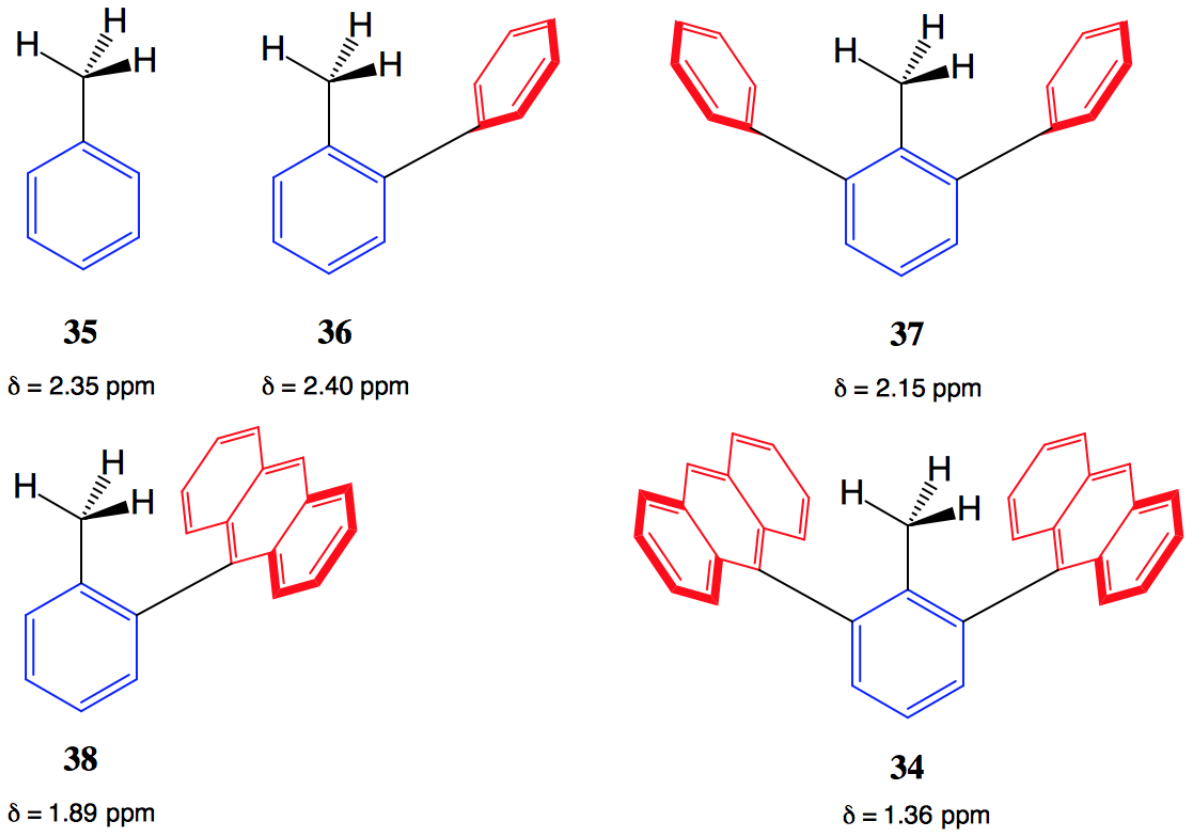

Figure 2.4. Series of phenyl and anthracenyl substituted toluene derivatives.[67–69]

Adding a single phenyl substituent barely changed the proton signal (2.40 ppm).[67] The almost negligible change can be attributed to the fact that the phenyl can almost freely rotate, resulting in the shielding and deshielding of the methyl group nearly canceling each other. This is significantly different than in the case of the naphthalene based **32** where introducing a phenyl group changed the methyl signal by -0.676 ppm.[64] The wider angle available in **36** must allow for a freer rotation. Adding two phenyl substituents surrounding

toluene (**37**) resulted in a slightly more downfield shift (2.25 ppm), but still not significantly shielded.[68] The monoanthracenyl toluene (**38**) proton NMR signal appears at 1.89 ppm, partly due to the wider induced magnetic field and and also partly due to the restricted rotational motion of anthracene. The new bisanthracenyl toluene (**34**) was found to have a proton NMR shift at 1.36 ppm. The larger difference between **34** and **38** can be explained by the same reason that **38** has a more upfield shift than **36** and **37** - that is, the restricted rotation of the anthracene substituents forces them to be close to perpendicular to the benzene ring scaffold.

The methyl proton signal in bistriptycenyltoluene **41** actually shifted slightly downfield (1.38 ppm) relative to **34**. This interesting result shows that the effect of decreasing the distance between two rings per substituent is negated by changing one of the rings on each substituent to be deshielding the methyl group. Furthermore, the triptycenyl proton peaks in the ^{1}H NMR spectrum are broad, which indicates that the triptycene substitutents are spinning, but not quickly.

2.3 Computational Results

In the last decade, Rablen and Bally published quantum mechanical procedures to calculate proton signals accurately in organic molecules.[77,78] In particular, these procedures do a good job of account for the shielding and deshielding effects of aromatic rings by utilizing specific internal options detailed in the experimental section. First, **34** and **41** geometries were optimized using the B3LYP method with a 6-31G(d) basis set. Then the chemical shift of the methyl group was calculated from the optimized structures using GIAO/WP04/cc-pVDZ in chloroform. The proton shifts were averaged and scaled according to Rablen's and Bally's results.[77,78] In the case of the bisanthracenyltoluene **34**, the calculated results were only $\sim$0.01 ppm different. Experimentally, the methyl group of **34** was found to be at 1.36 ppm and the calculated results suggested the shift to be at 1.3528 ppm. However, in the case of the bistriptycenyltoluene **41**, the calculated value (1.473 ppm) is significantly different than

the experimental value (1.38 ppm) by nearly ∼0.1 ppm.

2.4 Concluding Remarks and Future Work

We have successfully synthesized and characterized the triptycenyl flower **41** and demonstrated the methyl substituent is shielded by the triptycenyl benzene rings. The first order of business will be to obtain a crystal structure of **41**. The calculation procedure should be adapted for a better fit to the experimental results. The triptycenyl flowers should be synthesized with a variety of groups including R = H, CH_3, BH_2, NH_2, ^{t}Bu, ^{i}Pr, OCH_3, OH, SH, PH_2.

The gearing motion of **41** should also be studied using variable temperature (VT) NMR studies. Furthermore, this synthetic route can be applied to a variety of substrates to make a variety of molecular gears to be studied. In a first attempt to apply this synthetic route to a related system, we arrived at a naphthobarrelene product **46** (Scheme 2.5). A crystal structure of **46** was obtained, but with a refinement value of 12.4%.

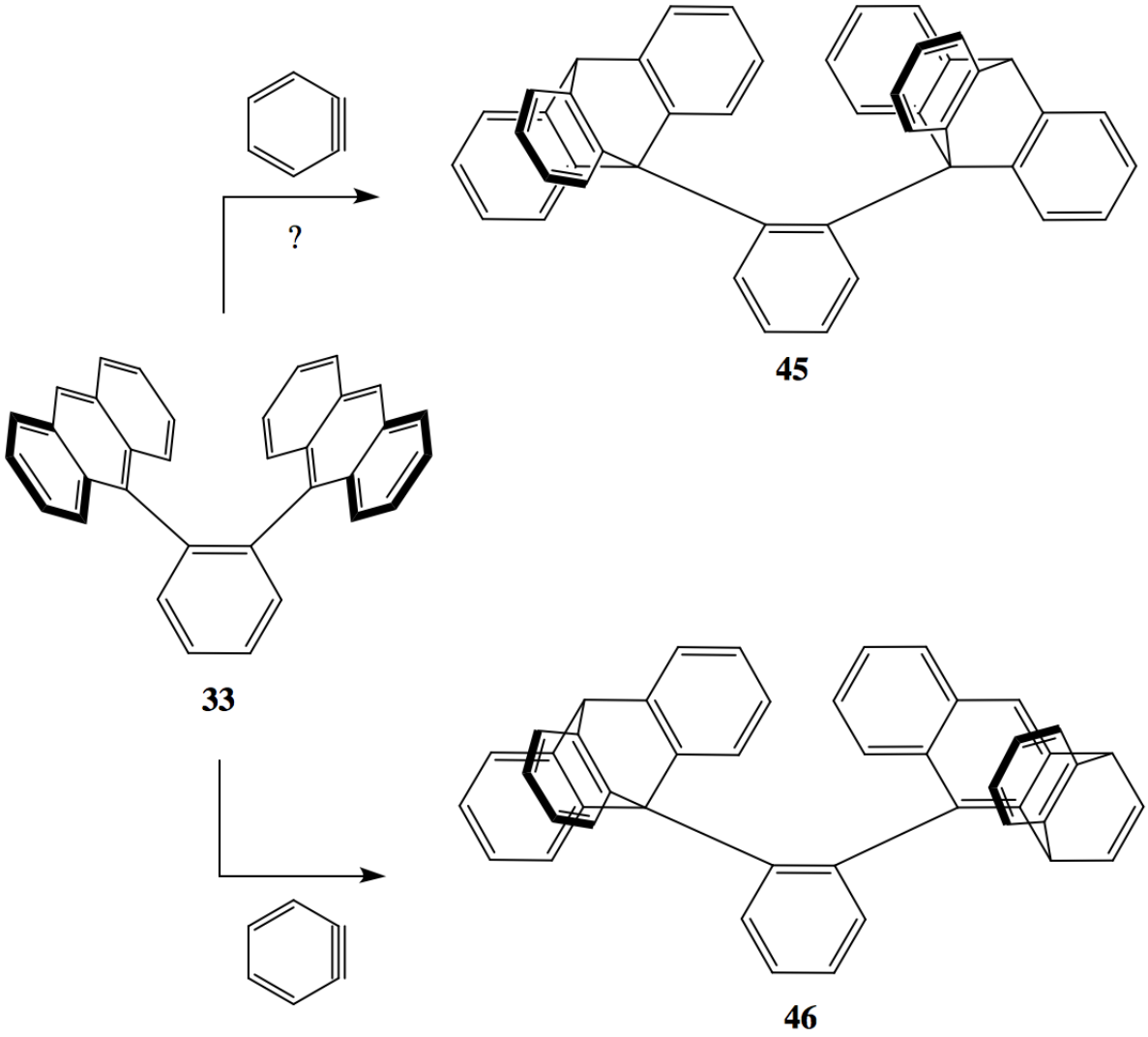

Scheme 2.5. First synthetic attempt at making a ortho-bistriptycenylbenzene molecular gear **45**.

Product **46** is apparent from the alkene proton signals. However, there appears to be multiple proton signals attributed to the bridgehead position of the triptycene, which suggests that there is a mixture of **45** and **46**. Further work is needed to determine if **45** is indeed formed. Additionally, density functional calculations showed that the naphthobarrelene product was more stable do to the steric strain induced by the bistriptycene product, but not enough to suggest that **45** is not formed at all.

Experimental Procedures

3.1 General Remarks

All solvents and reagents were used as obtained from commercial sources. Flash chromatography was performed on pre-packed silica gel columns (70-230 mesh). NMR spectra were recorded at 500 MHz for ^{1}H and 125 MHz for ^{13}C in $CDCl_3$. The shifts are reported in δ ppm and referenced to either tetramethylsilane (TMS) or the residual proton signal from the solvent. Exact masses were found using time of flight mass spectrometry (TOF-MS) equipped with a direct analysis in real time (DART) ion source in positive ionization mode (DART-TOF-MS).

3.2 9,9'-(2-methyl-1,3-phenylene)dianthracene (34)

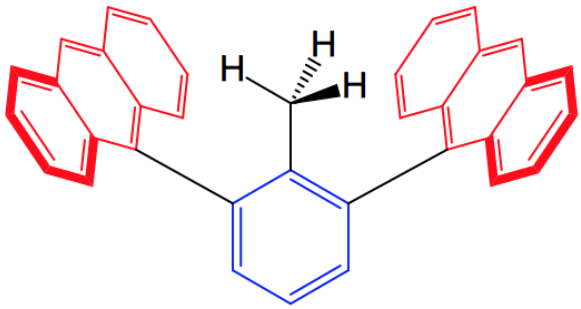

To a stirring solution of anthracen-9-ylboronic acid (1.8 g, 8.0 mmol) dissolved in toluene (60 mL) and ethanol (30 mL) in a pressure flask, was added 1,3-dibromo-2-methylbenzene (276 μL, 500 mg, 2.0 mmol) and 2M aqueous sodium carbonate (40 mL, 80 mmol). Argon was vigorously bubbled through the stirring mixture for 15 minutes before adding the tetrakis(triphenylphosphine)palladium(0) catalyst (361 mg, 0.31 mmol). After a few minutes of stirring, the reaction was heated to 110 °C for 24 h before quenching the reaction with water (20 mL). The reaction was extracted with dichloromethane (2 x 40 mL) and washed with water (40 mL) and brine (40 mL). The crude was purified by flash chromatography on silica gel (hexanes $\longrightarrow$ 20% dichloromethane $\longrightarrow$ 50% dichloromethane) to obtain **34** as a yellow-white solid (110 mg, 0.25 mmol, 25%) after recrystallization from toluene. ^{1}H NMR: δ 8.51 (s, 2H), 8.07 (d, J = 8.2 Hz, 4H), 7.77 (d, J = 8.3 Hz, 4H), 7.58

(t, J = 7.6 Hz, 1H), 7.53-7.42 (m, 12H); ^{13}C NMR: δ 138.9, 136.5, 131.5, 131.0, 130.1, 128.6, 128.2, 126.5, 126.4, 125.8, 125.7, 125.1, 16.9.

3.3 9,9'-(2-methyl-1,3-phenylene)bis(9,10-dihydro-9,10-[1,2]benzenoanthracene) (41)

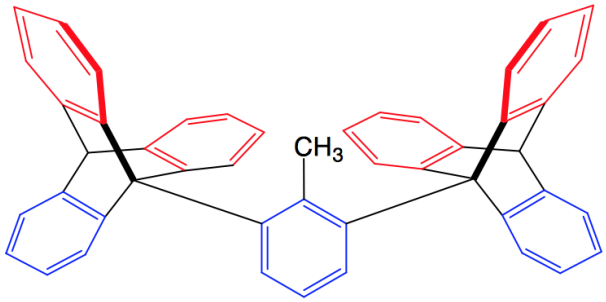

To a stirring solution of **34** (44 mg, 0.1 mmol) in toluene (1 mL) and acetonitrile (1 mL) in a microwave vial, was added cesium fluoride (130 mg, 0.86 mmol). The microwave vial was sealed and heated to 85 C for 10 min before adding 2-(trimethylsilyl)phenyl trifluoromethanesulfonate (130 μL, 0.3 mmol) to the milky white solution and allowing the reaction to stir for 24 h. After 24 h, additional 2-(trimethylsilyl)phenyl trifluoromethanesulfonate (130 μL, 0.3 mmol) was added. Within 3 h after the second addition, the solution cleared to a yellow color. Following 24 h after the second addition, the reaction was cooled, poured over silica gel, and dried by reduced pressure. The crude mixture was purified by flash chromatography on silica gel (hexanes $\longrightarrow$ 20% dichloromethane $\longrightarrow$ 50% dichloromethane) to obtain **34** (25 mg, 0.042 mmol, 42%) as a white needle-like solid. ^{1}H NMR: δ 8.57 (d, J = 7.9 Hz, 2H), 8.05 (s, 2H), 7.79-7.66 (m, 2H), 7.49 (t, J = 7.7 Hz 1H), 7.43 (s, 2H), 7.43-7.32 (m, 3H), 7.18-7.11 (m, 4H), 7.06-6.88 (m, 16H), 5.39 (s, 2H), 1.38 (s, 3H); HRMS (ESI-TOF) calc'd for $C_{47}H_{33}^{+}$ 597.2582, found 597.2579.

3.4 Computational Methods

All calculations were performed using Gaussin 09[41]. The geometries of **34** and **41** were optimized at B3LYP/6-31G(d) followed by vibrational frequency calculations at the same level of theory. The WP04[79] functional was invoked in Gaussian by entering the BLYP keyword and adding the internal options: iop (3/76=1000001189,3/77=0961409999,3/78=0000109999).[64,77]

The GIAO/WP04/cc-pVDZ chemical shift was scaled by the following: δ = (31.844 - calculated isotropic magnetic shielding)/1.0205.[64,78]

3.5 X-ray Structure Determination

Single crystals of **34** were prepared by the slow evaporation of hexanes/dichloromethane or by recrystallization from toluene. X-ray data were acquired at 173 K using a Bruker Smart Apex CCD diffractometer with graphite monochromated Mo Kα radiation (λ = 0.71073 Å). The data was processed with he Bruker Apex3 suite of programs[42] and the frames were integrated using the Bruker SAINT software[43] with a narrow-frame algorithm. The data was corrected for absorption effects using the multi-scan method SADABS[44]. Structure solution and refinement by least-squares on F^2 was done by using the Bruker SHELXTL software package[45]. Nonhydrogen atoms were refined anisotropically and hydrogen atoms were calculated using a riding model. The .cif files were validated with the checkCIF/Platon facility using enCIFer[46].

References

[1] Kirmse, W. (1964). *Carbene Chemistry*. New York: Academic Press.

[2] H. Staudinger and O. Kupfer, *Berichte der deutschen chmischen Gesellschaft*, **1912**, *45*, 501.

[3] W. Doering, A. K. Hoffman, *J. Am. Chem. Soc.*, **1954**, *76*, 23.

[4] E. Whittle, D. A. Dows, G. Pimentel, *J. Chem. Phys.*, **1943**, *21*, 11.

[5] E. O. Fischer, A. Maasböl, *Angewandte Chemie*, **1964**, *3*, 8.

[6] A. Igau, H. Grutzmacher, A. Baceiredo, G. Bertrand, *J. Am. Chem. Soc.*, **1988**, *110*, 6463.

[7] A. J. Arduengo, R. L Harlow and M. Kline, *J. Am. Chem. Soc.*, **1991**, *113*, 1.

[8] Bertrand, G. (2005). *Carbene Chemistry: From Fleeting Intermediates to Powerful Reagents*. New York: FontisMedia and Markel Dekker, Inc.

[9] R. Grainger and K. Munro, *Tetrahedron*, **2015**, *71*, 7795.

[10] H. Huang and M. Platz, *J. Am. Chem. Soc.*, **1988**, *120*, 5990.

[11] A. N. Van Nhien, E. Soriano, J. Marco-Contelles and D. Postel, *Carbohydr. Res.*, **2009**, *344*, 1605.

[12] J. Tseng, M.L McKee and P.B. Shevlin, *J. Am. Chem. Soc.*, **1987**, *109*, 5474.

[13] D. B. Richardson, L. R. Durrett, J. M. Martin, W. E. Putnam, S. C. Slaymaker and I. Dvoretzky, *J. Am. Chem. Soc.*, **1965**, *87*, 599.

[14] J. E. Chateauneuf, R. P. Johnson and M. M. Kirchoff, *J. Am. Chem. Soc*, **1990**, *112*, 3217.

[15] K. A. Moore, J. S. Vidaurri-Martinez and D. M. Thamattoor, *J. Am. Chem. Soc.*, **2012**, *134*, 20037.

[16] R. Knorr, *Chem. Rev.*, **2004**, *104*, 3975.

[17] C. Wentrup, R. Blanch, H. Briehl and G. Gross, *J. Am. Chem. Soc.*, **1988**, *110*, 1874.

[18] K. L. Erickson and J. Wolinsky, *J. Am. Chem. Soc.*, **1965**, *87*, 1142.

[19] T. Harada, K. Iwazaki, T. Otani and A. Oku, *J. Org. Chem.*, **1998**, *63*, 9007.

[20] T. S. Hardikar, M. A. Warren and D. M. Thamattoor, *Tetrahedron Letters*, **2015**, *56*, 6751.

[21] Nate Flanders, Honors Chemistry Thesis 2015.

[22] Christine Wamsley, Honors Chemistry Thesis 2015.

[23] J. M. Medina, T. C. McMahon, G. Jiménez-Osés, K. N. Houk, and N. K. Garg, *J. Am. Chem. Soc.*, **2014**, *136*, 14706.

[24] D. H. R. Barton, G. Bashiardes and J. L. Fourrey, *Tetrahedron*, **1988**, *44*, 147.

[25] M. Al-Omari, K. Banert and M. Hagedorn, *Angew. Chem., Int. Ed.*, **2006**, *45*, 309.

[26] G. Wittig and U. Mayer, *Chemische Berichte*, **1962**, *96*, 342.

[27] G. Wittig and A. Krebs, *Chemische Berichte*, **1961**, *94*, 3260.

[28] C. M. Gampe and E. M. Carreira, *Chemistry: A European Journal*, **2012**, *18*, 15761.

[29] C. M. Gampe and E. M. Carreira, *Angewandte Minireviews*, **2012**, *51*, 3766.

[30] J. M. Nguyen and D. M. Thamattoor, *Synthesis*, **2007**, *14* 2093.

[31] K. S. Graves, D. M. Thamattoor, P. R. Rablen, *J. Org. Chem.*, **2011**, *76*, 1584.

[32] N. A. Petasis and E. I. Bzowei, *Tet. Lett.*, **1993**, *34*, 943.

[33] G. W. Griffin and K. A. Horn, *Org. Prep. and Proc. Int.*, **1985**, *17*, 187.

[34] T. Takeda, R. Sasaki and T. Fujiwara, *J. Org. Chem.*, **1998**, *63*, 7286.

[35] R. P. Johnson and K. J. Daoust, *J. Am. Chem. Soc.*, **1995** *117*, 362.

[36] S. Matsubara, M. Horiuchi, K. Takai and K. Utimoto, *Chem. Lett.*, **1995**, 259.

[37] Y. Tobe, N. Iwasa, R. Umeda, M. Sonoda, *Tetrahedron Letters*, **2001**, *42*, 5485.

[38] H. E. Baumgarten and Andris Staklis, *J. Am. Chem. Soc.*, **1965**, *87*, 1142.

[39] Y. L. Choi, C. Yu, B. T. Kim J. Heo, *J. Org. Chem.*, **2009**, *74*, 3948.

[40] Y. H. Kim, H. Lee, Y. J. Kim, B. T. Kim and J. Heo, *J. Org. Chem.*, **2007**, *73*, 495.

[41] M. J. Frisch, G. W. Trucks, H. B. Schlegel, G. E. Scuseria, M. A. Robb, J. R. Cheeseman, G. Scalmani, V. Barone, B. Mennucci, G. A. Petersson, H. Nakatsuji, M. Caricato, X. Li, H. P. Hratchian, A. F. Izmaylov, J. Bloino, G. Zheng, J. L. Sonnenberg, M. Hada, M. Ehara, K. Toyota, R. Fukuda, J. Hasegawa, M. Ishida, T. Nakajima, Y. Honda, O. Kitao, H. Nakai, T. Vreven, J. A. Montgomery, Jr., J. E. Peralta, F. Ogliaro, M. Bearpark, J. J. Heyd, E. Brothers, K. N. Kudin, V. N. Staroverov, R. Kobayashi, J. Normand, K. Raghavachari, A. Rendell, J. C. Burant, S. S. Iyengar, J. Tomasi, M. Cossi, N. Rega, J. M. Millam, M. Klene, J. E. Knox, J. B. Cross, V. Bakken, C. Adamo, J. Jaramillo, R. Gomperts, R. E. Stratmann, O. Yazyev, A. J. Austin, R. Cammi, C. Pomelli, J. W. Ochterski, R. L. Martin, K. Morokuma, V. G. Zakrzewski, G. A. Voth, P. Salvador, J. J. Dannenberg, S. Dapprich, A. D. Daniels, O. Farkas, J. B. Foresman, J. V. Ortiz, J. Cioslowski, and D. J. Fox, Gaussian 09, Revision A.02, Gaussian, Inc., Wallingford CT, 2009.

[42] APEX3; Bruker AXS Inc., Madison, Wisconsin, USA.

[43] SAINT; Bruker AXS Inc., Madison, Wisconsin, USA.

[44] SADABS; G. M. Sheldrick, University of Gottingen, Germany; Bruker AXS Inc., Madison, Wisconsin, USA.

[45] XPREP; XS; XL; G. M. Sheldrick, University of Gottingen, Germany; Bruker AXS Inc., Madison, Wisconsin, USA.

[46] F. H. Allen, O. Johnson, G. P. Shields, B. R. Smith and M. Towler, *J. Appl. Crystallogr.*, **2004**, *37*, 335.

[47] A. Kekulé, *Bull. Soc. Chim. Fr.*, **1865**, *3*, 98.

[48] Hückel, *Z. Phys.*, **1931**, *70*, 204.

[49] Hückel, *Z. Phys.*, **1931**, *72*, 310.

[50] Hückel, *Z. Phys.*, **1932**, *76*, 628.

[51] Hückel, *Z. Phys.*, **1933**, *83*, 632.

[52] J. A. N. F. Gomes and R. B. Mallion, *Chem. Rev.*, **2001**, *101*, 1349.

[53] C. S. Wannere and P. von Ragué Schleyer, *Org. Lett.*, **2003**, *5*, 605.

[54] L. Pauling, *J. Chem. Phys.*, **1936**, *4*, 673.

[55] K. Lonsdale, *Proc. R. Soc. A*, **1937**, *159*, 149.

[56] F. London, *J. Phys. Radium*, **1937**, *8*, 397.

[57] U. Fleischer, W. Kutzelnigg, P. Lazzeretti and V. Muehlenkamp, *J. Am. Chem. Soc.*, **1994**, *116*, 5298.

[58] R. G. Vigilone, R. Zanasi and P. Lazzeretti, *Org. Lett.*, **2004**, *6*, 2265.

[59] J. A. Pople, *J. Chem. Phys.*, **1956**, *24*, 1111.

[60] R. A. Pascal Jr., R. B. Grossman and D. Van Engen, *J. Am. Chem. Soc.*, **1987**, *109*, 6878.

[61] L. Lemmerz, M. Nieger and F. Vögtle, *J. Chem. Soc., Chem. Comm.*, **1993**, 1168.

[62] T. K. Vinod and H. Hart, *J. Am. Chem. Soc.*, **1988**, *110*, 6574.

[63] T. K. Vinod and H. Hart, *J. Org. Chem.*, **1990**, *55*, 881.

[64] C. W. Anson and D. M. Thamattoor, *J. Org. Chem.*, **2012**, *77*, 1693.

[65] R. A. Pascal Jr., *Eur. J. Org. Chem.*, **2004**, 3763.

[66] T. Nishiuchi, S. Uno, Y. Hirao and T. Kubo, *J. Org. Chem.*, **2016**, *81*, 2106.

[67] P. D. Stevens, J. Fan, H. M. R. Gardimalla, M. Yen and Y. Gao, *Org. Lett.*, **2005**, *7*, 2085.

[68] Q. Teng, S. Mo, J. Pan, N. Wu, H. Wang and Y. Pan, *Synthesis*, **2016**, *48*, 455.

[69] D. Schaarschmidt, M. Grumbt, A. Hildebrandt and H. Lang, *Eur. J. Org. Chem.*, **2014**, *30*, 6676.

[70] G. Wittig, *Org. Synth.*, **1959**, *39*, 75.

[71] F. Cozzi, A. Guenzi, C. A. Johnson and K. Mislow, *J. Am. Chem. Soc.*, **1981**, *103*, 957.

[72] J. M. Chance, J. H. Geiger and K. Mislow, *J. Am. Chem. Soc.*, **1989**, *111*, 2326.

[73] J. C. Bryan, R. A. Sachleben, A. A. Gakh and G. J. Bunick, *Chem. Cryst.*, **1999**, 513.

[74] H. Huang, Q. Fu, S. Zhuang, Y. Liu, L. Wang, J. Chen, D. Ma and C. Yang, *J. Phys. Chem.*, **2011**, *115*, 4872.

[75] K. Suzuki, A. Seno, H. Tanabe and K Ueno, *Synthetic Metals*, **2004**, *143*, 89.

[76] I. Yoon, S. Suh, S. A. Barros and D. M. Chenoweth, *Org. Lett.*, **2016**, *18*, 1096.

[77] R. Jain, T. Bally and P. R. Rablen, *J. Org. Chem.*, **2009**, *74*, 4017.

[78] T. Bally and P. R. Rablen, *J. Org. Chem.*, **2011**, *76*, 4818.

[79] K. W. Wiitala, T. R. Hoye and C. J. Cramer, *J. Chem. Theory Comput.*, **2006**, *2*, 1085.

Appendix A

Characterization Data

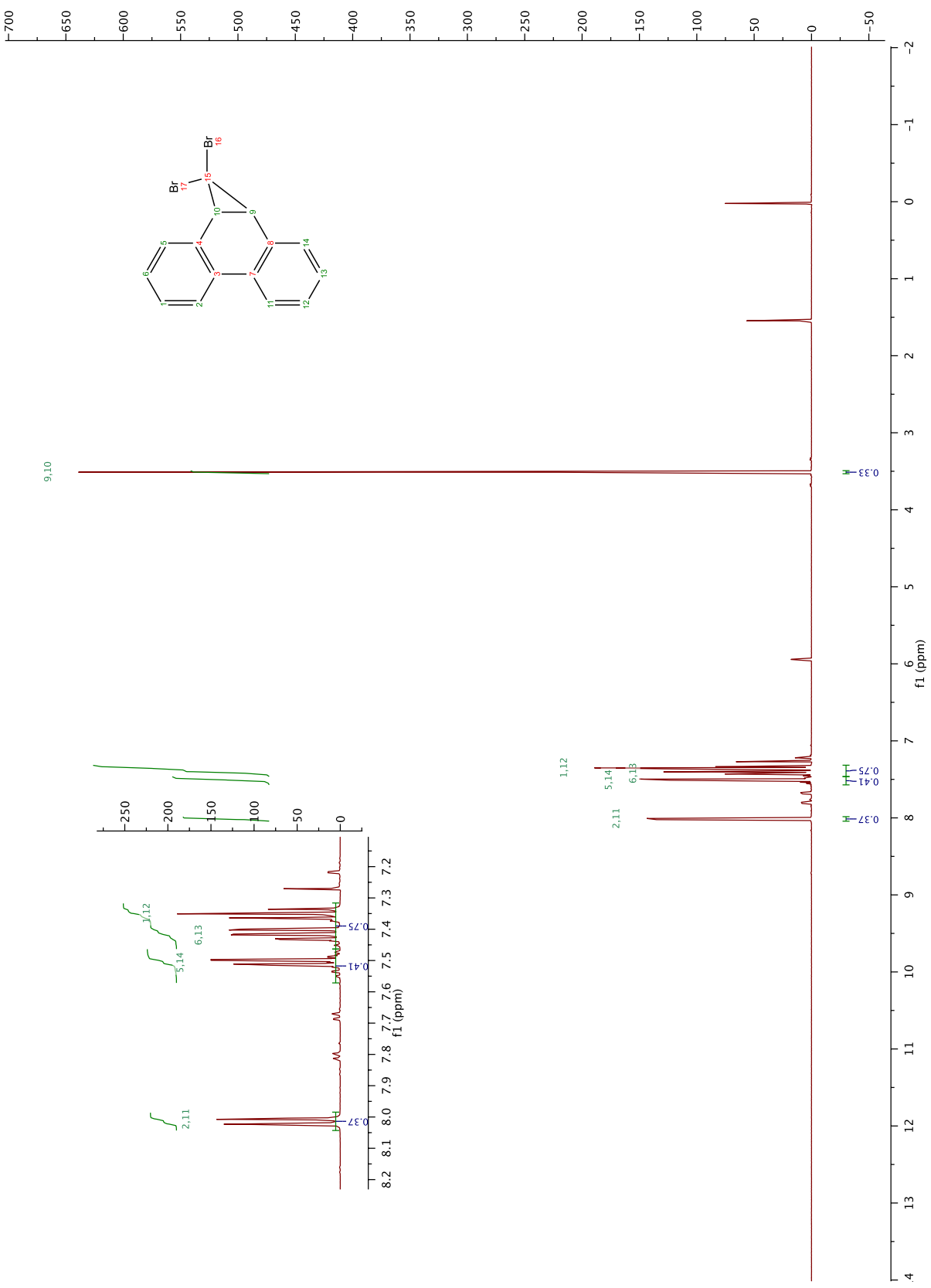

Figure A.1. ^{1}H NMR Spectrum of **19**.

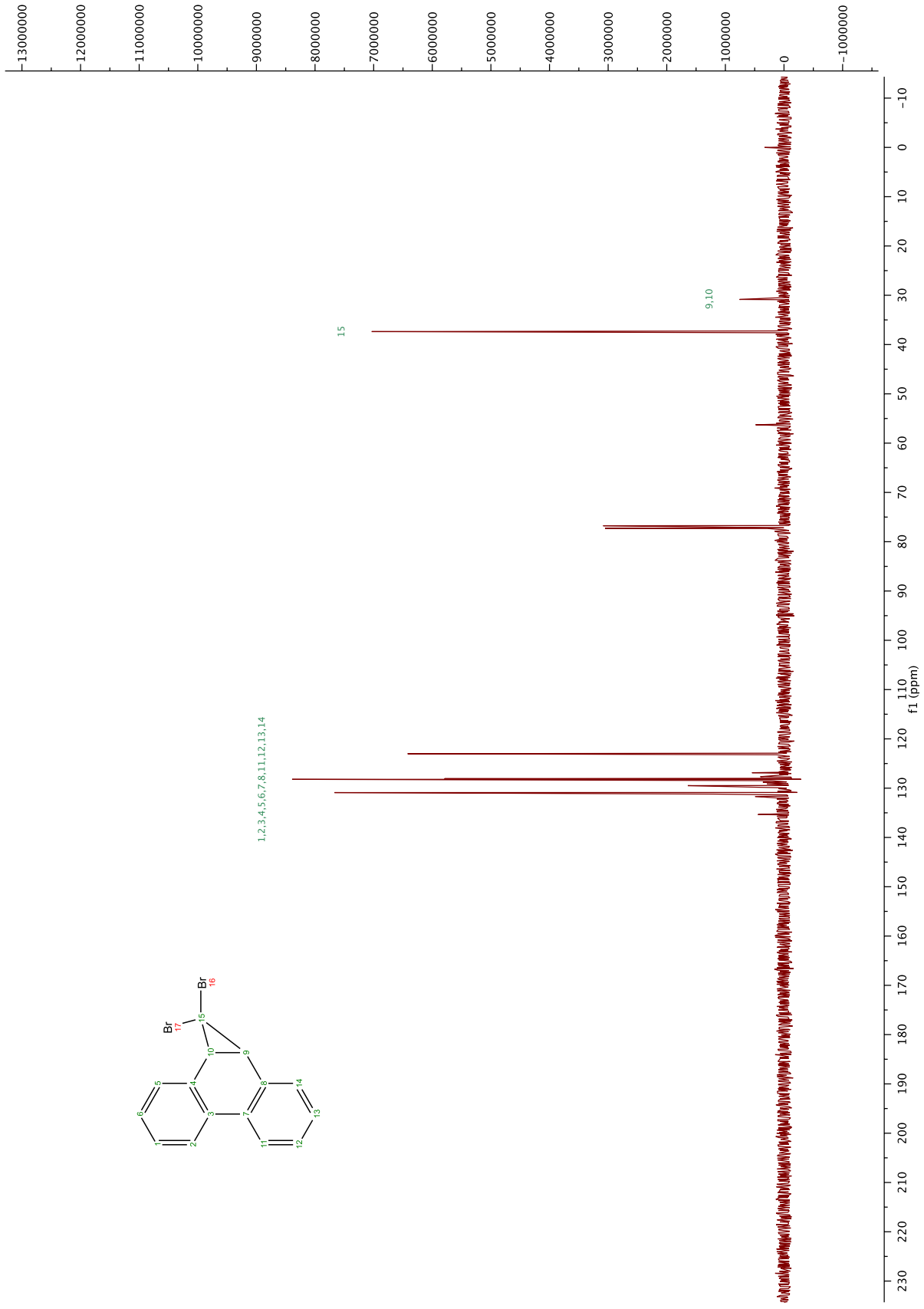

Figure A.2. ^{13}C NMR Spectrum of **19**.

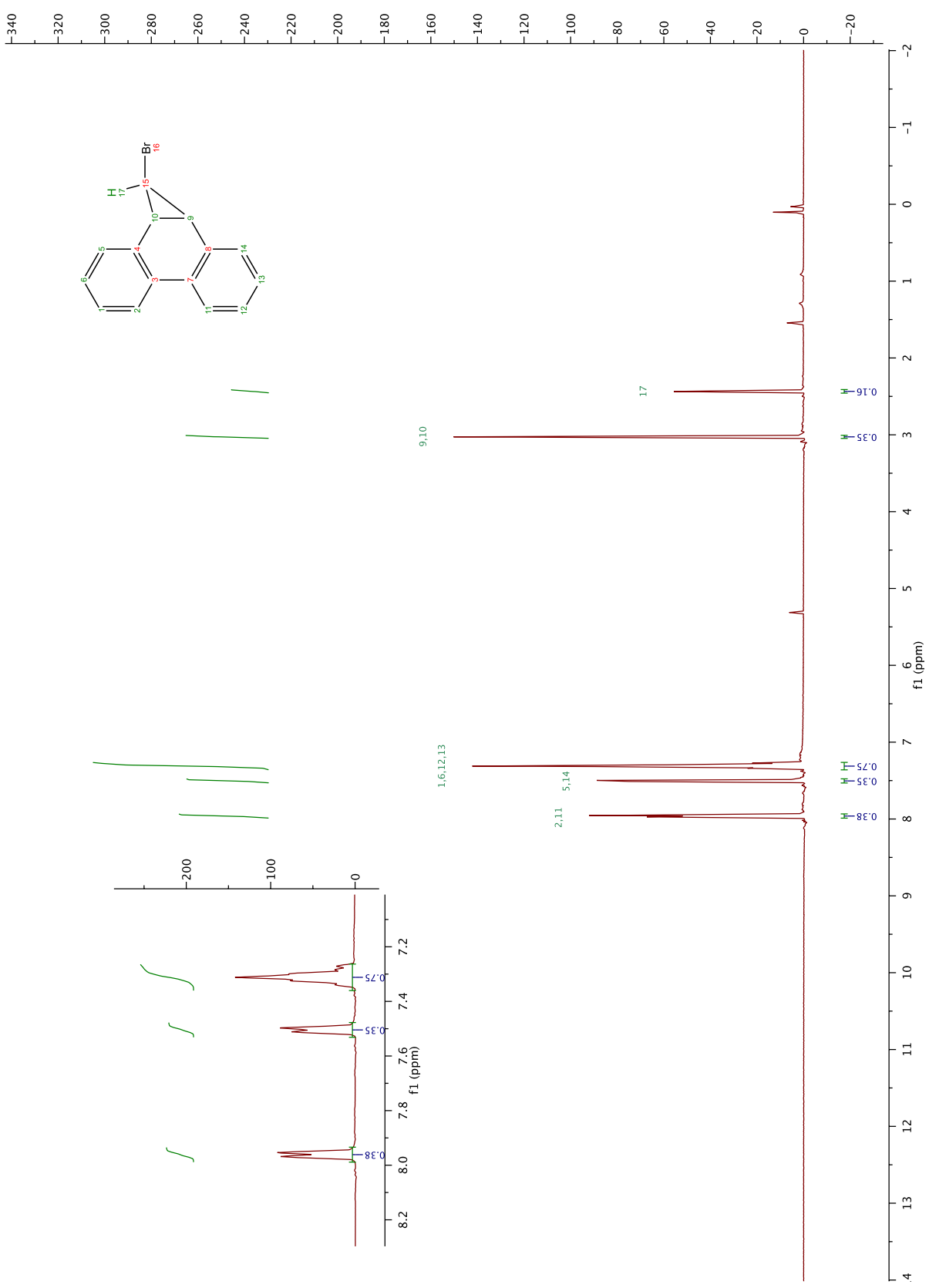

Figure A.3. ^{1}H NMR Spectrum of **22**.

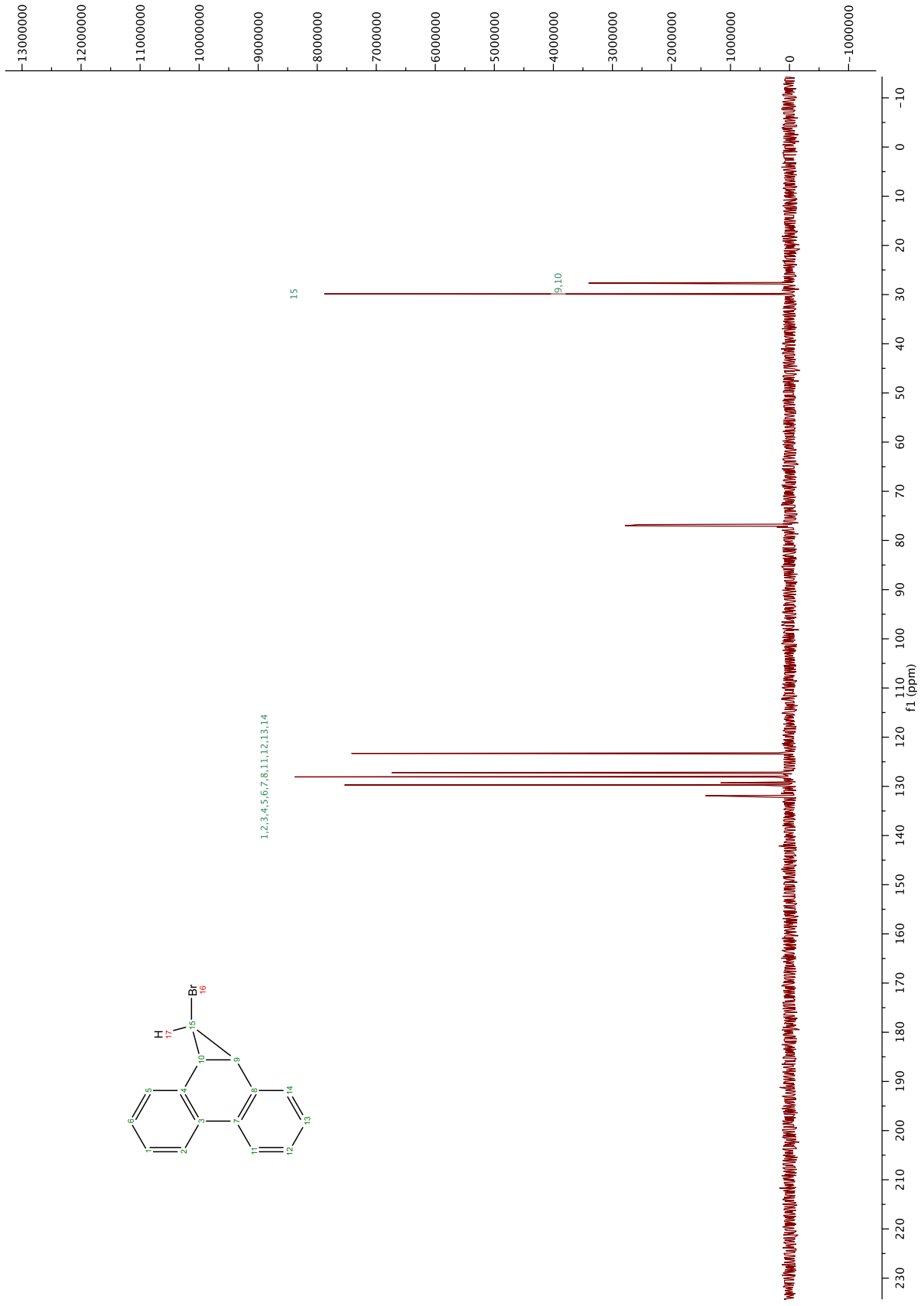

Figure A.4. ^{13}C NMR Spectrum of **22**.

```
File       :D:\1\data\Dan\DM092515002.D
Operator   : Dan
Acquired   : 25 Sep 2015  16:28     using AcqMethod DASLAB3MIN.M
Instrument :    GCMS1
Sample Name: monobromo
Misc Info  : from xy
Vial Number: 1
```

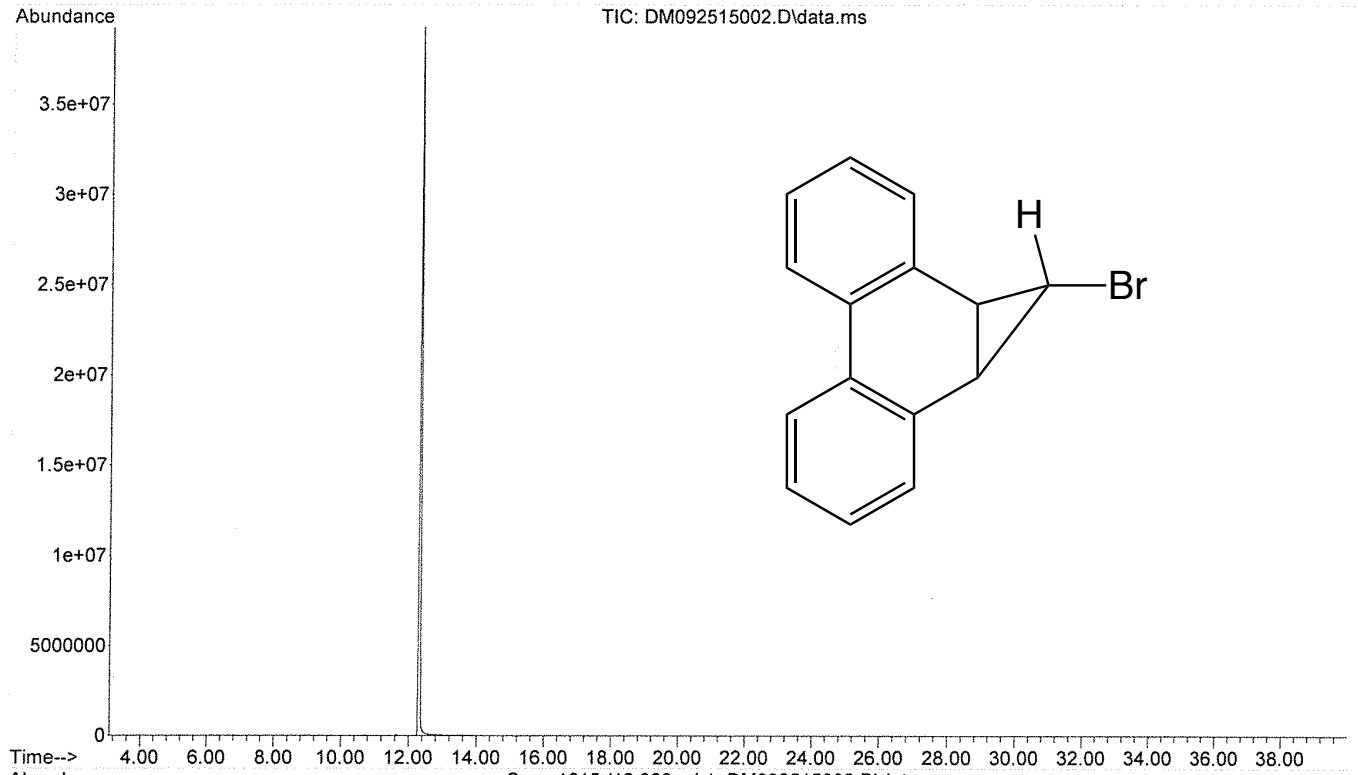

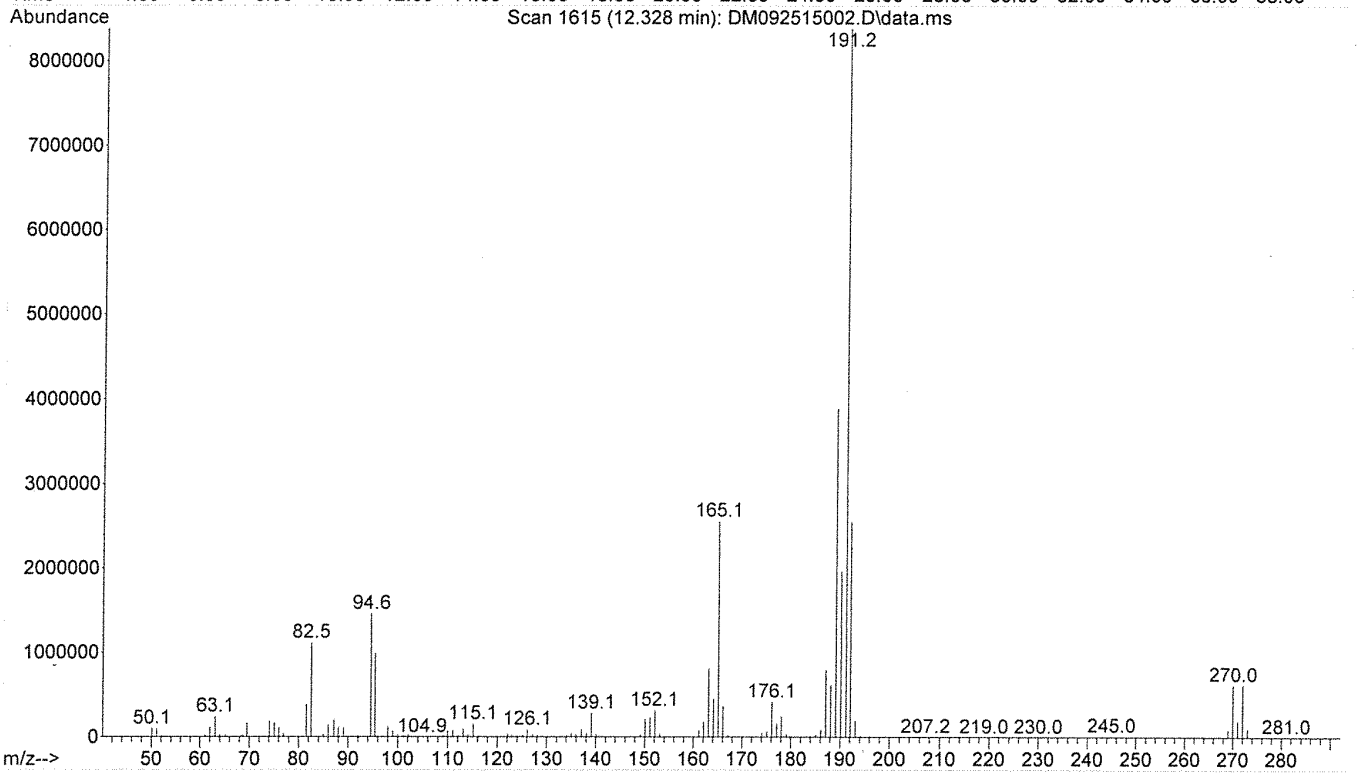

Figure A.5. GC/MS data for **22**.

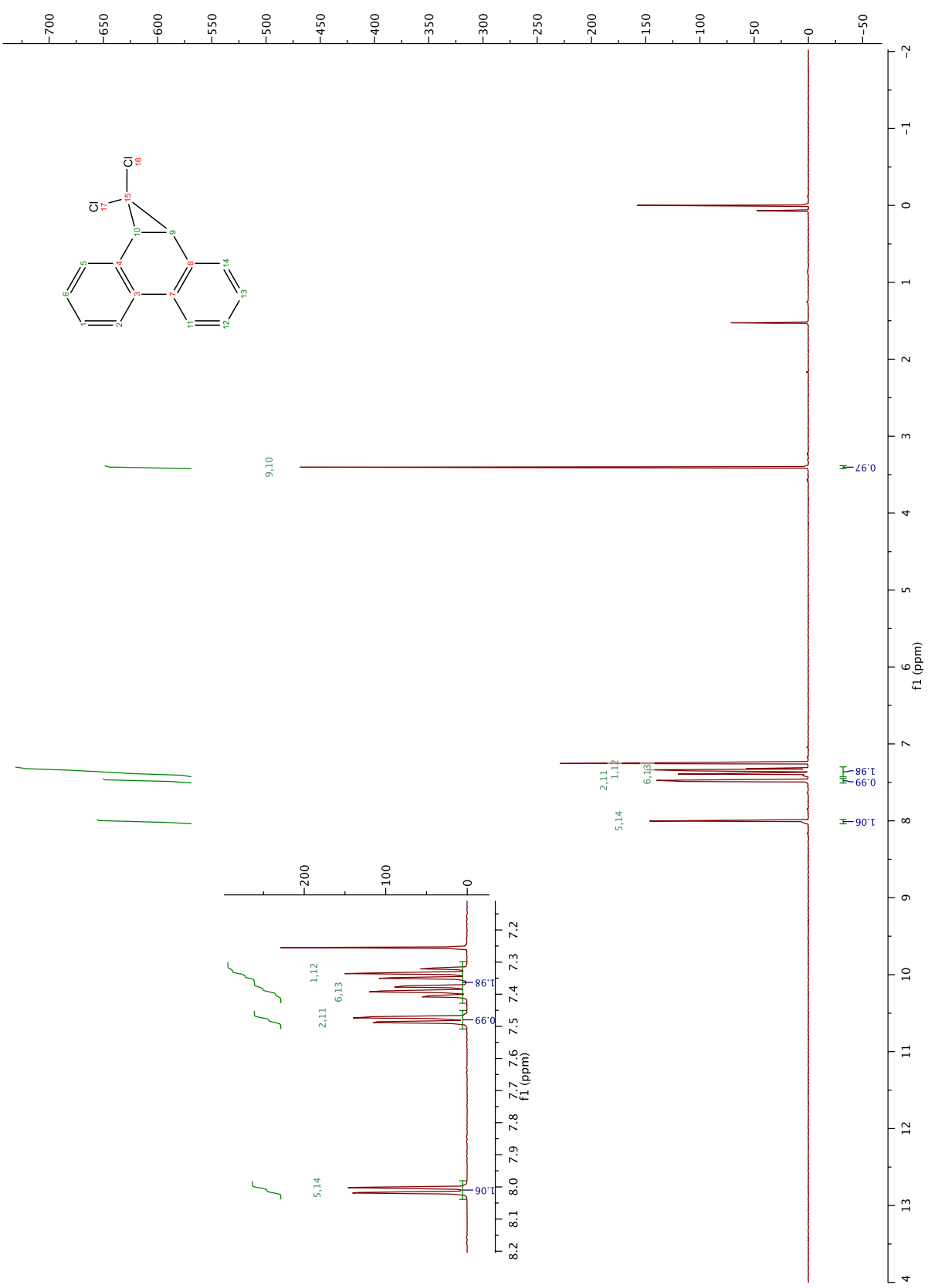

Figure A.6. ^{1}H NMR Spectrum of **25**.

```
File       :D:\1\data\Dan\DM011916001.D
Operator   : dan
Acquired   : 19 Jan 2016  10:28     using AcqMethod DASLAB3MIN.M
Instrument :    GCMS1
Sample Name: dichloro recryst
Misc Info  :
Vial Number: 1
```

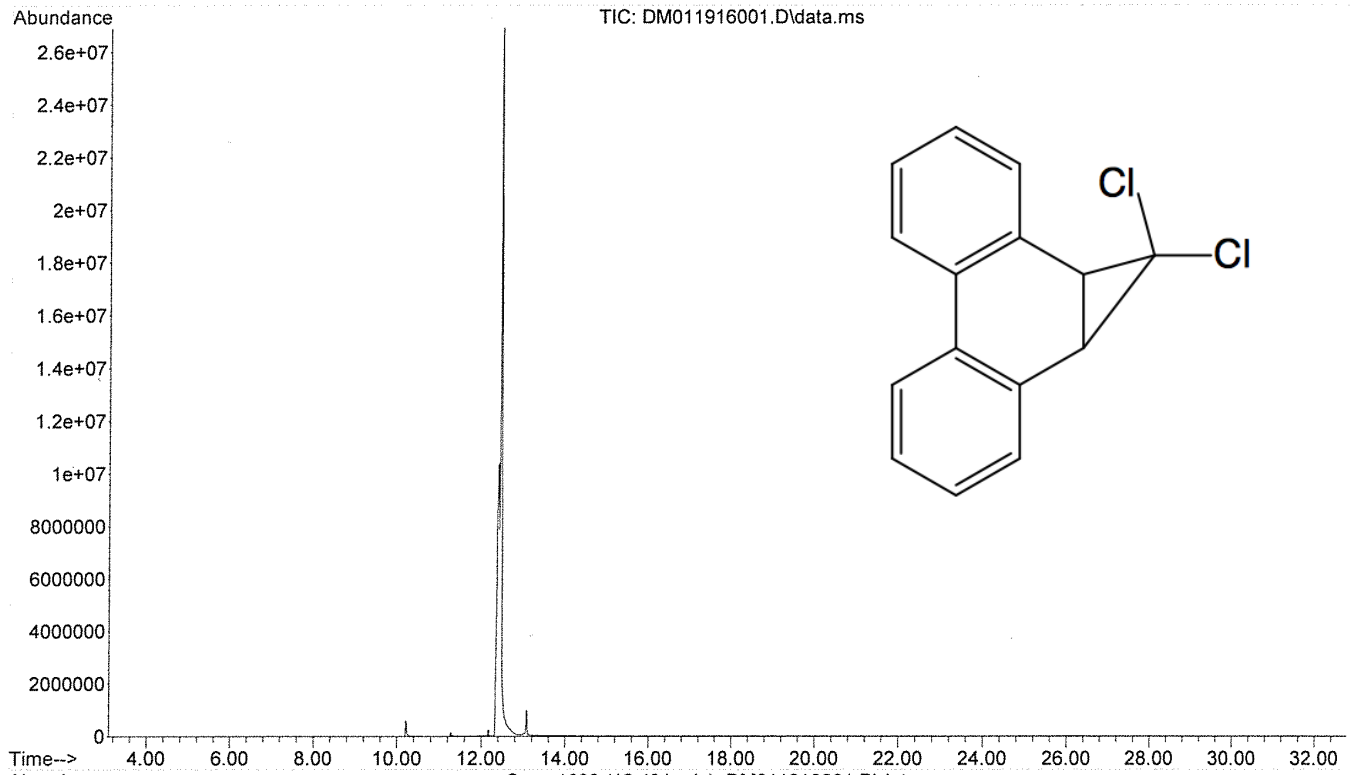

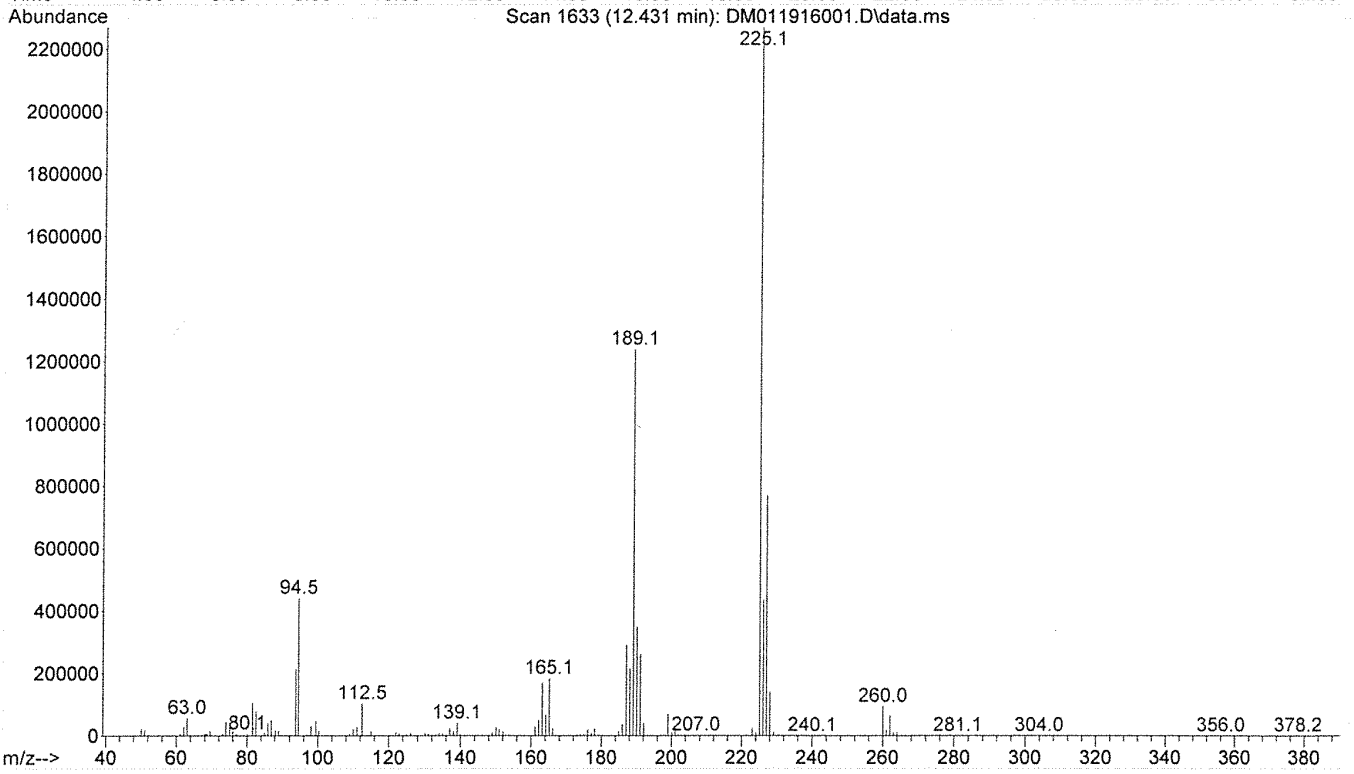

Figure A.7. GC/MS data for **25**.

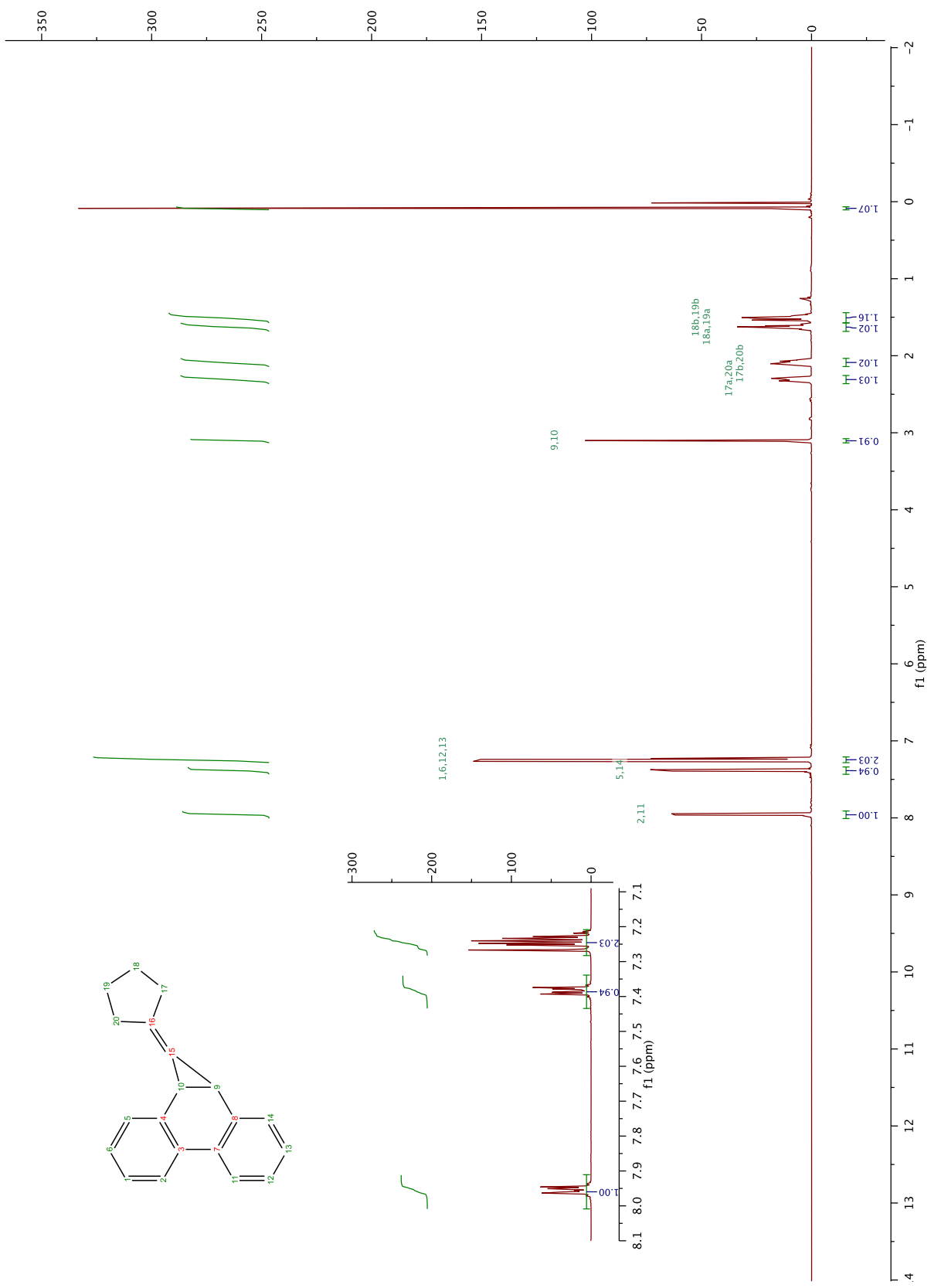

Figure A.8. ^{1}H NMR Spectrum of **11**.

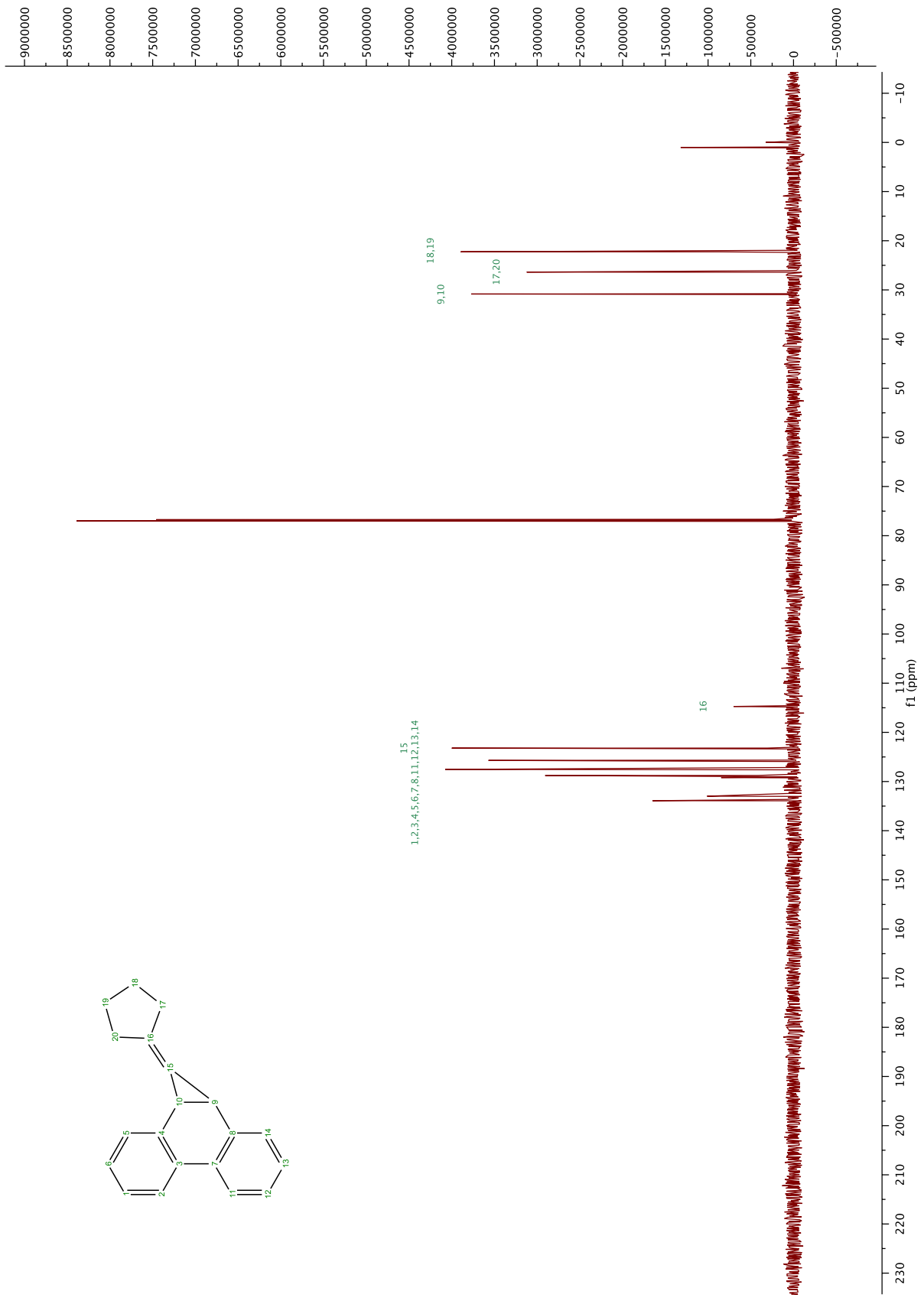

Figure A.9. ^{13}C NMR Spectrum of **11**.

```
File       :D:\1\data\Dan\DM040616003.D
Operator   : dan
Acquired   :  6 Apr 2016  12:54     using AcqMethod DASLAB3MIN.M
Instrument :    GCMS1
Sample Name: 5ring prec
Misc Info  : pure
Vial Number: 1
```

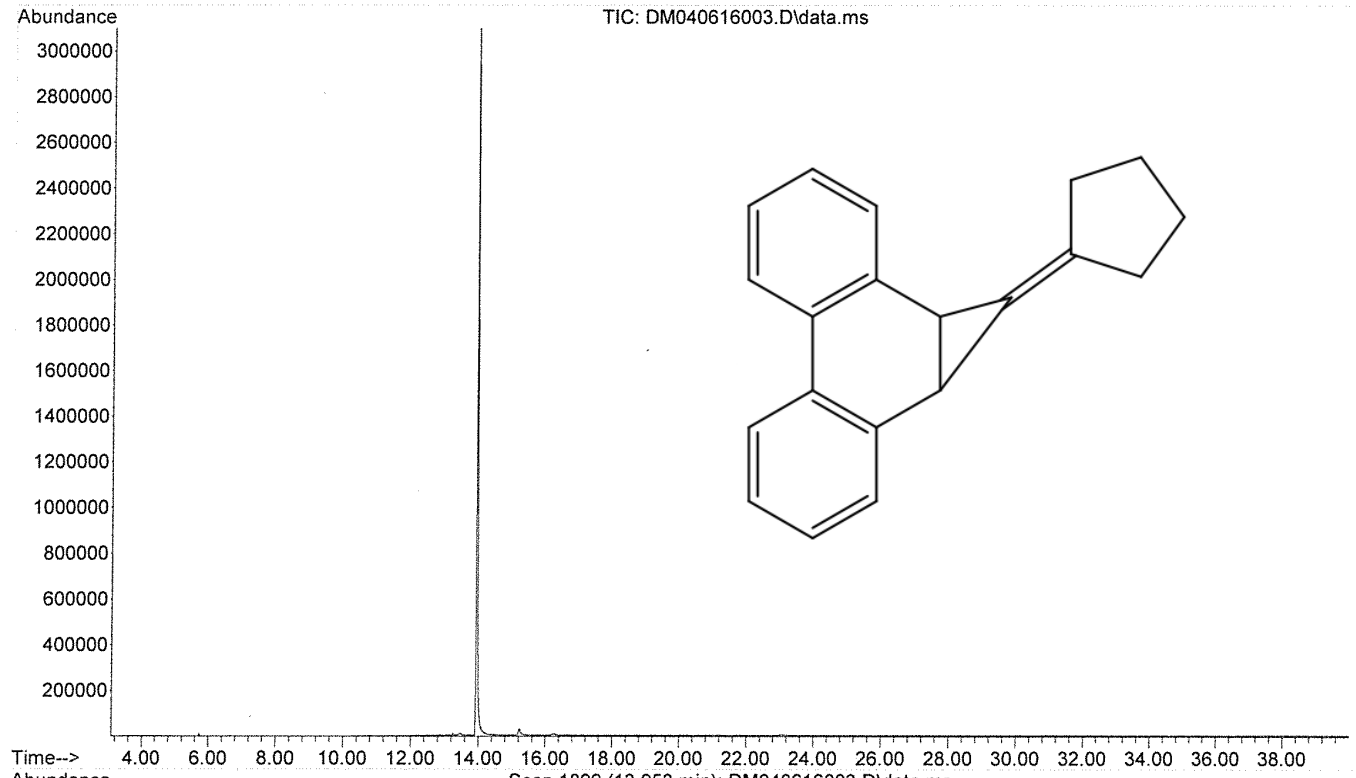

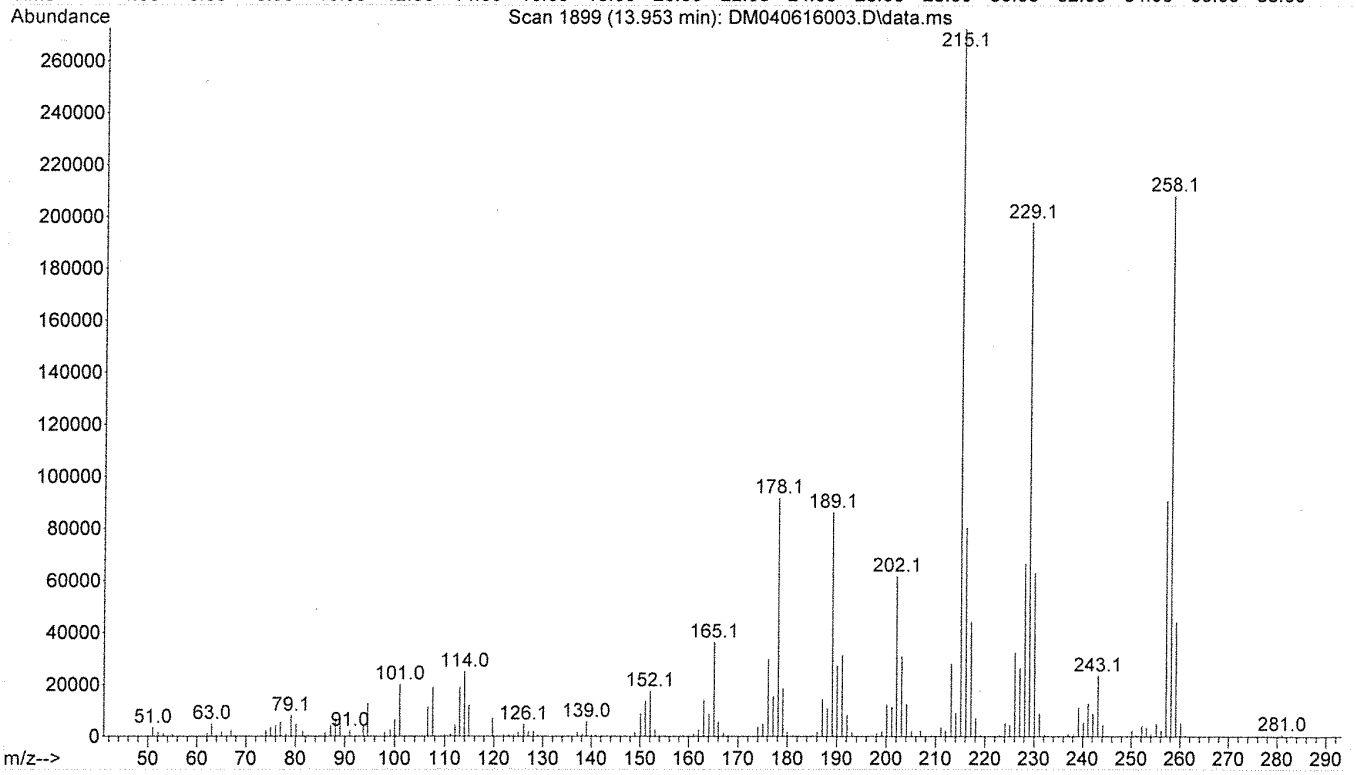

Figure A.10. GC/MS data for **11**.

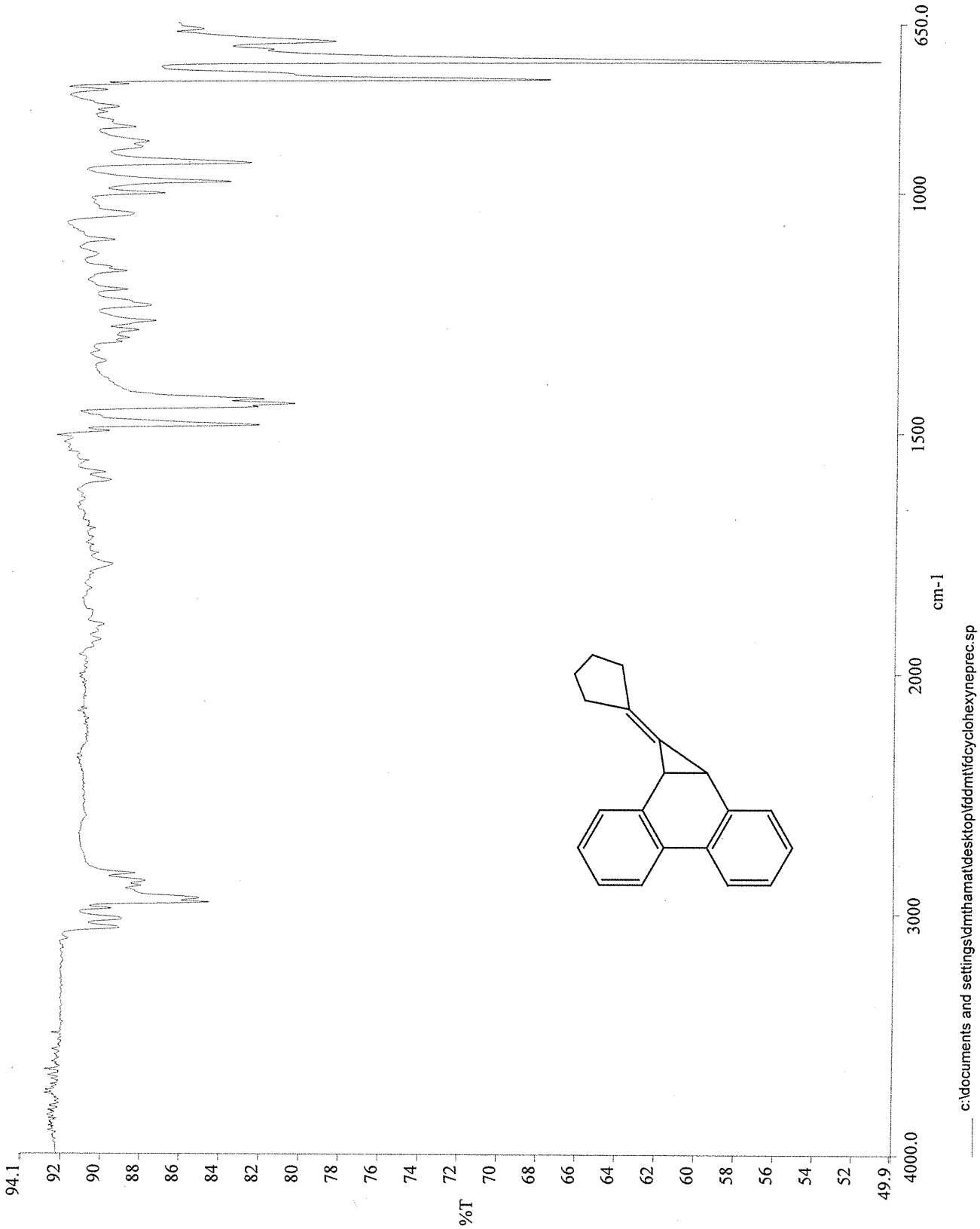

Figure A.11. IR Spectrum of **11**.

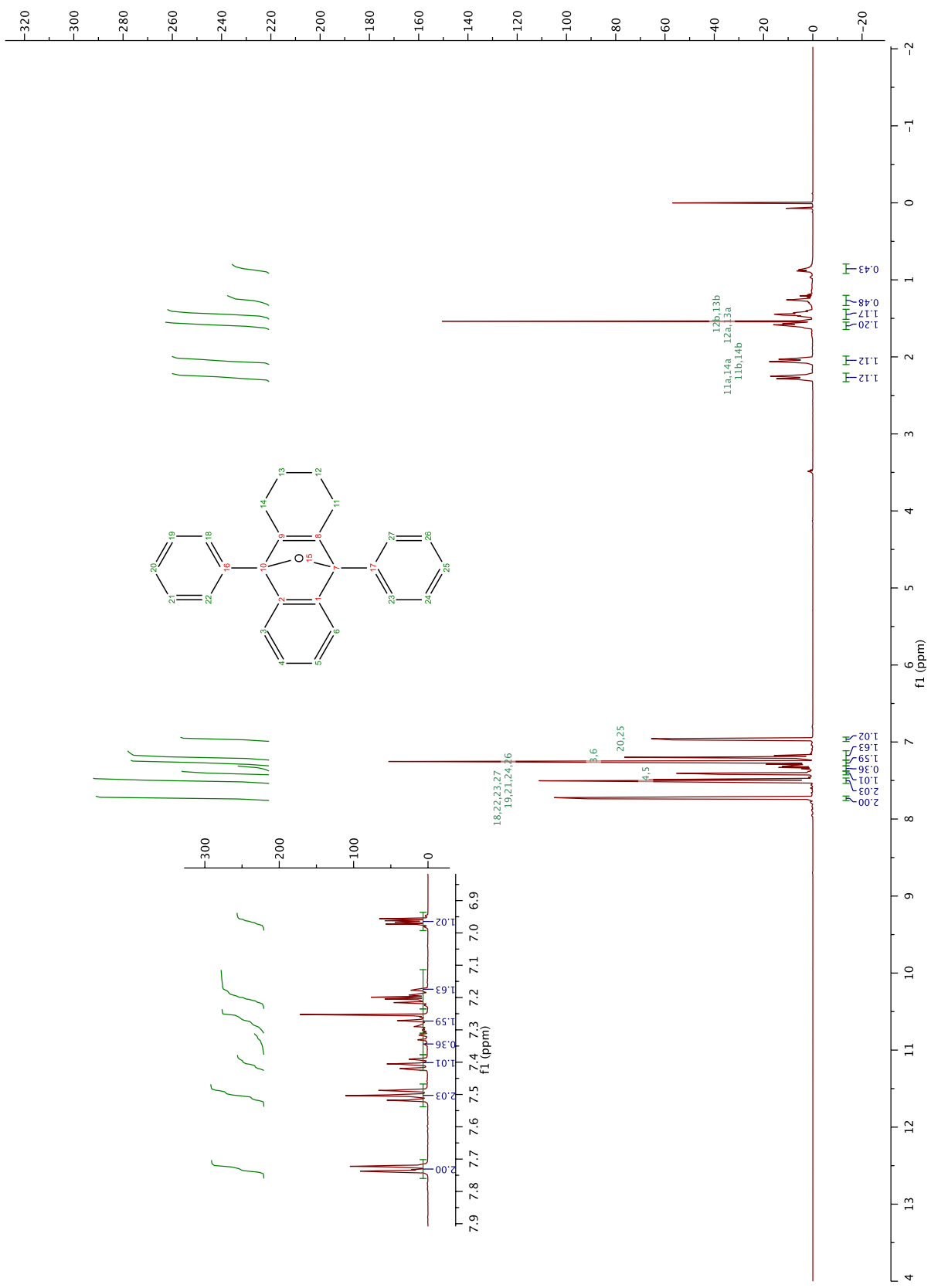

Figure A.12. ^{1}H NMR Spectrum of **16**.

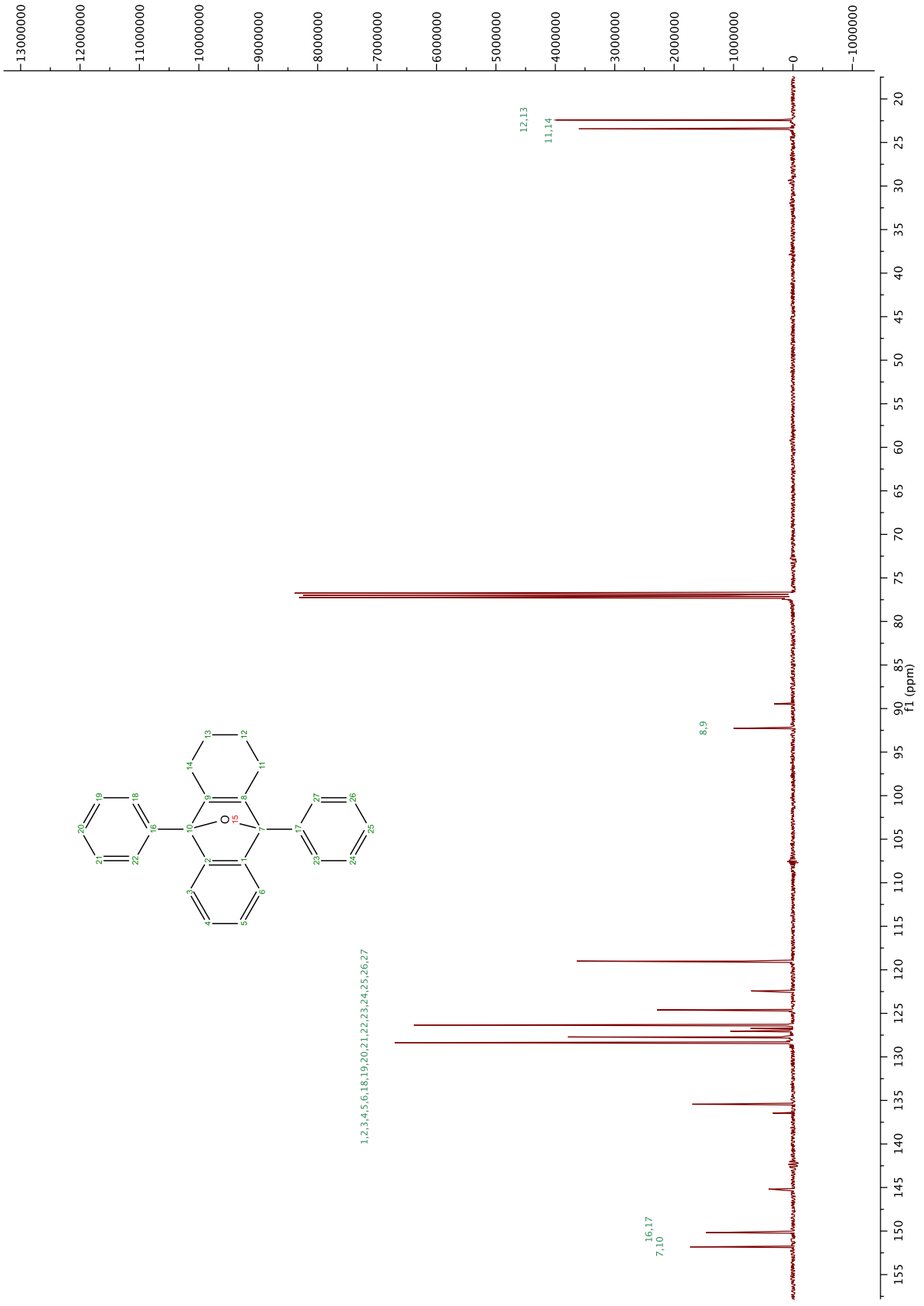

Figure A.13. ^{13}C NMR Spectrum of **16**.

```
File       :D:\1\data\Dan\DM073114006.D
Operator   : Dan
Acquired   : 31 Jul 2014  14:28     using AcqMethod DASLAB3MIN.M
Instrument :    GCMS1
Sample Name: cyclohexyne isobenzofuran trap
Misc Info  : 95 mg 20 hr photol fraction 32
Vial Number: 1
```

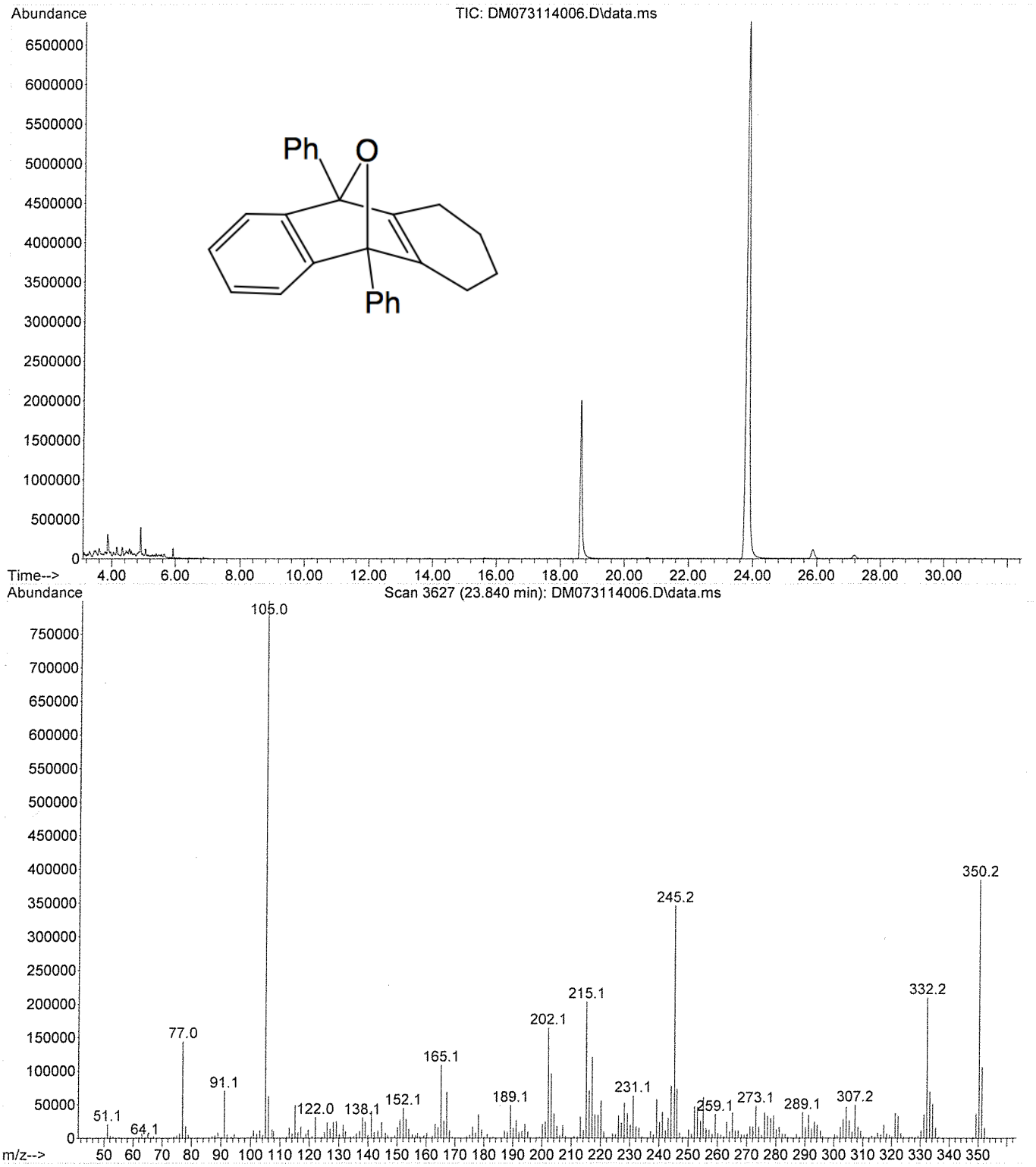

Figure A.14. GC/MS data for **16**.

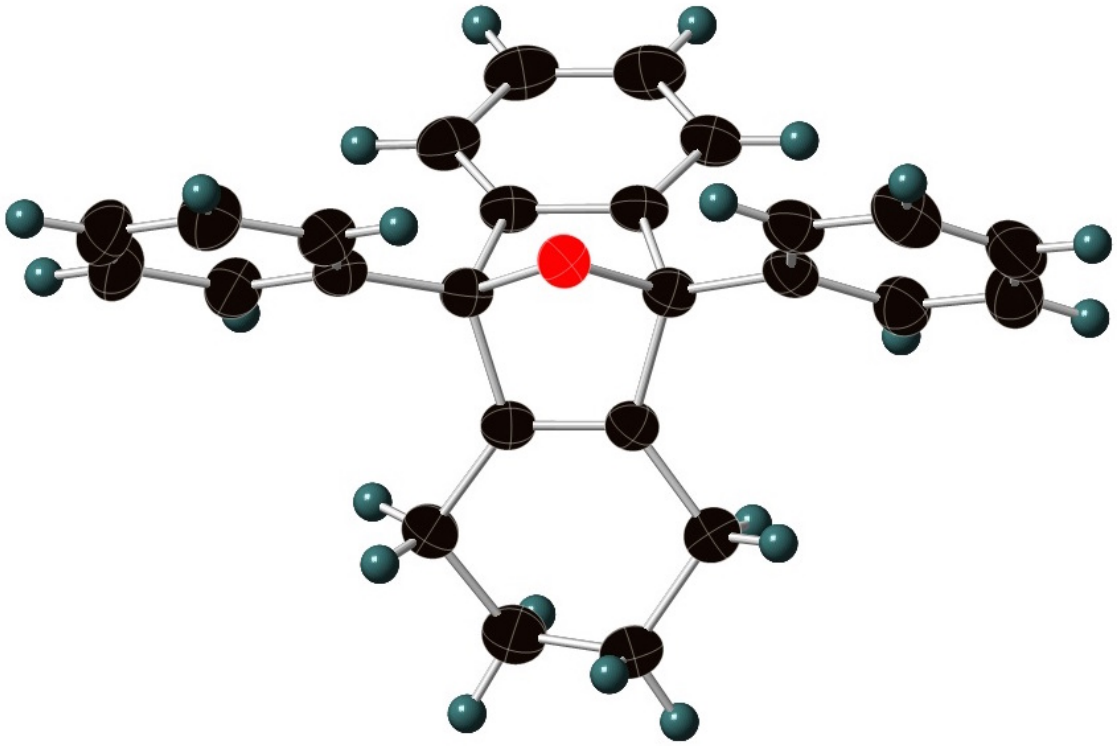

Figure A.15. X-ray Crystal Structure of **16**.

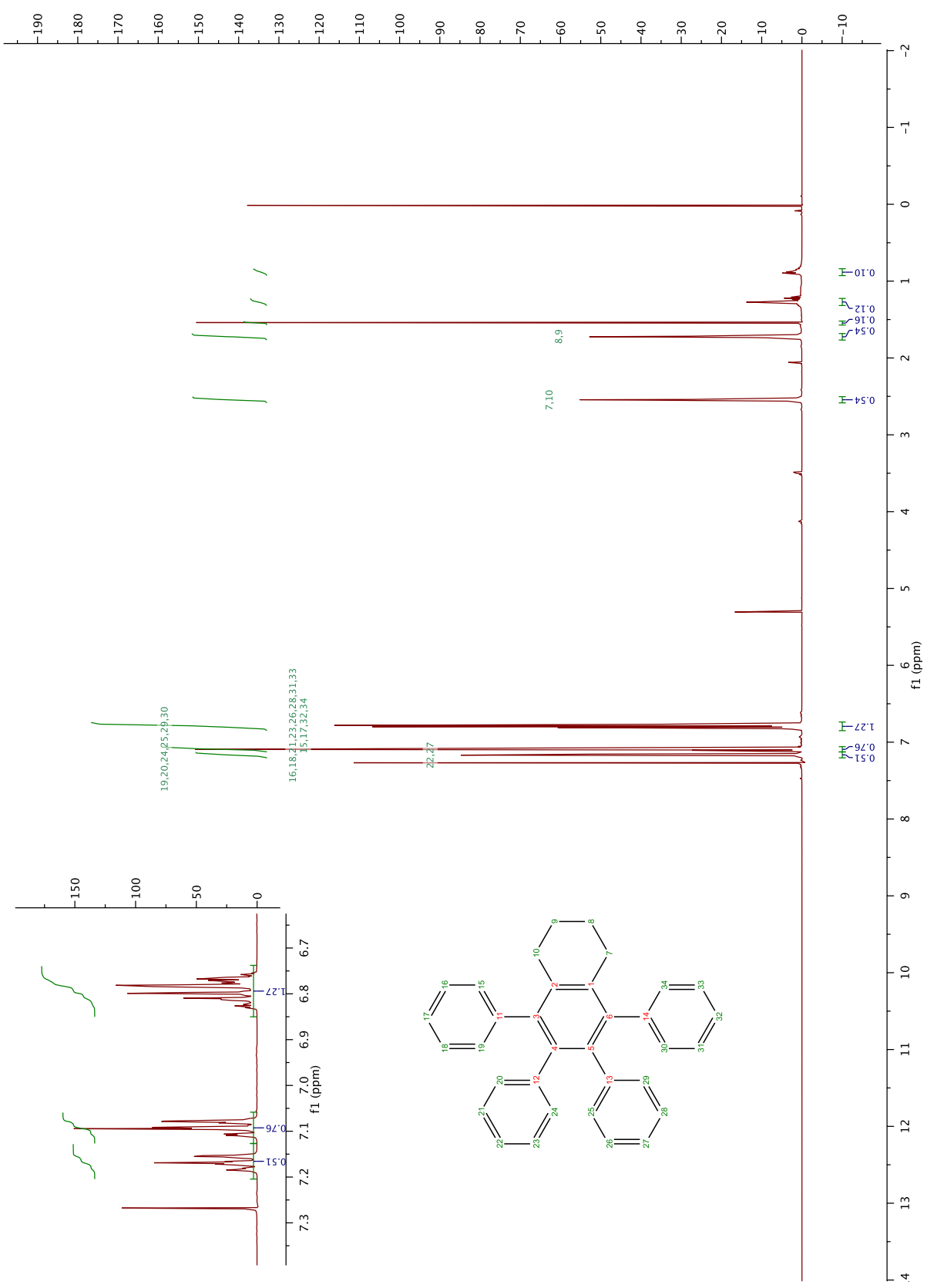

Figure A.16. ^{1}H NMR Spectrum of **18**.

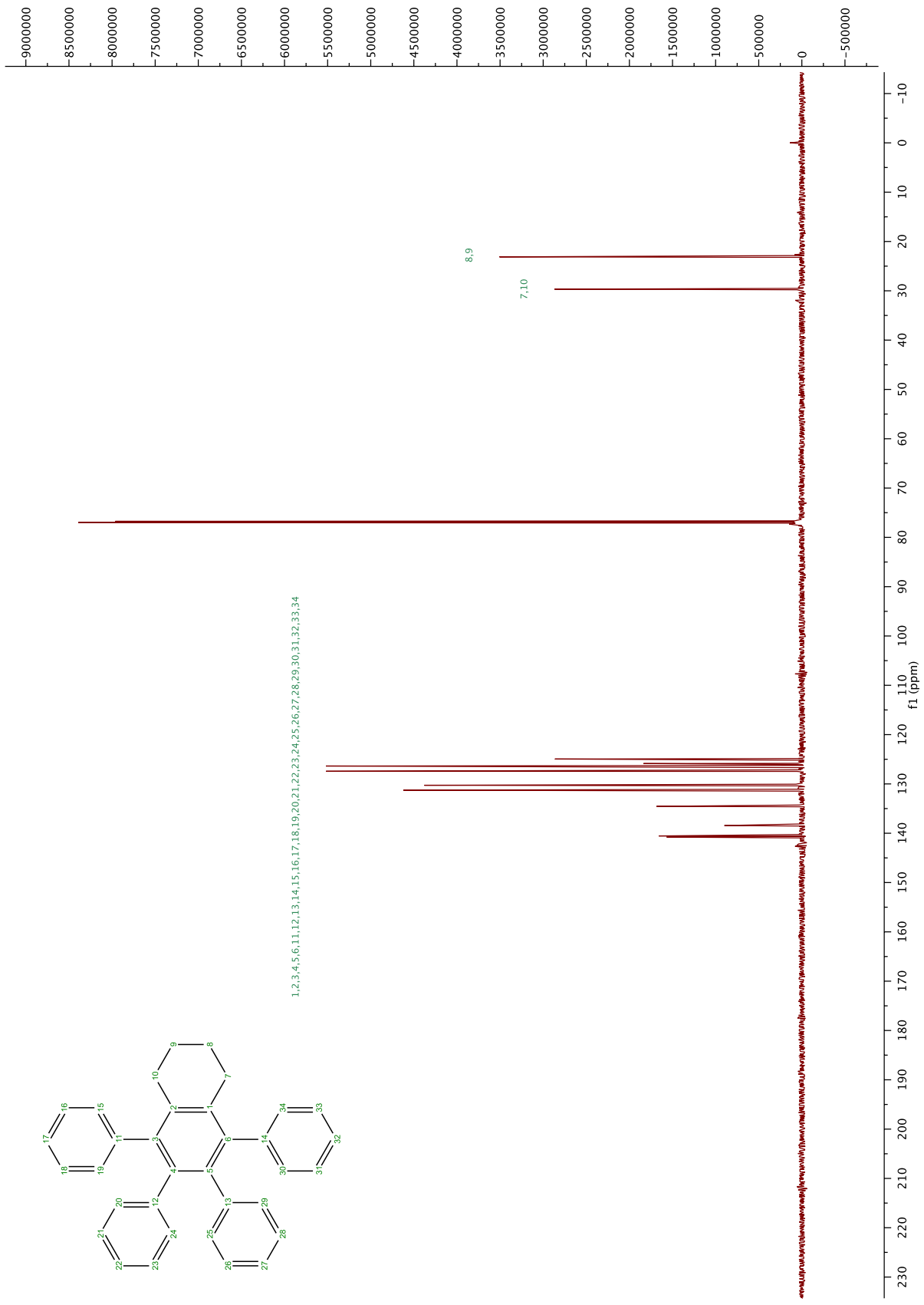

Figure A.17. ^{13}C NMR Spectrum of **18**.

```
File       :D:\1\data\Dan\DM073014003.D
Operator   : Dan
Acquired   : 30 Jul 2014  16:01     using AcqMethod FD3MINSDLR.M
Instrument :    GCMS1
Sample Name: cyclohexyne tetraphenyol trap
Misc Info  : 40 hr photol column fraction 30
Vial Number: 1
```

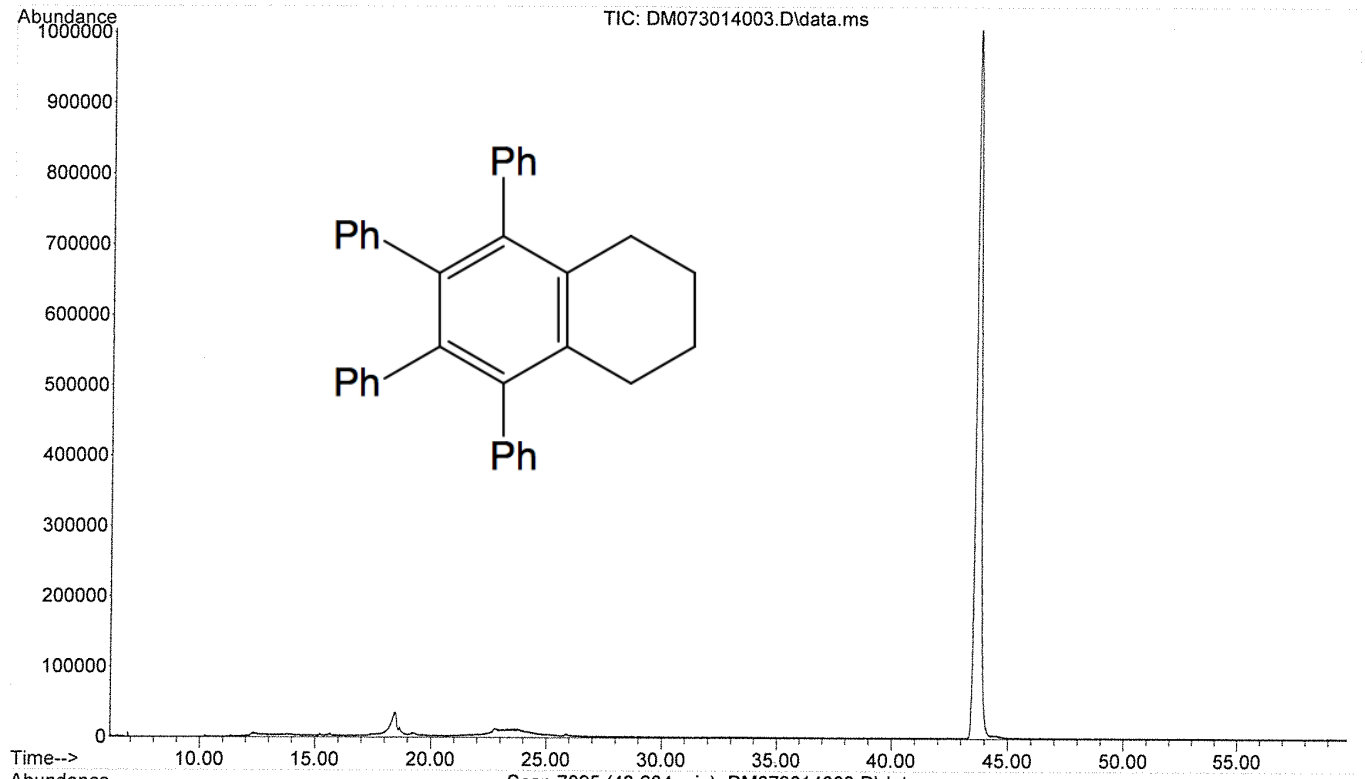

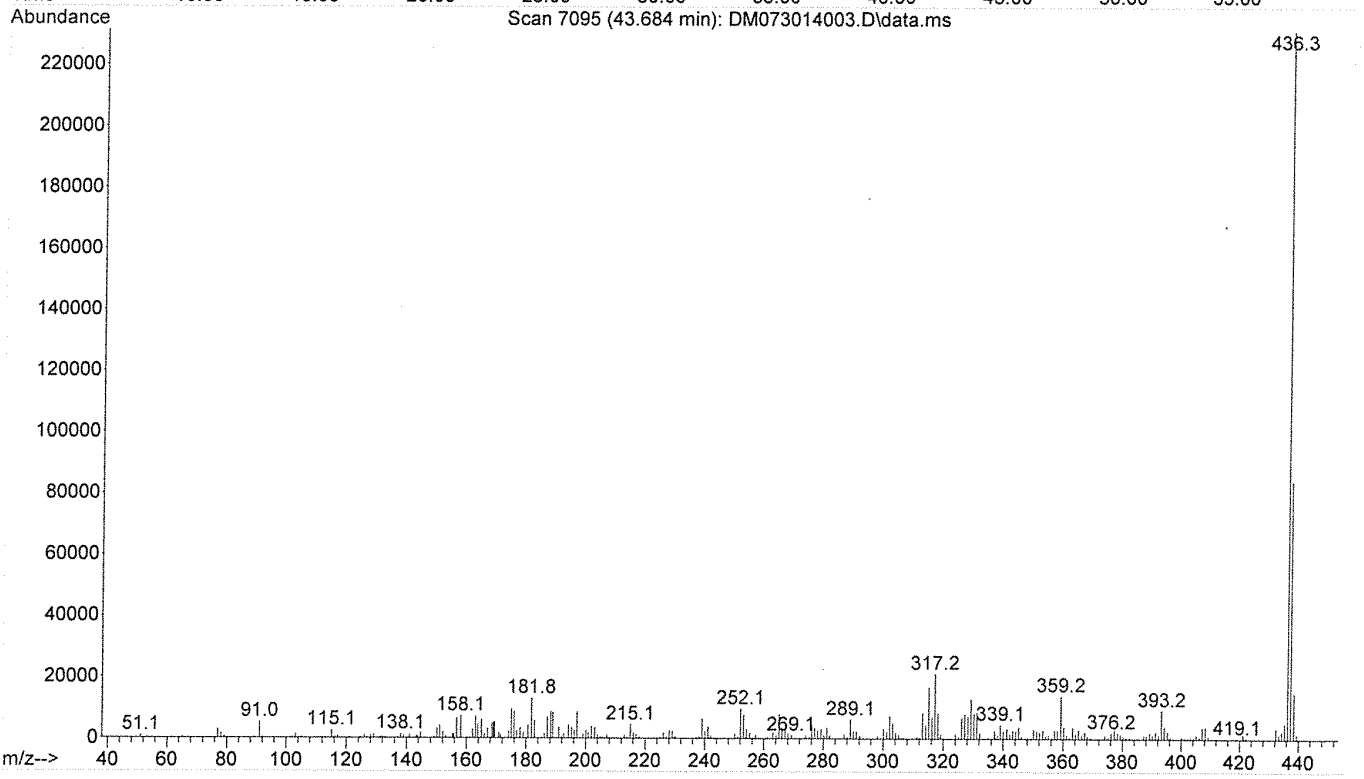

Figure A.18. GC/MS data for **18**.

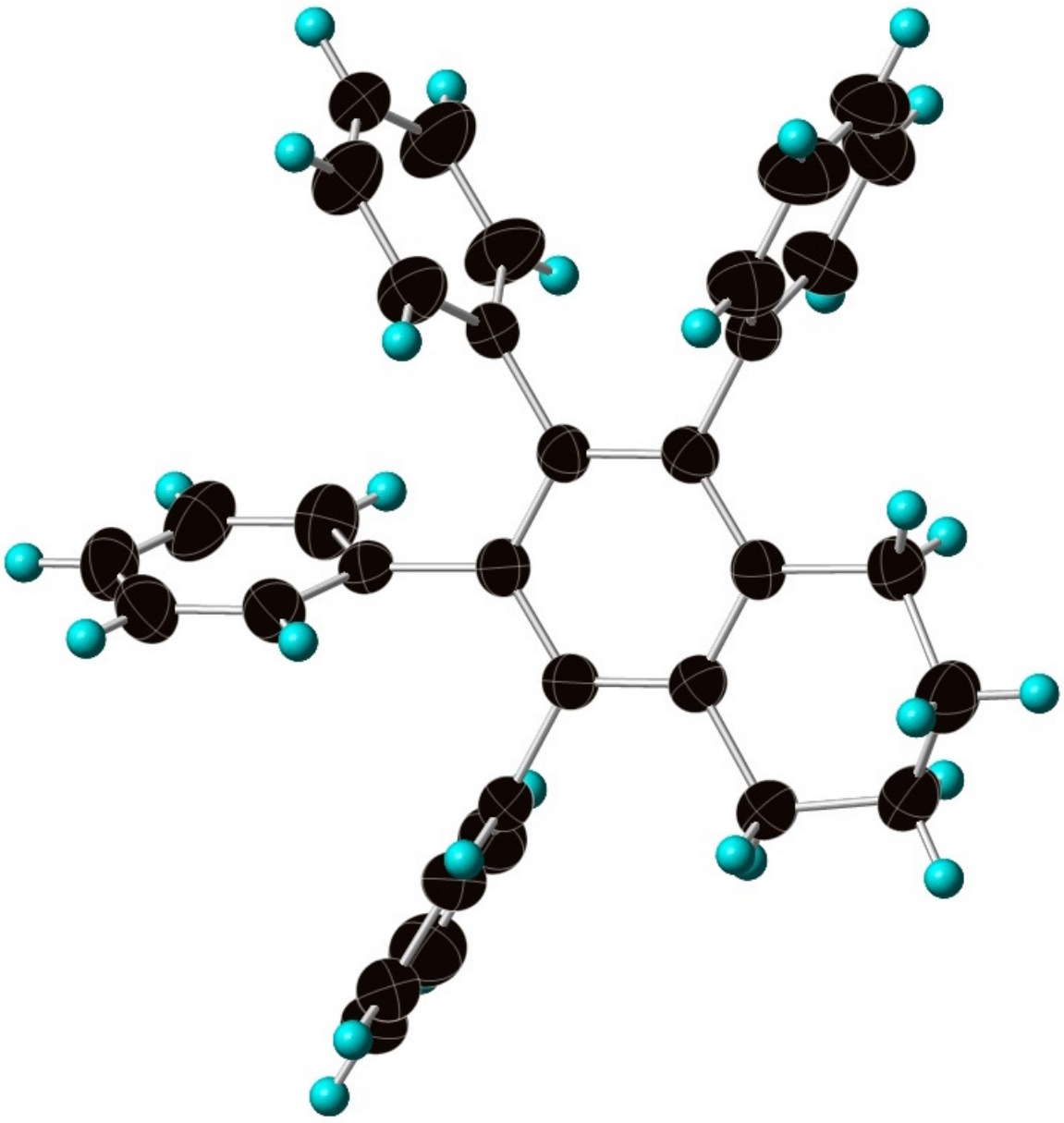

Figure A.19. X-ray Crystal Structure of **18**.

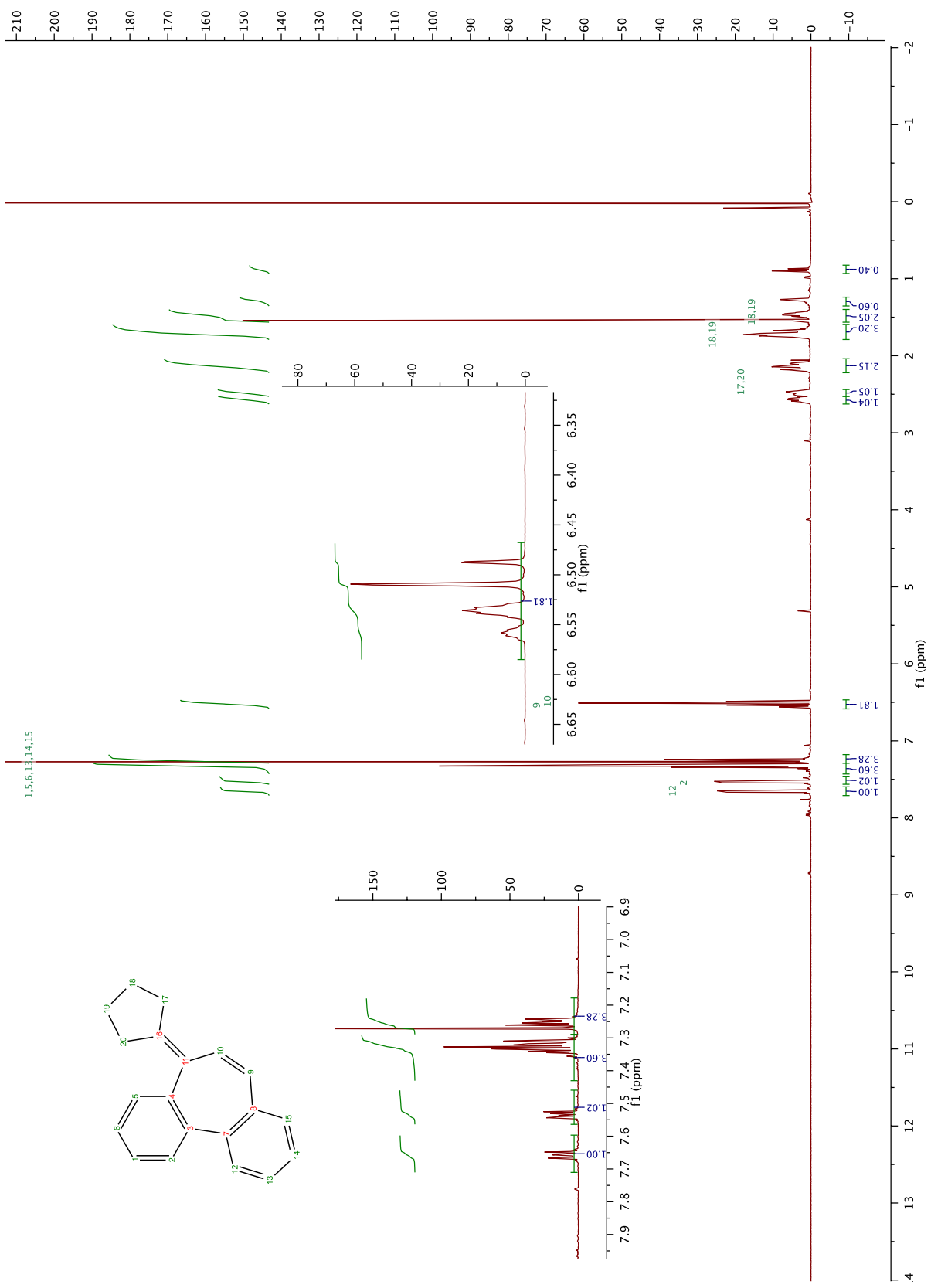

Figure A.20. ^{1}H NMR Spectrum of **26**.

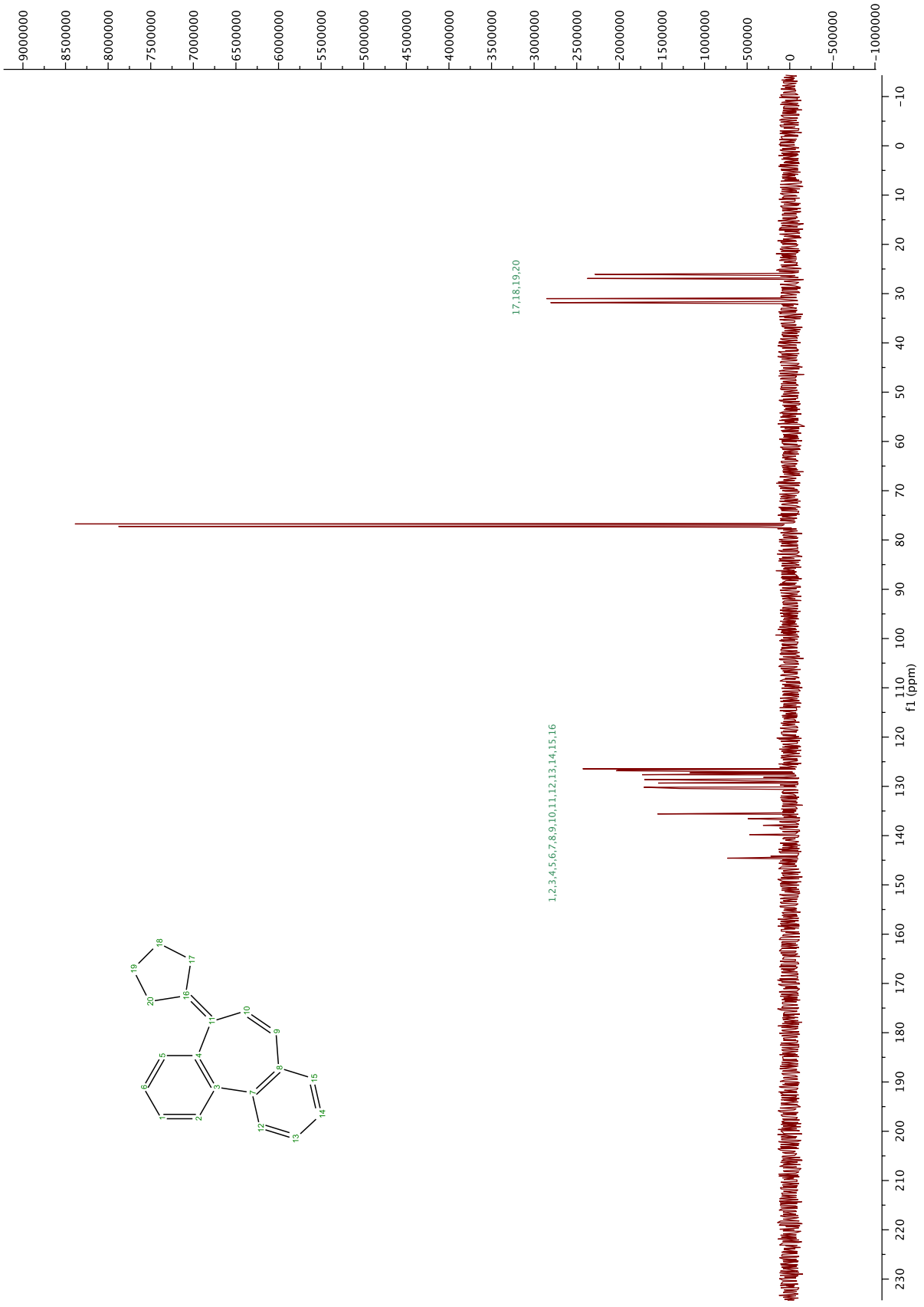

Figure A.21. ^{13}C NMR Spectrum of **26**.

```
File       :D:\1\data\Dan\DM040816002.D
Operator   : dan
Acquired   :  8 Apr 2016  14:27     using AcqMethod DASLAB3MIN.M
Instrument :    GCMS1
Sample Name: Rearranged Cyclopentylidene Precursor
Misc Info  : After prep TLC and filtration
Vial Number: 1
```

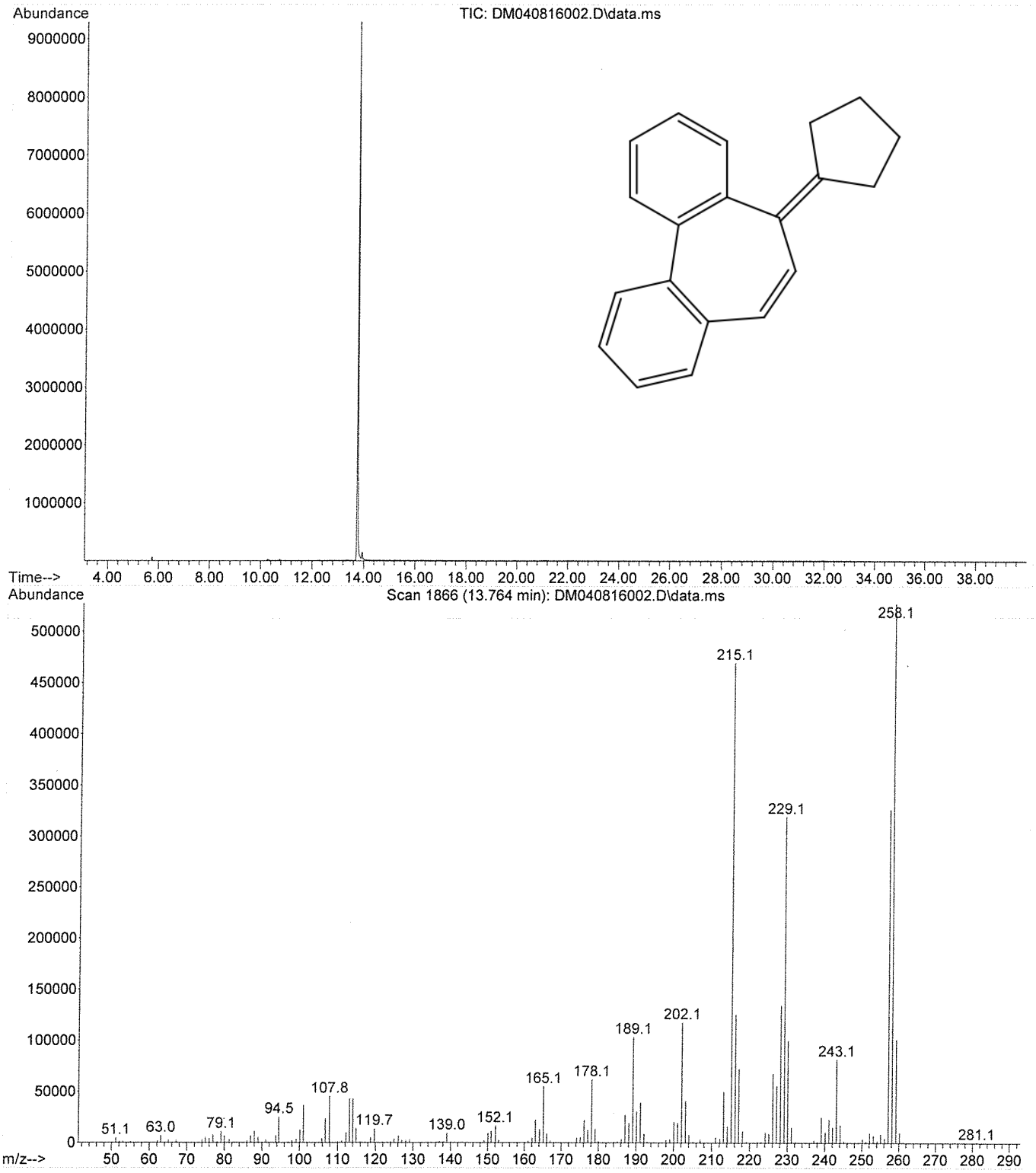

Figure A.22. GC/MS data for **26**.

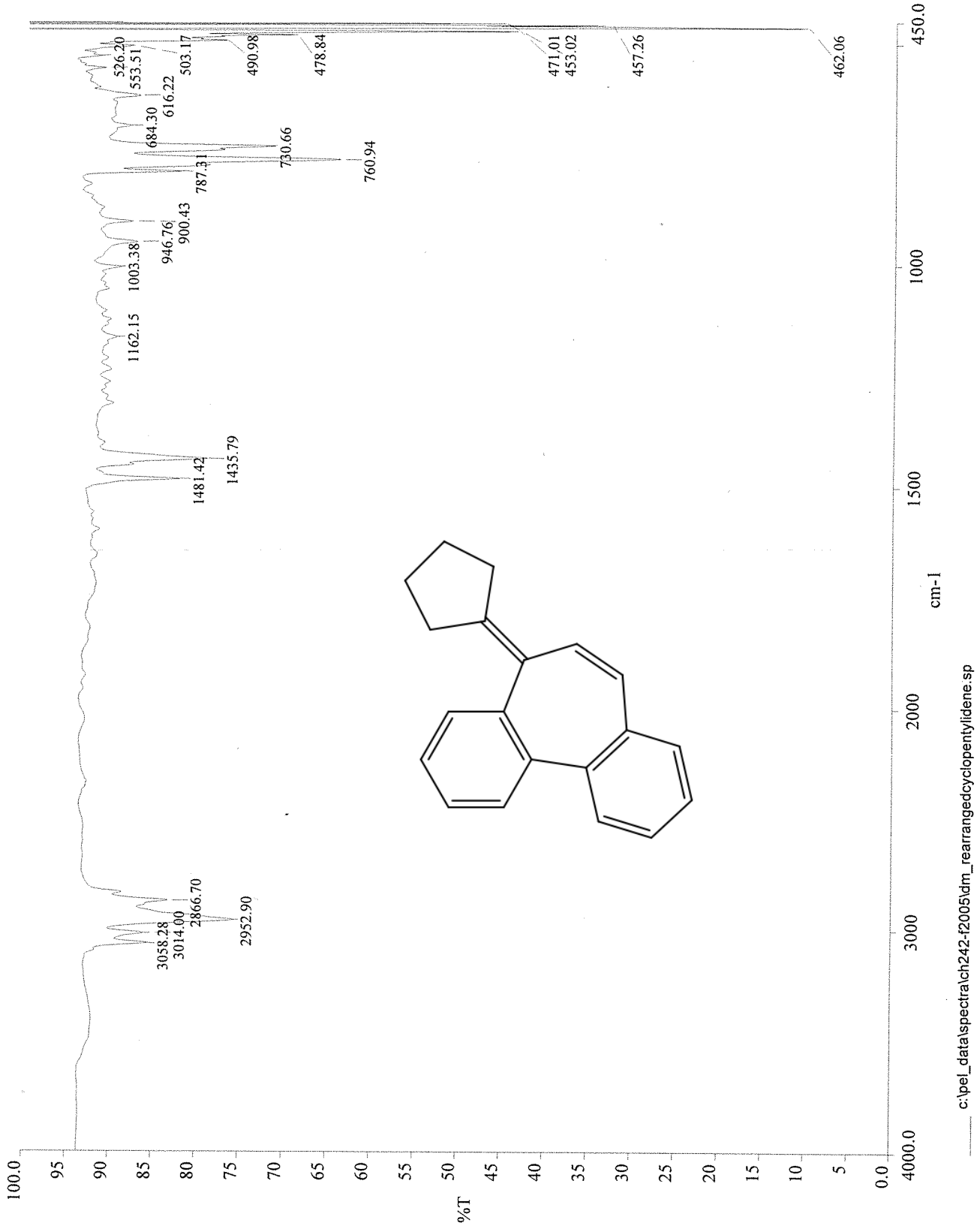

Figure A.23. IR Spectrum of **26**

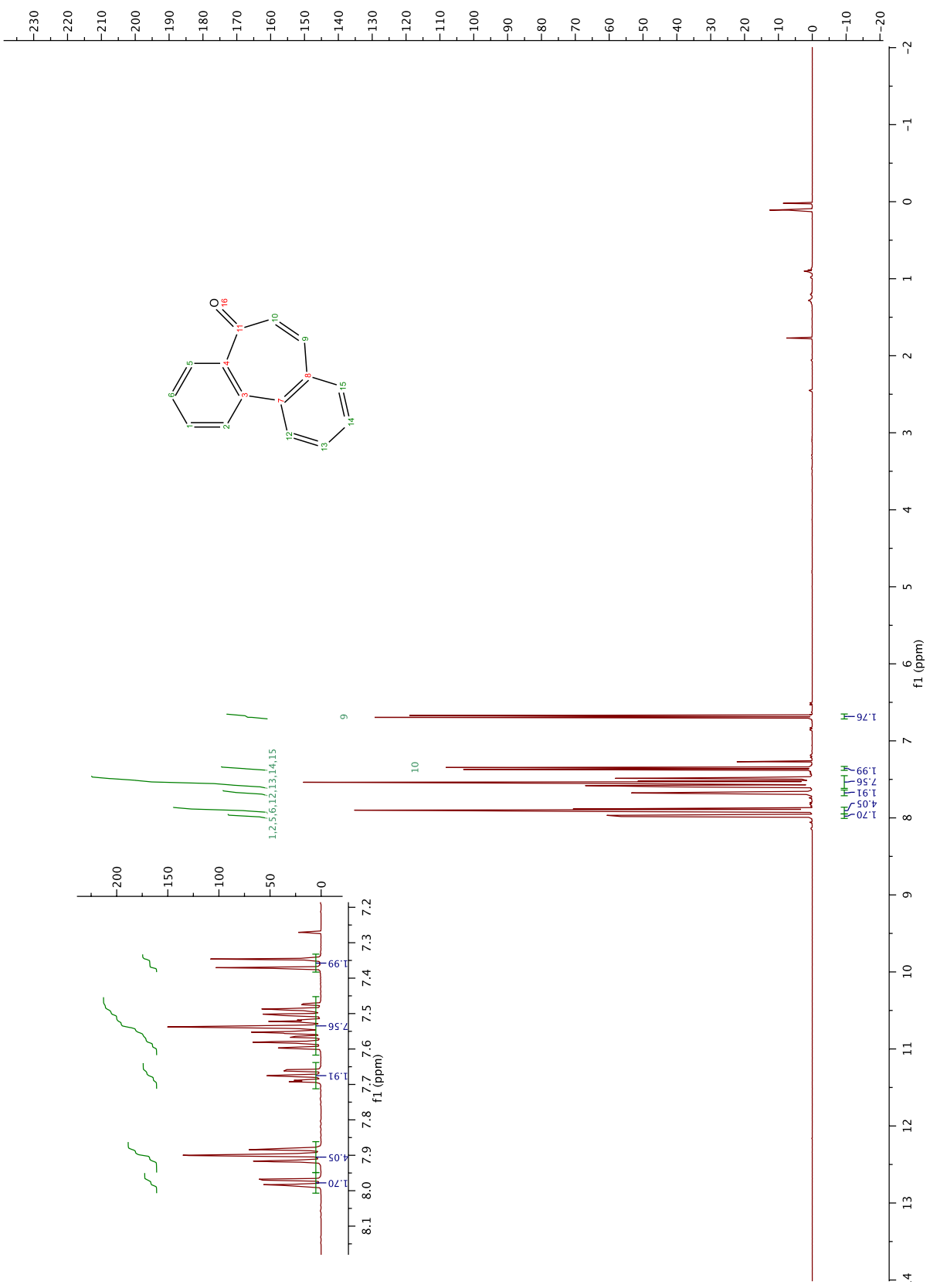

Figure A.24. ^{1}H NMR Spectrum of **27**.

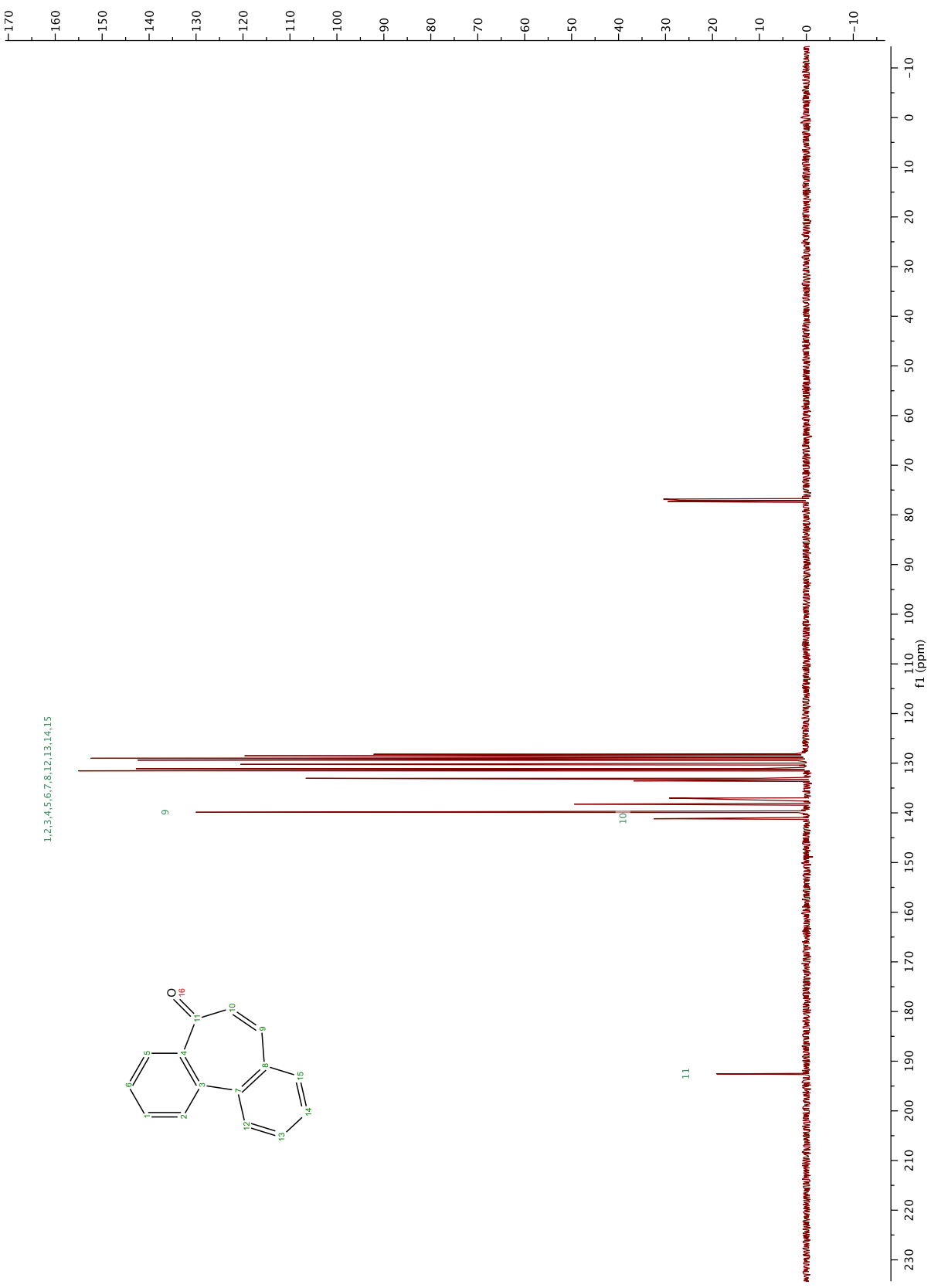

Figure A.25. ^{13}C NMR Spectrum of **27**.

```
File       :D:\1\data\Dan\DM012516001.D
Operator   : dan
Acquired   : 25 Jan 2016  10:08     using AcqMethod DASLAB3MIN.M
Instrument :    GCMS1
Sample Name: suzuki 7ring
Misc Info  : column frac 11
Vial Number: 1
```

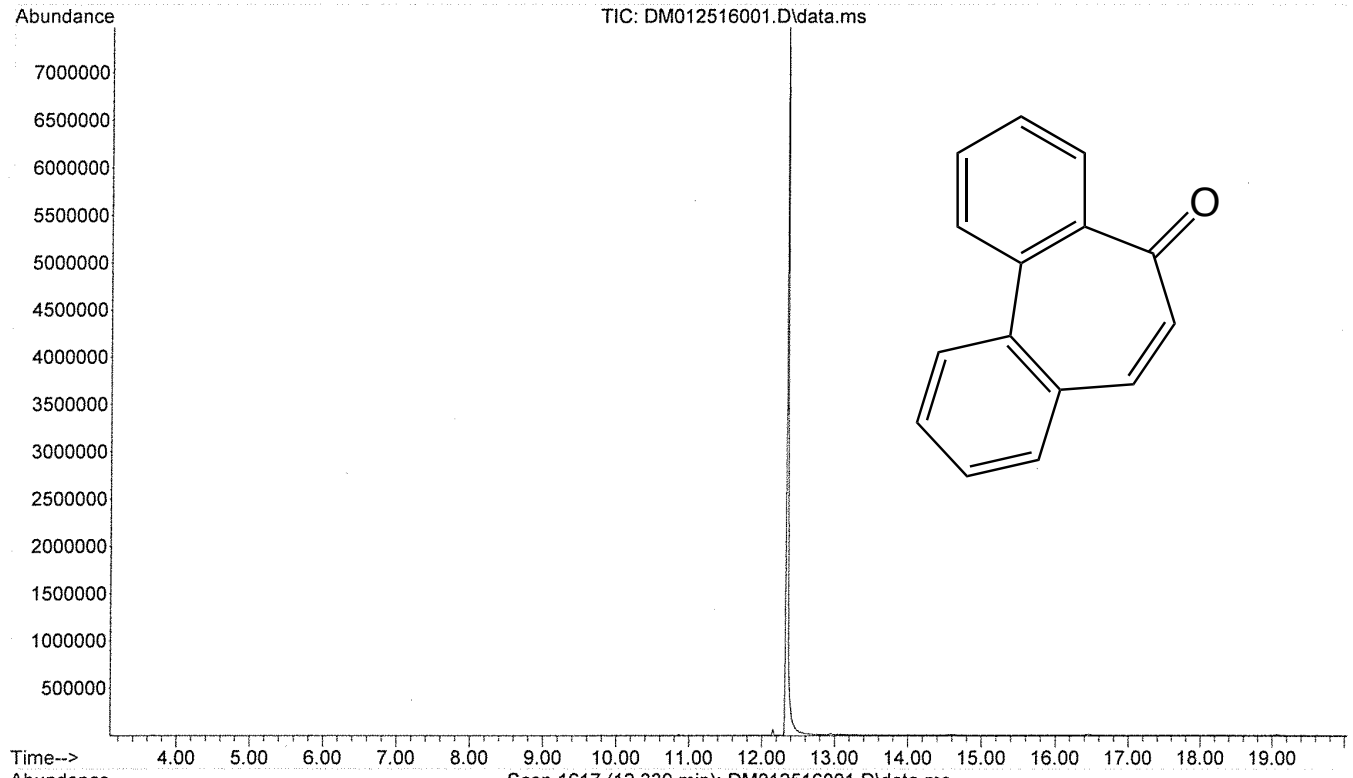

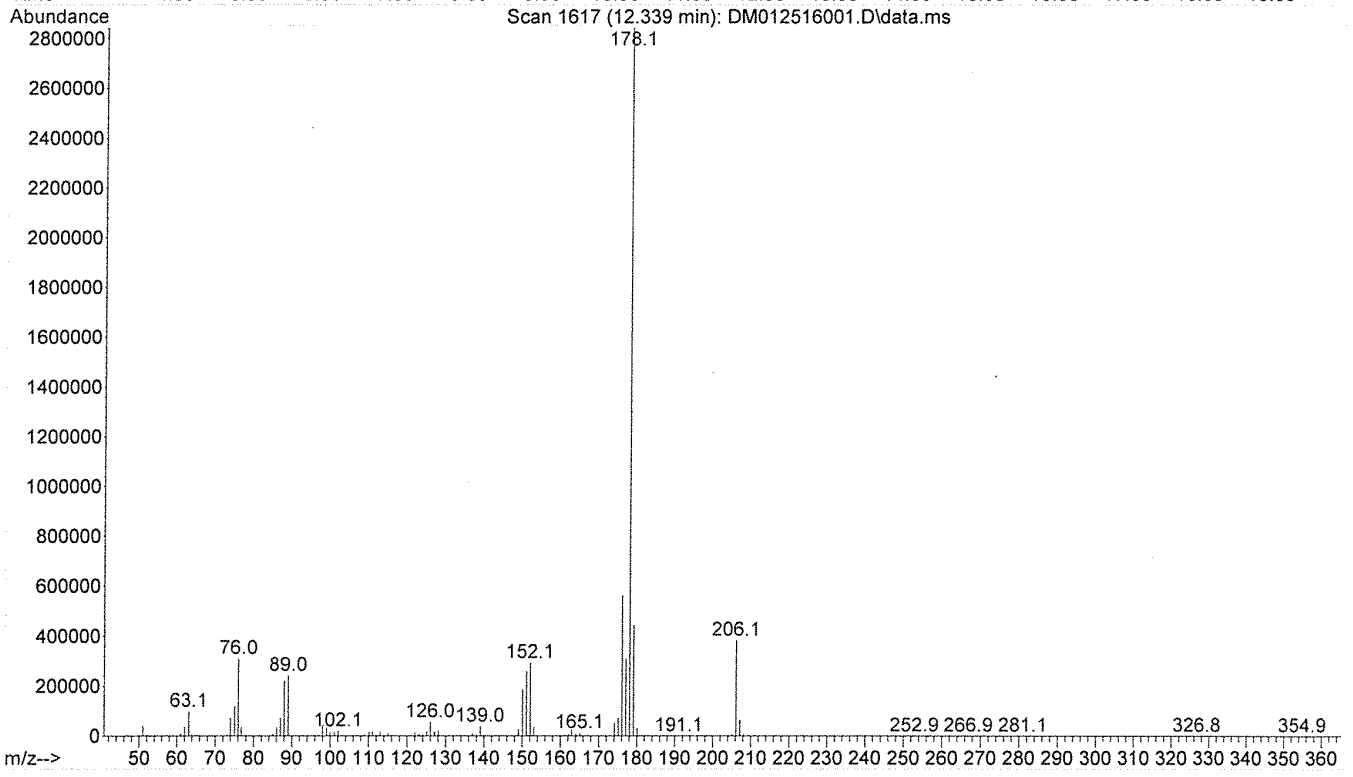

Figure A.26. GC/MS data for **27**.

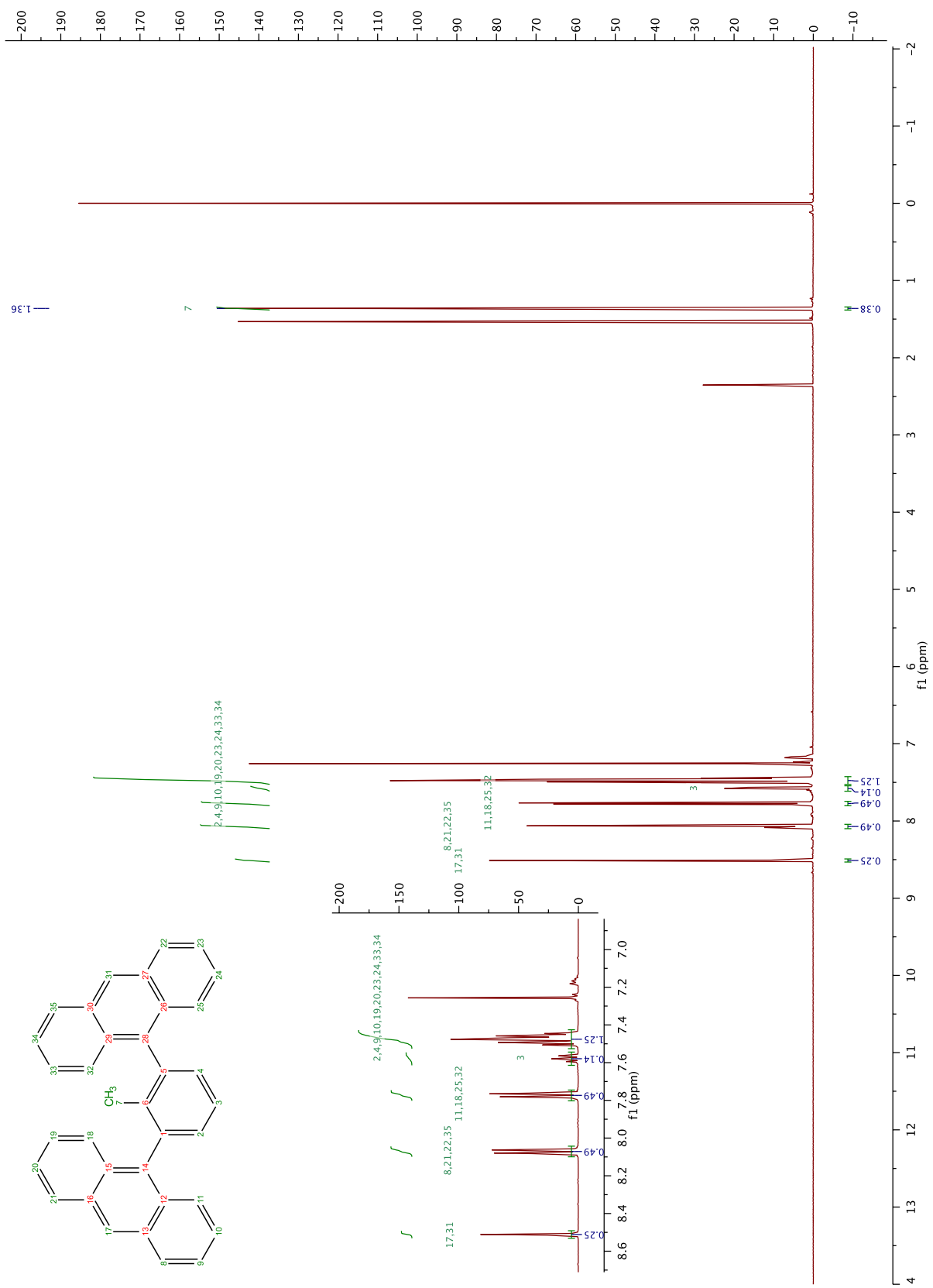

Figure A.27. ^{1}H NMR Spectrum of **34**.

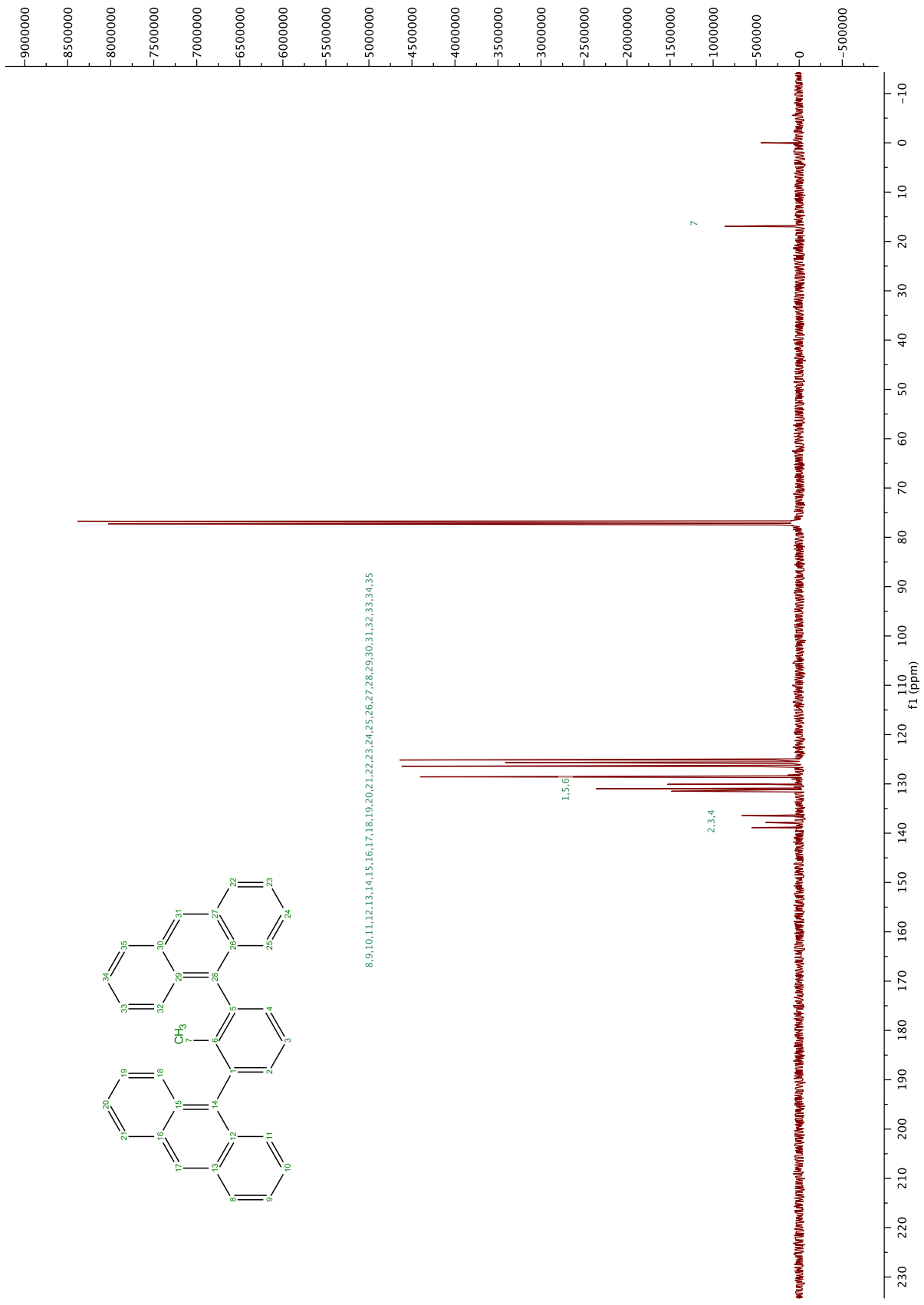

Figure A.28. [1]3C NMR Spectrum of **34**.

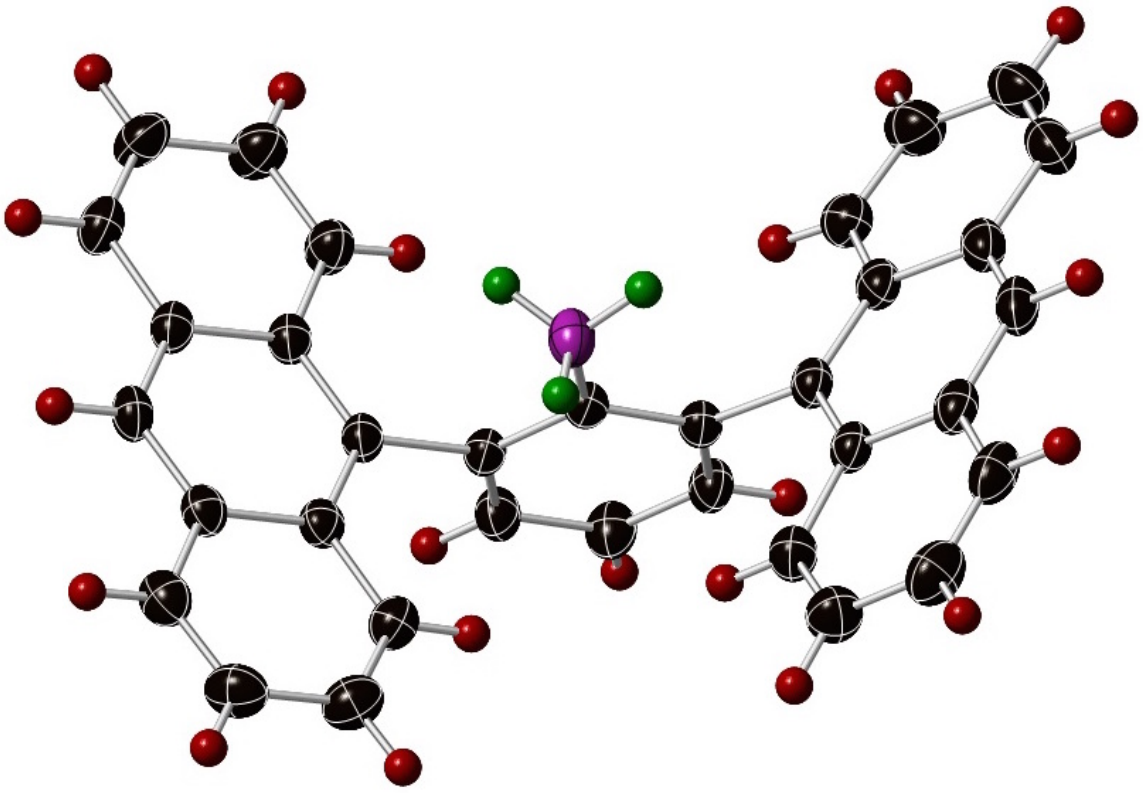

Figure A.29. X-ray Crystal Structure of **34**.

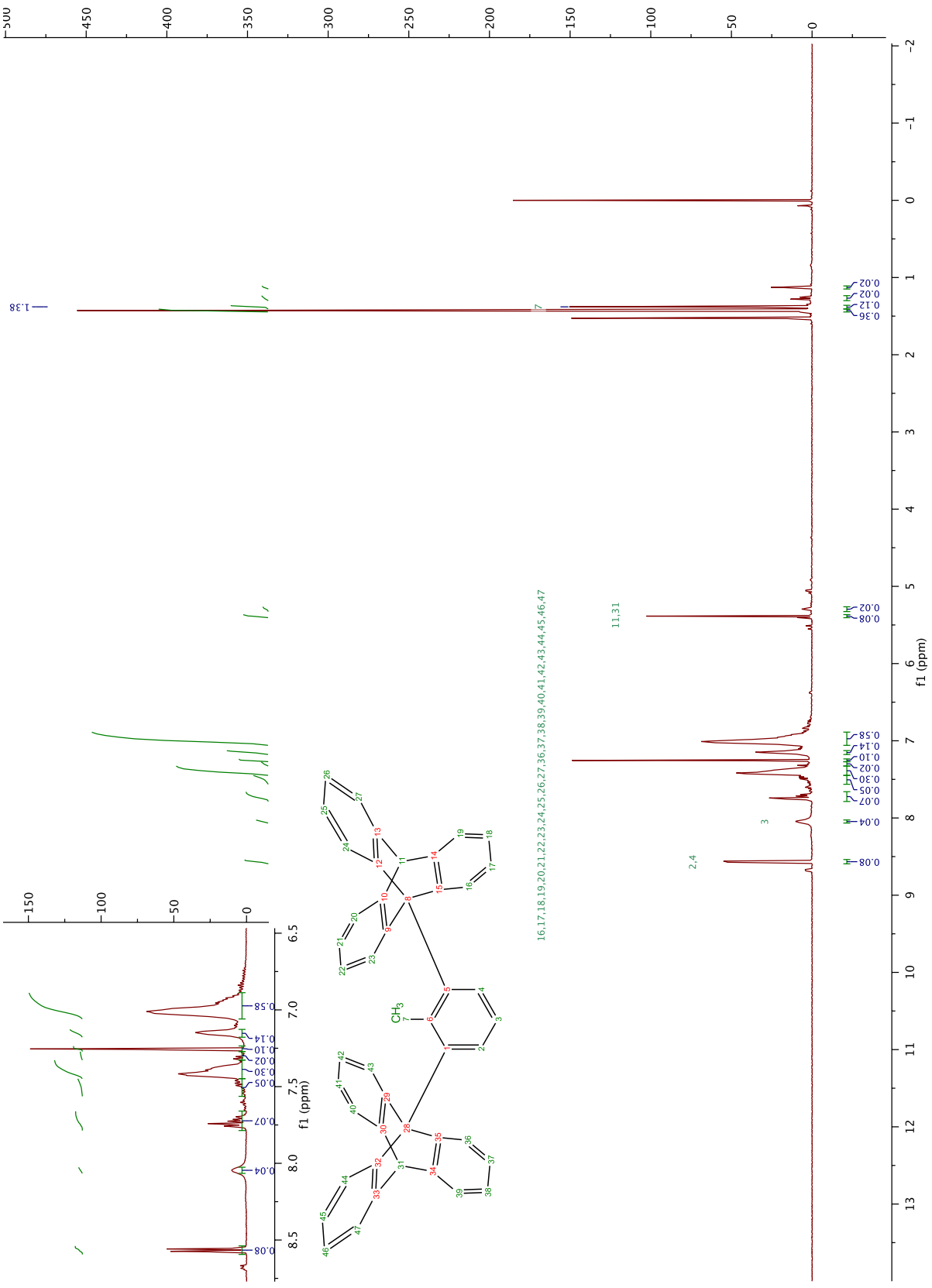

Figure A.30. ^{1}H NMR Spectrum of **34**.

Appendix B

Crystallographic Reports

Crystal Structure Report for CyclohexynePrecursor_1

A clear colourless plate-like specimen of $C_{20}H_{18}$, approximate dimensions 0.030 mm x 0.100 mm x 0.380 mm, was used for the X-ray crystallographic analysis. The X-ray intensity data were measured.

The total exposure time was 23.11 hours. The frames were integrated with the Bruker SAINT software package using a narrow-frame algorithm. The integration of the data using a triclinic unit cell yielded a total of 11940 reflections to a maximum θ angle of 26.42° (0.80 Å resolution), of which 5730 were independent (average redundancy 2.084, completeness = 98.8%, R_{int} = 3.91%, R_{sig} = 6.71%) and 3188 (55.64%) were greater than $2\sigma(F^2)$. The final cell constants of a = 4.9861(12) Å, b = 14.094(4) Å, c = 20.610(4) Å, α = 80.584(4)°, β = 86.129(3)°, γ = 81.535(3)°, volume = 1411.9(6) $Å^3$, are based upon the refinement of the XYZ-centroids of 1316 reflections above 20 σ(I) with 5.341° < 2θ < 46.07°. Data were corrected for absorption effects using the multi-scan method (SADABS). The ratio of minimum to maximum apparent transmission was 0.857. The calculated minimum and maximum transmission coefficients (based on crystal size) are 0.9740 and 0.9980.

The final anisotropic full-matrix least-squares refinement on F^2 with 361 variables converged at R1 = 6.53%, for the observed data and wR2 = 20.85% for all data. The goodness-of-fit was 0.994. The largest peak in the final difference electron density synthesis was 0.381 $e^-/Å^3$ and the largest hole was -0.167 $e^-/Å^3$ with an RMS deviation of 0.043 $e^-/Å^3$. On the basis of the final model, the calculated density was 1.218 g/cm^3 and F(000), 554 e^-.

Table 1. Sample and crystal data for CyclohexynePrecursor_1.

Identification code	CyclohexynePrecursor_1	
Chemical formula	$C_{20}H_{18}$	
Formula weight	258.36 g/mol	
Temperature	173(2) K	
Wavelength	0.71073 Å	
Crystal size	0.030 x 0.100 x 0.380 mm	
Crystal habit	clear colourless plate	
Crystal system	triclinic	
Space group	P -1	
Unit cell dimensions	a = 4.9861(12) Å	α = 80.584(4)°
	b = 14.094(4) Å	β = 86.129(3)°
	c = 20.610(4) Å	γ = 81.535(3)°
Volume	1411.9(6) $Å^3$	
Z	2	

Density (calculated)	1.218 g/cm^3
Absorption coefficient	0.068 mm^{-1}
F(000)	554

Table 2. Data collection and structure refinement for CyclohexynePrecursor_1.

Theta range for data collection	1.48 to 26.42°	
Index ranges	-6<=h<=6, -17<=k<=17, -23<=l<=25	
Reflections collected	11940	
Independent reflections	5730 [R(int) = 0.0391]	
Coverage of independent reflections	98.8%	
Absorption correction	multi-scan	
Max. and min. transmission	0.9980 and 0.9740	
Refinement method	Full-matrix least-squares on F^2	
Refinement program	SHELXL-2014/7 (Sheldrick, 2014)	
Function minimized	$\Sigma\ w(F_o^2 - F_c^2)^2$	
Data / restraints / parameters	5730 / 0 / 361	
Goodness-of-fit on F^2	0.994	
Final R indices	3188 data; $I>2\sigma(I)$	R1 = 0.0653, wR2 = 0.1586
	all data	R1 = 0.1282, wR2 = 0.2085
Weighting scheme	$w=1/[\sigma^2(F_o^2)+(0.1000P)^2]$ where $P=(F_o^2+2F_c^2)/3$	
Largest diff. peak and hole	0.381 and -0.167 $eÅ^{-3}$	
R.M.S. deviation from mean	0.043 $eÅ^{-3}$	

Table 3. Atomic coordinates and equivalent isotropic atomic displacement parameters ($Å^2$) for CyclohexynePrecursor_1.

U(eq) is defined as one third of the trace of the orthogonalized U_{ij} tensor.

	x/a	y/b	z/c	U(eq)
C1	0.9784(6)	0.3027(3)	0.25015(14)	0.0535(8)
C2	0.8096(7)	0.3872(2)	0.22970(14)	0.0537(8)
C3	0.6246(6)	0.3878(2)	0.18255(13)	0.0451(7)

	x/a	y/b	z/c	U(eq)
C4	0.6077(5)	0.30560(19)	0.15514(12)	0.0362(6)
C5	0.4150(5)	0.31218(19)	0.10244(12)	0.0379(6)
C6	0.5251(5)	0.29467(19)	0.03660(13)	0.0387(6)
C7	0.6909(5)	0.31780(19)	0.98614(13)	0.0370(6)
C8	0.8287(6)	0.4089(2)	0.97313(14)	0.0458(7)
C9	0.9861(6)	0.4036(2)	0.90736(14)	0.0510(8)
C10	0.8803(6)	0.9550(2)	0.15043(16)	0.0568(9)
C11	0.6815(7)	0.9544(2)	0.10714(17)	0.0602(9)
C12	0.5205(6)	0.0402(2)	0.08474(15)	0.0501(8)
C13	0.5542(5)	0.12708(19)	0.10478(13)	0.0377(6)
C14	0.3862(5)	0.21836(19)	0.07615(12)	0.0386(6)
C15	0.9614(6)	0.2199(2)	0.22466(13)	0.0458(7)
C16	0.7765(5)	0.2185(2)	0.17653(12)	0.0376(6)
C17	0.7506(5)	0.12776(19)	0.15043(13)	0.0382(6)
C18	0.9120(6)	0.0397(2)	0.17232(15)	0.0490(8)
C19	0.7838(5)	0.2574(2)	0.93308(13)	0.0436(7)
C20	0.0412(5)	0.2959(2)	0.90310(14)	0.0443(7)
C21	0.4650(6)	0.0301(2)	0.32193(16)	0.0542(8)
C22	0.2949(6)	0.0637(2)	0.37092(16)	0.0560(8)
C23	0.1119(6)	0.0054(2)	0.40398(15)	0.0513(8)
C24	0.0998(5)	0.9138(2)	0.38851(13)	0.0427(7)
C25	0.9112(6)	0.8518(2)	0.42791(14)	0.0471(7)
C26	0.0266(6)	0.7595(2)	0.46682(14)	0.0444(7)
C27	0.1849(5)	0.7126(2)	0.51359(13)	0.0409(7)
C28	0.2660(7)	0.6042(2)	0.52523(14)	0.0522(8)
C29	0.3685(7)	0.5831(2)	0.59416(16)	0.0635(9)
C30	0.4986(6)	0.6722(2)	0.60034(16)	0.0568(8)
C31	0.3103(6)	0.7559(2)	0.56414(14)	0.0517(8)
C32	0.8897(6)	0.7534(2)	0.40710(14)	0.0476(7)
C33	0.0605(6)	0.7253(2)	0.34960(14)	0.0458(7)
C34	0.0407(6)	0.6378(2)	0.32865(15)	0.0540(8)
C35	0.2095(7)	0.6053(3)	0.27854(16)	0.0618(9)
C36	0.3971(7)	0.6614(3)	0.24780(16)	0.0608(9)
C37	0.4162(6)	0.7496(2)	0.26640(14)	0.0522(8)
C38	0.2496(5)	0.7841(2)	0.31789(13)	0.0433(7)
C39	0.2692(5)	0.8798(2)	0.33740(13)	0.0413(7)
C40	0.4503(6)	0.9409(2)	0.30497(14)	0.0498(8)

Table 4. Bond lengths (Å) for CyclohexynePrecursor_1.

C1-C15	1.370(4)	C1-C2	1.376(4)
C1-H1	0.95	C2-C3	1.382(4)
C2-H8	0.95	C3-C4	1.385(4)
C3-H5	0.95	C4-C16	1.407(4)
C4-C5	1.481(3)	C5-C6	1.474(4)
C5-C14	1.537(4)	C5-H17	1.0
C6-C7	1.313(3)	C6-C14	1.469(4)
C7-C19	1.502(4)	C7-C8	1.522(4)
C8-C9	1.527(4)	C8-H14	0.99
C8-H13	0.99	C9-C20	1.519(4)
C9-H12	0.99	C9-H2	0.99
C10-C18	1.377(4)	C10-C11	1.379(5)
C10-H3	0.95	C11-C12	1.379(4)
C11-H4	0.95	C12-C13	1.390(4)
C12-H19	0.95	C13-C17	1.405(4)
C13-C14	1.485(4)	C14-H18	1.0
C15-C16	1.403(4)	C15-H7	0.95
C16-C17	1.492(4)	C17-C18	1.401(4)
C18-H6	0.95	C19-C20	1.520(4)
C19-H16	0.99	C19-H15	0.99
C20-H10	0.99	C20-H11	0.99
C21-C40	1.372(4)	C21-C22	1.373(4)
C21-H20	0.95	C22-C23	1.387(4)
C22-H29	0.95	C23-C24	1.390(4)
C23-H31	0.95	C24-C39	1.407(4)
C24-C25	1.487(4)	C25-C26	1.473(4)
C25-C32	1.538(4)	C25-H32	1.0
C26-C27	1.315(4)	C26-C32	1.467(4)
C27-C31	1.503(4)	C27-C28	1.505(4)
C28-C29	1.511(4)	C28-H25	0.99
C28-H24	0.99	C29-C30	1.523(4)
C29-H21	0.99	C29-H23	0.99
C30-C31	1.520(4)	C30-H22	0.99
C30-H37	0.99	C31-H27	0.99
C31-H26	0.99	C32-C33	1.485(4)
C32-H36	1.0	C33-C34	1.391(4)
C33-C38	1.404(4)	C34-C35	1.381(4)
C34-H35	0.95	C35-C36	1.370(5)
C35-H34	0.95	C36-C37	1.377(4)
C36-H28	0.95	C37-C38	1.409(4)
C37-H33	0.95	C38-C39	1.486(4)
C39-C40	1.402(4)	C40-H30	0.95

Table 5. Bond angles (°) for CyclohexynePrecursor_1.

C15-C1-C2	120.5(3)	C15-C1-H1	119.8
C2-C1-H1	119.8	C1-C2-C3	119.1(3)
C1-C2-H8	120.4	C3-C2-H8	120.4
C2-C3-C4	121.4(3)	C2-C3-H5	119.3
C4-C3-H5	119.3	C3-C4-C16	119.8(3)
C3-C4-C5	118.9(2)	C16-C4-C5	121.3(2)
C6-C5-C4	118.4(2)	C6-C5-C14	58.34(17)
C4-C5-C14	117.8(2)	C6-C5-H17	116.6
C4-C5-H17	116.6	C14-C5-H17	116.6
C7-C6-C14	146.9(3)	C7-C6-C5	147.7(3)
C14-C6-C5	63.00(18)	C6-C7-C19	125.8(3)
C6-C7-C8	125.5(3)	C19-C7-C8	108.7(2)
C7-C8-C9	104.7(2)	C7-C8-H14	110.8
C9-C8-H14	110.8	C7-C8-H13	110.8
C9-C8-H13	110.8	H14-C8-H13	108.9
C20-C9-C8	104.4(2)	C20-C9-H12	110.9
C8-C9-H12	110.9	C20-C9-H2	110.9
C8-C9-H2	110.9	H12-C9-H2	108.9
C18-C10-C11	120.3(3)	C18-C10-H3	119.8
C11-C10-H3	119.8	C10-C11-C12	119.1(3)
C10-C11-H4	120.4	C12-C11-H4	120.4
C11-C12-C13	121.5(3)	C11-C12-H19	119.3
C13-C12-H19	119.3	C12-C13-C17	119.7(3)
C12-C13-C14	119.3(3)	C17-C13-C14	121.0(2)
C6-C14-C13	118.1(2)	C6-C14-C5	58.66(17)
C13-C14-C5	118.1(2)	C6-C14-H18	116.5
C13-C14-H18	116.5	C5-C14-H18	116.5
C1-C15-C16	121.7(3)	C1-C15-H7	119.2
C16-C15-H7	119.2	C15-C16-C4	117.5(3)
C15-C16-C17	121.8(2)	C4-C16-C17	120.7(2)
C18-C17-C13	117.6(3)	C18-C17-C16	121.6(3)
C13-C17-C16	120.7(2)	C10-C18-C17	121.7(3)
C10-C18-H6	119.2	C17-C18-H6	119.2
C7-C19-C20	104.2(2)	C7-C19-H16	110.9
C20-C19-H16	110.9	C7-C19-H15	110.9
C20-C19-H15	110.9	H16-C19-H15	108.9
C9-C20-C19	103.9(2)	C9-C20-H10	111.0
C19-C20-H10	111.0	C9-C20-H11	111.0
C19-C20-H11	111.0	H10-C20-H11	109.0
C40-C21-C22	120.4(3)	C40-C21-H20	119.8
C22-C21-H20	119.8	C21-C22-C23	119.2(3)

C21-C22-H29	120.4	C23-C22-H29	120.4
C22-C23-C24	121.1(3)	C22-C23-H31	119.5
C24-C23-H31	119.5	C23-C24-C39	120.1(3)
C23-C24-C25	119.0(3)	C39-C24-C25	120.9(3)
C26-C25-C24	118.5(2)	C26-C25-C32	58.29(19)
C24-C25-C32	117.8(2)	C26-C25-H32	116.5
C24-C25-H32	116.5	C32-C25-H32	116.5
C27-C26-C32	146.2(3)	C27-C26-C25	149.5(3)
C32-C26-C25	63.1(2)	C26-C27-C31	126.8(3)
C26-C27-C28	124.3(3)	C31-C27-C28	108.9(2)
C27-C28-C29	104.0(2)	C27-C28-H25	111.0
C29-C28-H25	111.0	C27-C28-H24	111.0
C29-C28-H24	111.0	H25-C28-H24	109.0
C28-C29-C30	104.0(3)	C28-C29-H21	111.0
C30-C29-H21	111.0	C28-C29-H23	111.0
C30-C29-H23	111.0	H21-C29-H23	109.0
C31-C30-C29	103.7(2)	C31-C30-H22	111.0
C29-C30-H22	111.0	C31-C30-H37	111.0
C29-C30-H37	111.0	H22-C30-H37	109.0
C27-C31-C30	105.0(2)	C27-C31-H27	110.7
C30-C31-H27	110.7	C27-C31-H26	110.7
C30-C31-H26	110.7	H27-C31-H26	108.8
C26-C32-C33	117.9(2)	C26-C32-C25	58.65(19)
C33-C32-C25	118.2(2)	C26-C32-H36	116.5
C33-C32-H36	116.5	C25-C32-H36	116.5
C34-C33-C38	119.7(3)	C34-C33-C32	119.5(3)
C38-C33-C32	120.8(3)	C35-C34-C33	121.5(3)
C35-C34-H35	119.2	C33-C34-H35	119.2
C36-C35-C34	119.3(3)	C36-C35-H34	120.3
C34-C35-H34	120.3	C35-C36-C37	120.3(3)
C35-C36-H28	119.8	C37-C36-H28	119.8
C36-C37-C38	121.7(3)	C36-C37-H33	119.2
C38-C37-H33	119.2	C33-C38-C37	117.4(3)
C33-C38-C39	121.1(3)	C37-C38-C39	121.5(3)
C40-C39-C24	117.1(3)	C40-C39-C38	121.9(3)
C24-C39-C38	120.9(3)	C21-C40-C39	122.1(3)
C21-C40-H30	118.9	C39-C40-H30	118.9

Table 6. Torsion angles (°) for CyclohexynePrecursor_1.

C15-C1-C2-C3	-0.7(4)	C1-C2-C3-C4	-0.6(4)
C2-C3-C4-C16	1.6(4)	C2-C3-C4-C5	-176.9(2)

C3-C4-C5-C6	117.0(3)	C16-C4-C5-C6	-61.5(3)
C3-C4-C5-C14	-175.9(2)	C16-C4-C5-C14	5.5(3)
C4-C5-C6-C7	-55.5(5)	C14-C5-C6-C7	-162.3(5)
C4-C5-C6-C14	106.8(3)	C14-C6-C7-C19	12.8(6)
C5-C6-C7-C19	163.1(4)	C14-C6-C7-C8	-164.9(4)
C5-C6-C7-C8	-14.6(6)	C6-C7-C8-C9	-177.2(3)
C19-C7-C8-C9	4.7(3)	C7-C8-C9-C20	-26.0(3)
C18-C10-C11-C12	1.8(5)	C10-C11-C12-C13	0.0(4)
C11-C12-C13-C17	-2.0(4)	C11-C12-C13-C14	176.4(2)
C7-C6-C14-C13	55.3(5)	C5-C6-C14-C13	-107.5(3)
C7-C6-C14-C5	162.7(5)	C12-C13-C14-C6	-116.4(3)
C17-C13-C14-C6	62.1(3)	C12-C13-C14-C5	176.2(2)
C17-C13-C14-C5	-5.4(3)	C4-C5-C14-C6	-107.8(2)
C6-C5-C14-C13	107.4(2)	C4-C5-C14-C13	-0.4(3)
C2-C1-C15-C16	1.0(4)	C1-C15-C16-C4	0.0(4)
C1-C15-C16-C17	-177.8(2)	C3-C4-C16-C15	-1.3(4)
C5-C4-C16-C15	177.2(2)	C3-C4-C16-C17	176.5(2)
C5-C4-C16-C17	-5.0(4)	C12-C13-C17-C18	2.1(4)
C14-C13-C17-C18	-176.3(2)	C12-C13-C17-C16	-175.3(2)
C14-C13-C17-C16	6.2(3)	C15-C16-C17-C18	-0.7(4)
C4-C16-C17-C18	-178.4(2)	C15-C16-C17-C13	176.7(2)
C4-C16-C17-C13	-1.0(4)	C11-C10-C18-C17	-1.7(4)
C13-C17-C18-C10	-0.3(4)	C16-C17-C18-C10	177.1(2)
C6-C7-C19-C20	-159.8(3)	C8-C7-C19-C20	18.3(3)
C8-C9-C20-C19	37.6(3)	C7-C19-C20-C9	-34.3(3)
C40-C21-C22-C23	1.3(4)	C21-C22-C23-C24	0.4(4)
C22-C23-C24-C39	-1.8(4)	C22-C23-C24-C25	176.5(2)
C23-C24-C25-C26	-116.5(3)	C39-C24-C25-C26	61.9(4)
C23-C24-C25-C32	176.5(2)	C39-C24-C25-C32	-5.2(4)
C24-C25-C26-C27	59.7(6)	C32-C25-C26-C27	166.5(5)
C24-C25-C26-C32	-106.8(3)	C32-C26-C27-C31	170.8(4)
C25-C26-C27-C31	12.8(7)	C32-C26-C27-C28	-10.1(6)
C25-C26-C27-C28	-168.2(4)	C26-C27-C28-C29	-162.9(3)
C31-C27-C28-C29	16.3(3)	C27-C28-C29-C30	-33.5(3)
C28-C29-C30-C31	38.3(3)	C26-C27-C31-C30	-173.4(3)
C28-C27-C31-C30	7.4(3)	C29-C30-C31-C27	-27.9(3)
C27-C26-C32-C33	-60.0(5)	C25-C26-C32-C33	107.7(3)
C27-C26-C32-C25	-167.7(5)	C24-C25-C32-C26	108.0(3)
C26-C25-C32-C33	-107.2(3)	C24-C25-C32-C33	0.8(4)
C26-C32-C33-C34	114.1(3)	C25-C32-C33-C34	-178.5(2)
C26-C32-C33-C38	-63.2(3)	C25-C32-C33-C38	4.2(4)
C38-C33-C34-C35	2.2(4)	C32-C33-C34-C35	-175.2(3)
C33-C34-C35-C36	-1.4(5)	C34-C35-C36-C37	-0.4(5)
C35-C36-C37-C38	1.3(5)	C34-C33-C38-C37	-1.3(4)

C32-C33-C38-C37	176.0(2)	C34-C33-C38-C39	177.8(2)
C32-C33-C38-C39	-4.9(4)	C36-C37-C38-C33	-0.4(4)
C36-C37-C38-C39	-179.4(3)	C23-C24-C39-C40	1.5(4)
C25-C24-C39-C40	-176.9(2)	C23-C24-C39-C38	-176.9(2)
C25-C24-C39-C38	4.8(4)	C33-C38-C39-C40	-177.9(2)
C37-C38-C39-C40	1.1(4)	C33-C38-C39-C24	0.4(4)
C37-C38-C39-C24	179.4(2)	C22-C21-C40-C39	-1.7(4)
C24-C39-C40-C21	0.3(4)	C38-C39-C40-C21	178.6(3)

Table 7. Anisotropic atomic displacement parameters (Å^2) for CyclohexynePrecursor_1.

The anisotropic atomic displacement factor exponent takes the form: $-2\pi^2[h^2 a^{*2} U_{11} + ... + 2 h k a^* b^* U_{12}]$

	U_{11}	U_{22}	U_{33}	U_{23}	U_{13}	U_{12}
C1	0.0537(18)	0.073(2)	0.0382(17)	-0.0067(16)	-0.0065(14)	-0.0219(17)
C2	0.069(2)	0.058(2)	0.0400(17)	-0.0130(15)	0.0048(15)	-0.0249(17)
C3	0.0525(17)	0.0464(17)	0.0365(16)	-0.0061(13)	0.0013(13)	-0.0088(14)
C4	0.0352(13)	0.0436(16)	0.0298(14)	-0.0051(12)	0.0036(11)	-0.0083(12)
C5	0.0338(13)	0.0425(16)	0.0345(15)	-0.0028(12)	-0.0005(11)	0.0005(12)
C6	0.0361(14)	0.0455(17)	0.0340(14)	-0.0043(12)	-0.0031(12)	-0.0049(12)
C7	0.0295(13)	0.0447(16)	0.0363(15)	-0.0040(12)	-0.0031(11)	-0.0052(12)
C8	0.0437(15)	0.0410(17)	0.0514(18)	-0.0040(13)	0.0010(14)	-0.0069(13)
C9	0.0479(16)	0.0515(19)	0.0503(18)	0.0013(14)	0.0051(14)	-0.0093(14)
C10	0.0521(18)	0.0431(19)	0.069(2)	-0.0028(16)	0.0116(17)	0.0013(15)
C11	0.065(2)	0.0433(19)	0.073(2)	-0.0148(16)	0.0154(19)	-0.0116(16)
C12	0.0475(17)	0.0534(19)	0.0531(18)	-0.0136(15)	0.0057(14)	-0.0169(15)
C13	0.0337(13)	0.0429(16)	0.0370(15)	-0.0049(12)	0.0084(12)	-0.0129(12)
C14	0.0307(13)	0.0491(17)	0.0365(15)	-0.0050(12)	-0.0008(11)	-0.0089(12)
C15	0.0406(15)	0.0562(19)	0.0388(16)	0.0020(14)	-0.0060(13)	-0.0090(14)

	U_{11}	U_{22}	U_{33}	U_{23}	U_{13}	U_{12}
C16	0.0333(13)	0.0464(17)	0.0313(14)	-0.0005(12)	0.0054(11)	-0.0085(12)
C17	0.0351(13)	0.0412(16)	0.0363(15)	-0.0032(12)	0.0075(12)	-0.0060(12)
C18	0.0455(16)	0.0489(19)	0.0492(18)	-0.0022(14)	0.0040(14)	-0.0038(14)
C19	0.0371(14)	0.0521(18)	0.0426(16)	-0.0078(13)	0.0005(12)	-0.0097(13)
C20	0.0352(14)	0.0532(18)	0.0439(16)	-0.0078(13)	0.0028(12)	-0.0055(13)
C21	0.0488(17)	0.052(2)	0.058(2)	0.0127(16)	-0.0081(15)	-0.0150(15)
C22	0.061(2)	0.0465(19)	0.058(2)	0.0049(15)	-0.0195(17)	-0.0066(16)
C23	0.0520(18)	0.0479(19)	0.0489(18)	0.0033(14)	-0.0073(15)	0.0004(15)
C24	0.0391(15)	0.0439(17)	0.0401(16)	0.0067(13)	-0.0102(12)	-0.0004(13)
C25	0.0406(15)	0.0485(18)	0.0460(17)	0.0057(14)	0.0000(13)	-0.0010(13)
C26	0.0431(15)	0.0443(17)	0.0421(16)	0.0026(13)	0.0028(13)	-0.0062(13)
C27	0.0420(15)	0.0398(16)	0.0385(15)	-0.0018(12)	0.0003(12)	-0.0040(12)
C28	0.0636(19)	0.0431(18)	0.0463(18)	-0.0034(14)	-0.0033(15)	0.0009(15)
C29	0.072(2)	0.056(2)	0.055(2)	0.0069(16)	-0.0097(17)	0.0010(17)
C30	0.0474(17)	0.070(2)	0.0506(19)	0.0004(16)	-0.0054(15)	-0.0091(16)
C31	0.0636(19)	0.0484(18)	0.0440(17)	-0.0061(14)	0.0005(15)	-0.0129(15)
C32	0.0396(15)	0.0506(18)	0.0496(18)	0.0072(14)	-0.0054(13)	-0.0115(13)
C33	0.0397(15)	0.0534(19)	0.0433(17)	0.0033(14)	-0.0152(13)	-0.0085(14)
C34	0.0530(19)	0.057(2)	0.055(2)	0.0001(16)	-0.0143(16)	-0.0190(16)
C35	0.072(2)	0.063(2)	0.054(2)	-0.0110(17)	-0.0214(18)	-0.0092(18)
C36	0.061(2)	0.072(2)	0.050(2)	-0.0107(17)	-0.0087(16)	-0.0067(18)
C37	0.0498(18)	0.061(2)	0.0438(17)	0.0004(15)	-0.0041(14)	-0.0094(15)
C38	0.0363(14)	0.0499(18)	0.0408(16)	0.0038(13)	-0.0121(12)	-0.0039(13)
C39	0.0364(14)	0.0440(17)	0.0391(15)	0.0077(13)	-0.0099(12)	-0.0028(12)

Crystal Structure Report for IBFTrap

A clear colourless rectangular-like specimen of $C_{26}H_{22}O$, approximate dimensions 0.150 mm x 0.180 mm x 0.460 mm, was used for the X-ray crystallographic analysis. The X-ray intensity data were measured.

The total exposure time was 15.41 hours. The frames were integrated with the Bruker SAINT software package using a narrow-frame algorithm. The integration of the data using an orthorhombic unit cell yielded a total of 18897 reflections to a maximum θ angle of 29.45° (0.72 Å resolution), of which 4908 were independent (average redundancy 3.850, completeness = 93.9%, R_{int} = 2.16%, R_{sig} = 2.01%) and 4526 (92.22%) were greater than $2\sigma(F^2)$. The final cell constants of a = 8.0338(5) Å, b = 12.0424(7) Å, c = 19.9450(12) Å, volume = 1929.6(2) $Å^3$, are based upon the refinement of the XYZ-centroids of 7063 reflections above 20 σ(I) with 5.303° < 2θ < 55.60°. Data were corrected for absorption effects using the multi-scan method (SADABS). The ratio of minimum to maximum apparent transmission was 0.891. The calculated minimum and maximum transmission coefficients (based on crystal size) are 0.9680 and 0.9890.

The final anisotropic full-matrix least-squares refinement on F^2 with 244 variables converged at R1 = 4.89%, for the observed data and wR2 = 14.23% for all data. The goodness-of-fit was 1.096. The largest peak in the final difference electron density synthesis was 0.315 $e^-/Å^3$ and the largest hole was -0.164 $e^-/Å^3$ with an RMS deviation of 0.048 $e^-/Å^3$. On the basis of the final model, the calculated density was 1.206 g/cm^3 and F(000), 744 e^-.

Table 1. Sample and crystal data for IBFTrap.

Identification code	IBFTrap	
Chemical formula	$C_{26}H_{22}O$	
Formula weight	350.43 g/mol	
Temperature	173(2) K	
Wavelength	0.71073 Å	
Crystal size	0.150 x 0.180 x 0.460 mm	
Crystal habit	clear colourless rectangular	
Crystal system	orthorhombic	
Space group	P 21 21 21	
Unit cell dimensions	a = 8.0338(5) Å	α = 90°
	b = 12.0424(7) Å	β = 90°
	c = 19.9450(12) Å	γ = 90°
Volume	1929.6(2) $Å^3$	
Z	4	
Density (calculated)	1.206 g/cm^3	
Absorption coefficient	0.072 mm^{-1}	

F(000)	744

Table 2. Data collection and structure refinement for IBFTrap.

Theta range for data collection	1.98 to 29.45°	
Index ranges	-10<=h<=10, -16<=k<=16, -24<=l<=26	
Reflections collected	18897	
Independent reflections	4908 [R(int) = 0.0216]	
Coverage of independent reflections	93.9%	
Absorption correction	multi-scan	
Max. and min. transmission	0.9890 and 0.9680	
Refinement method	Full-matrix least-squares on F^2	
Refinement program	SHELXL-2014/7 (Sheldrick, 2014)	
Function minimized	$\Sigma\, w(F_o^2 - F_c^2)^2$	
Data / restraints / parameters	4908 / 0 / 244	
Goodness-of-fit on F^2	1.096	
Final R indices	4526 data; I>2σ(I)	R1 = 0.0489, wR2 = 0.1365
	all data	R1 = 0.0531, wR2 = 0.1423
Weighting scheme	$w=1/[\sigma^2(F_o^2)+(0.1000P)^2]$ where $P=(F_o^2+2F_c^2)/3$	
Absolute structure parameter	0.3(5)	
Largest diff. peak and hole	0.315 and -0.164 eÅ^{-3}	
R.M.S. deviation from mean	0.048 eÅ^{-3}	

Table 3. Atomic coordinates and equivalent isotropic atomic displacement parameters (Å^2) for IBFTrap.

U(eq) is defined as one third of the trace of the orthogonalized U_{ij} tensor.

	x/a	y/b	z/c	U(eq)
O1	0.77747(16)	0.30586(11)	0.22241(7)	0.0311(3)
C1	0.8560(4)	0.1929(2)	0.46139(11)	0.0503(6)
C2	0.9489(3)	0.11638(19)	0.42562(12)	0.0498(6)
C3	0.9518(3)	0.12061(16)	0.35588(11)	0.0407(5)
C4	0.8632(2)	0.20243(16)	0.32165(9)	0.0320(4)

	x/a	y/b	z/c	U(eq)
C5	0.8681(2)	0.20897(15)	0.24672(9)	0.0296(4)
C6	0.8022(2)	0.28648(15)	0.15139(9)	0.0296(4)
C7	0.7185(2)	0.37338(15)	0.10923(10)	0.0336(4)
C8	0.6352(3)	0.46142(17)	0.13899(12)	0.0403(5)
C9	0.5506(3)	0.53827(19)	0.09929(14)	0.0519(6)
C10	0.5495(3)	0.5270(2)	0.03017(14)	0.0550(6)
C11	0.7671(3)	0.2737(2)	0.42795(12)	0.0483(5)
C12	0.7702(3)	0.27931(17)	0.35841(11)	0.0382(4)
C13	0.7823(2)	0.11753(15)	0.20497(10)	0.0311(4)
C14	0.7409(2)	0.16492(15)	0.14666(10)	0.0307(4)
C15	0.7205(3)	0.36384(18)	0.03960(11)	0.0422(5)
C16	0.6352(3)	0.4409(2)	0.00024(13)	0.0529(6)
C17	0.9940(2)	0.28016(15)	0.15069(10)	0.0318(4)
C18	0.1138(3)	0.31380(17)	0.10558(11)	0.0385(4)
C19	0.2806(3)	0.2956(2)	0.12256(12)	0.0463(5)
C20	0.3237(2)	0.24536(19)	0.18265(12)	0.0452(5)
C21	0.2006(2)	0.21022(17)	0.22824(12)	0.0390(4)
C22	0.0360(2)	0.22969(15)	0.21152(10)	0.0313(4)
C23	0.6577(3)	0.10632(17)	0.08995(11)	0.0381(4)
C24	0.5823(4)	0.99810(19)	0.11647(12)	0.0520(6)
C25	0.7040(4)	0.9338(2)	0.15885(14)	0.0598(7)
C26	0.7597(3)	0.99760(17)	0.22164(11)	0.0432(5)

Table 4. Bond lengths (Å) for IBFTrap.

O1-C6	1.449(2)	O1-C5	1.458(2)
C1-C11	1.379(3)	C1-C2	1.384(3)
C1-H1	0.95	C2-C3	1.392(3)
C2-H3	0.95	C3-C4	1.394(3)
C3-H4	0.95	C4-C12	1.398(3)
C4-C5	1.497(3)	C5-C22	1.541(3)
C5-C13	1.543(3)	C6-C7	1.501(2)
C6-C17	1.543(2)	C6-C14	1.547(2)
C7-C8	1.387(3)	C7-C15	1.394(3)
C8-C9	1.395(3)	C8-H7	0.95
C9-C10	1.385(4)	C9-H6	0.95
C10-C16	1.380(4)	C10-H2	0.95
C11-C12	1.389(3)	C11-H22	0.95
C12-H21	0.95	C13-C14	1.338(3)
C13-C26	1.493(3)	C14-C23	1.491(3)
C15-C16	1.396(3)	C15-H5	0.95

C16-H8	0.95	C17-C18	1.378(3)
C17-C22	1.398(3)	C18-C19	1.400(3)
C18-H12	0.95	C19-C20	1.387(3)
C19-H9	0.95	C20-C21	1.409(3)
C20-H11	0.95	C21-C22	1.383(3)
C21-H10	0.95	C23-C24	1.531(3)
C23-H20	0.99	C23-H13	0.99
C24-C25	1.506(4)	C24-H19	0.99
C24-H14	0.99	C25-C26	1.536(3)
C25-H15	0.99	C25-H18	0.99
C26-H17	0.99	C26-H16	0.99

Table 5. Bond angles (°) for IBFTrap.

C6-O1-C5	97.34(13)	C11-C1-C2	120.0(2)
C11-C1-H1	120.0	C2-C1-H1	120.0
C1-C2-C3	120.0(2)	C1-C2-H3	120.0
C3-C2-H3	120.0	C2-C3-C4	120.4(2)
C2-C3-H4	119.8	C4-C3-H4	119.8
C3-C4-C12	118.97(19)	C3-C4-C5	120.84(17)
C12-C4-C5	120.19(17)	O1-C5-C4	111.15(15)
O1-C5-C22	98.98(13)	C4-C5-C22	119.10(15)
O1-C5-C13	99.69(13)	C4-C5-C13	119.30(16)
C22-C5-C13	105.12(15)	O1-C6-C7	111.96(15)
O1-C6-C17	98.84(14)	C7-C6-C17	118.45(15)
O1-C6-C14	99.70(14)	C7-C6-C14	118.86(15)
C17-C6-C14	105.70(14)	C8-C7-C15	119.66(19)
C8-C7-C6	120.60(19)	C15-C7-C6	119.71(18)
C7-C8-C9	119.9(2)	C7-C8-H7	120.0
C9-C8-H7	120.0	C10-C9-C8	120.2(2)
C10-C9-H6	119.9	C8-C9-H6	119.9
C16-C10-C9	120.0(2)	C16-C10-H2	120.0
C9-C10-H2	120.0	C1-C11-C12	120.6(2)
C1-C11-H22	119.7	C12-C11-H22	119.7
C11-C12-C4	120.1(2)	C11-C12-H21	120.0
C4-C12-H21	120.0	C14-C13-C26	125.19(18)
C14-C13-C5	106.01(16)	C26-C13-C5	128.62(17)
C13-C14-C23	124.68(17)	C13-C14-C6	105.75(16)
C23-C14-C6	129.54(17)	C7-C15-C16	120.0(2)
C7-C15-H5	120.0	C16-C15-H5	120.0
C10-C16-C15	120.1(2)	C10-C16-H8	120.0
C15-C16-H8	120.0	C18-C17-C22	121.71(18)

C18-C17-C6	133.53(19)	C22-C17-C6	104.75(16)
C17-C18-C19	117.7(2)	C17-C18-H12	121.2
C19-C18-H12	121.2	C20-C19-C18	121.1(2)
C20-C19-H9	119.5	C18-C19-H9	119.5
C19-C20-C21	120.92(19)	C19-C20-H11	119.5
C21-C20-H11	119.5	C22-C21-C20	117.7(2)
C22-C21-H10	121.2	C20-C21-H10	121.2
C21-C22-C17	120.90(19)	C21-C22-C5	134.36(18)
C17-C22-C5	104.74(15)	C14-C23-C24	108.54(17)
C14-C23-H20	110.0	C24-C23-H20	110.0
C14-C23-H13	110.0	C24-C23-H13	110.0
H20-C23-H13	108.4	C25-C24-C23	112.0(2)
C25-C24-H19	109.2	C23-C24-H19	109.2
C25-C24-H14	109.2	C23-C24-H14	109.2
H19-C24-H14	107.9	C24-C25-C26	112.9(2)
C24-C25-H15	109.0	C26-C25-H15	109.0
C24-C25-H18	109.0	C26-C25-H18	109.0
H15-C25-H18	107.8	C13-C26-C25	109.74(18)
C13-C26-H17	109.7	C25-C26-H17	109.7
C13-C26-H16	109.7	C25-C26-H16	109.7
H17-C26-H16	108.2		

Table 6. Torsion angles (°) for IBFTrap.

C11-C1-C2-C3	-0.4(4)	C1-C2-C3-C4	0.8(4)
C2-C3-C4-C12	-0.6(3)	C2-C3-C4-C5	178.9(2)
C6-O1-C5-C4	-178.70(14)	C6-O1-C5-C22	55.20(14)
C6-O1-C5-C13	-51.95(15)	C3-C4-C5-O1	-175.44(17)
C12-C4-C5-O1	4.1(2)	C3-C4-C5-C22	-61.4(2)
C12-C4-C5-C22	118.06(19)	C3-C4-C5-C13	69.5(2)
C12-C4-C5-C13	-111.0(2)	C5-O1-C6-C7	178.85(14)
C5-O1-C6-C17	-55.52(15)	C5-O1-C6-C14	52.20(14)
O1-C6-C7-C8	2.2(2)	C17-C6-C7-C8	-111.8(2)
C14-C6-C7-C8	117.6(2)	O1-C6-C7-C15	-175.95(17)
C17-C6-C7-C15	70.0(2)	C14-C6-C7-C15	-60.5(2)
C15-C7-C8-C9	1.5(3)	C6-C7-C8-C9	-176.61(18)
C7-C8-C9-C10	0.0(3)	C8-C9-C10-C16	-1.4(4)
C2-C1-C11-C12	-0.1(4)	C1-C11-C12-C4	0.3(4)
C3-C4-C12-C11	0.1(3)	C5-C4-C12-C11	-179.37(19)
O1-C5-C13-C14	32.28(18)	C4-C5-C13-C14	153.32(16)
C22-C5-C13-C14	-69.85(18)	O1-C5-C13-C26	-152.4(2)
C4-C5-C13-C26	-31.4(3)	C22-C5-C13-C26	105.5(2)

C26-C13-C14-C23	3.1(3)	C5-C13-C14-C23	178.65(17)
C26-C13-C14-C6	-175.07(19)	C5-C13-C14-C6	0.46(19)
O1-C6-C14-C13	-33.31(17)	C7-C6-C14-C13	-155.13(17)
C17-C6-C14-C13	68.81(19)	O1-C6-C14-C23	148.62(19)
C7-C6-C14-C23	26.8(3)	C17-C6-C14-C23	-109.3(2)
C8-C7-C15-C16	-1.7(3)	C6-C7-C15-C16	176.45(19)
C9-C10-C16-C15	1.2(4)	C7-C15-C16-C10	0.4(3)
O1-C6-C17-C18	-144.1(2)	C7-C6-C17-C18	-23.2(3)
C14-C6-C17-C18	113.1(2)	O1-C6-C17-C22	34.86(18)
C7-C6-C17-C22	155.83(16)	C14-C6-C17-C22	-67.90(18)
C22-C17-C18-C19	0.1(3)	C6-C17-C18-C19	178.9(2)
C17-C18-C19-C20	0.1(3)	C18-C19-C20-C21	0.5(4)
C19-C20-C21-C22	-1.3(3)	C20-C21-C22-C17	1.5(3)
C20-C21-C22-C5	-177.7(2)	C18-C17-C22-C21	-0.9(3)
C6-C17-C22-C21	179.95(17)	C18-C17-C22-C5	178.47(17)
C6-C17-C22-C5	-0.66(19)	O1-C5-C22-C21	145.8(2)
C4-C5-C22-C21	25.4(3)	C13-C5-C22-C21	-111.6(2)
O1-C5-C22-C17	-33.51(17)	C4-C5-C22-C17	-153.91(17)
C13-C5-C22-C17	69.15(18)	C13-C14-C23-C24	16.9(3)
C6-C14-C23-C24	-165.4(2)	C14-C23-C24-C25	-47.7(3)
C23-C24-C25-C26	61.6(3)	C14-C13-C26-C25	7.5(3)
C5-C13-C26-C25	-167.0(2)	C24-C25-C26-C13	-38.8(3)

Table 7. Anisotropic atomic displacement parameters (Å^2) for IBFTrap.

The anisotropic atomic displacement factor exponent takes the form: $-2\pi^2[h^2 a^{*2} U_{11} + ... + 2 h k a^* b^* U_{12}]$

	U_{11}	U_{22}	U_{33}	U_{23}	U_{13}	U_{12}
O1	0.0270(6)	0.0313(6)	0.0349(6)	0.0009(5)	0.0009(5)	0.0044(5)
C1	0.0632(15)	0.0535(13)	0.0343(10)	-0.0040(10)	-0.0078(10)	0.0009(12)
C2	0.0635(15)	0.0439(11)	0.0421(12)	-0.0001(9)	-0.0125(11)	0.0066(11)
C3	0.0456(11)	0.0376(10)	0.0391(10)	-0.0029(8)	-0.0052(9)	0.0074(9)
C4	0.0296(9)	0.0313(8)	0.0350(9)	-0.0021(7)	-0.0027(7)	-0.0011(7)

	U_{11}	U_{22}	U_{33}	U_{23}	U_{13}	U_{12}
C5	0.0251(8)	0.0276(8)	0.0359(9)	0.0002(7)	-0.0018(6)	0.0022(6)
C6	0.0245(8)	0.0297(8)	0.0345(9)	0.0006(7)	0.0017(6)	-0.0001(6)
C7	0.0238(8)	0.0328(8)	0.0440(10)	0.0077(8)	-0.0017(7)	-0.0024(7)
C8	0.0339(10)	0.0344(9)	0.0526(12)	0.0045(9)	-0.0010(9)	0.0006(8)
C9	0.0425(11)	0.0377(10)	0.0754(17)	0.0137(11)	0.0003(11)	0.0085(9)
C10	0.0483(13)	0.0473(12)	0.0693(16)	0.0242(12)	-0.0104(12)	0.0006(11)
C11	0.0511(12)	0.0515(13)	0.0422(11)	-0.0110(10)	0.0003(10)	0.0068(10)
C12	0.0368(9)	0.0378(10)	0.0399(10)	-0.0044(8)	-0.0021(8)	0.0050(8)
C13	0.0269(8)	0.0307(8)	0.0358(9)	-0.0008(7)	0.0001(7)	-0.0021(6)
C14	0.0247(7)	0.0316(8)	0.0357(9)	0.0009(7)	0.0006(6)	-0.0013(6)
C15	0.0410(10)	0.0401(10)	0.0454(11)	0.0077(9)	-0.0009(9)	-0.0014(9)
C16	0.0535(14)	0.0547(13)	0.0504(13)	0.0185(11)	-0.0089(11)	-0.0048(11)
C17	0.0254(8)	0.0287(8)	0.0414(9)	-0.0018(7)	0.0011(7)	-0.0020(6)
C18	0.0316(9)	0.0391(10)	0.0448(10)	-0.0002(8)	0.0053(8)	-0.0061(8)
C19	0.0285(9)	0.0536(12)	0.0568(13)	-0.0068(10)	0.0082(9)	-0.0072(9)
C20	0.0229(9)	0.0503(12)	0.0623(13)	-0.0095(10)	0.0002(8)	-0.0006(9)
C21	0.0296(9)	0.0375(9)	0.0498(11)	-0.0064(9)	-0.0061(8)	0.0032(8)
C22	0.0250(8)	0.0286(8)	0.0404(9)	-0.0036(7)	0.0004(7)	-0.0001(6)
C23	0.0392(10)	0.0373(10)	0.0379(10)	-0.0010(8)	-0.0029(8)	-0.0013(8)
C24	0.0658(16)	0.0434(12)	0.0468(12)	-0.0019(10)	-0.0115(11)	-0.0164(11)
C25	0.086(2)	0.0361(11)	0.0578(15)	0.0018(10)	-0.0180(14)	-0.0095(13)
C26	0.0547(12)	0.0322(9)	0.0427(11)	0.0046(8)	-0.0075(9)	-0.0072(8)

Table 8. Hydrogen atomic coordinates and isotropic atomic displacement parameters (Å^2) for IBFTrap.

	x/a	y/b	z/c	U(eq)
H1	0.8534	0.1898	0.5090	0.06
H3	1.0107	0.0610	0.4487	0.06
H4	1.0146	0.0674	0.3315	0.049
H7	0.6357	0.4693	0.1864	0.048
H6	0.4935	0.5985	0.1197	0.062

	x/a	y/b	z/c	U(eq)
H2	0.4898	0.5786	0.0034	0.066
H22	0.7033	0.3260	0.4527	0.058
H21	0.7089	0.3355	0.3358	0.046
H5	0.7799	0.3049	0.0189	0.051
H8	0.6360	0.4341	-0.0472	0.063
H12	1.0842	0.3481	0.0644	0.046
H9	1.3658	0.3181	0.0924	0.056
H11	1.4378	0.2345	0.1932	0.054
H10	1.2295	0.1744	0.2690	0.047
H20	0.7398	0.0899	0.0543	0.046
H13	0.5692	0.1538	0.0707	0.046
H19	0.4824	0.0155	0.1435	0.062
H14	0.5469	-0.0485	0.0781	0.062
H15	0.8031	-0.0844	0.1315	0.072
H18	0.6518	-0.1370	0.1728	0.072
H17	0.6750	-0.0104	0.2574	0.052
H16	0.8659	-0.0335	0.2384	0.052

Crystal Structure Report for TetraPhenTrap

A clear colourless block-like specimen of $C_{34}H_{28}$, approximate dimensions 0.140 mm x 0.140 mm x 0.400 mm, was used for the X-ray crystallographic analysis. The X-ray intensity data were measured.

The total exposure time was 5.13 hours. The frames were integrated with the Bruker SAINT software package using a narrow-frame algorithm. The integration of the data using a tetragonal unit cell yielded a total of 42329 reflections to a maximum θ angle of 26.37° (0.80 Å resolution), of which 5132 were independent (average redundancy 8.248, completeness = 100.0%, R_{int} = 6.03%, R_{sig} = 3.37%) and 3253 (63.39%) were greater than $2\sigma(F^2)$. The final cell constants of a = 24.1562(17) Å, b = 24.1562(17) Å, c = 17.2185(12) Å, volume = 10047.4(16) $Å^3$, are based upon the refinement of the XYZ-centroids of 3827 reflections above 20 σ(I) with 4.451° < 2θ < 39.78°. Data were corrected for absorption effects using the multi-scan method (SADABS). The ratio of minimum to maximum apparent transmission was 0.864. The calculated minimum and maximum transmission coefficients (based on crystal size) are 0.9740 and 0.9910.

The final anisotropic full-matrix least-squares refinement on F^2 with 307 variables converged at R1 = 5.65%, for the observed data and wR2 = 18.74% for all data. The goodness-of-fit was 1.095. The largest peak in the final difference electron density synthesis was 0.386 $e^-/Å^3$ and the largest hole was -0.187 $e^-/Å^3$ with an RMS deviation of 0.038 $e^-/Å^3$. On the basis of the final model, the calculated density was 1.154 g/cm^3 and F(000), 3712 e^-.

Table 1. Sample and crystal data for TetraPhenTrap.

Identification code	TetraPhenTrap	
Chemical formula	$C_{34}H_{28}$	
Formula weight	436.56 g/mol	
Temperature	173(2) K	
Wavelength	0.71073 Å	
Crystal size	0.140 x 0.140 x 0.400 mm	
Crystal habit	clear colourless block	
Crystal system	tetragonal	
Space group	I 41/a	
Unit cell dimensions	a = 24.1562(17) Å	α = 90°
	b = 24.1562(17) Å	β = 90°
	c = 17.2185(12) Å	γ = 90°
Volume	10047.4(16) $Å^3$	
Z	16	

Density (calculated)	1.154 g/cm^3
Absorption coefficient	0.065 mm^{-1}
F(000)	3712

Table 2. Data collection and structure refinement for TetraPhenTrap.

Theta range for data collection	1.45 to 26.37°	
Index ranges	-30<=h<=30, -30<=k<=30, -21<=l<=20	
Reflections collected	42329	
Independent reflections	5132 [R(int) = 0.0603]	
Coverage of independent reflections	100.0%	
Absorption correction	multi-scan	
Max. and min. transmission	0.9910 and 0.9740	
Refinement method	Full-matrix least-squares on F^2	
Refinement program	SHELXL-2014/7 (Sheldrick, 2014)	
Function minimized	$\Sigma\, w(F_o^2 - F_c^2)^2$	
Data / restraints / parameters	5132 / 0 / 307	
Goodness-of-fit on F^2	1.095	
Final R indices	3253 data; $I>2\sigma(I)$	R1 = 0.0565, wR2 = 0.1535
	all data	R1 = 0.0970, wR2 = 0.1874
Weighting scheme	$w=1/[\sigma^2(F_o^2)+(0.1000P)^2]$ where $P=(F_o^2+2F_c^2)/3$	
Largest diff. peak and hole	0.386 and -0.187 $eÅ^{-3}$	
R.M.S. deviation from mean	0.038 $eÅ^{-3}$	

Table 3. Atomic coordinates and equivalent isotropic atomic displacement parameters ($Å^2$) for TetraPhenTrap.

U(eq) is defined as one third of the trace of the orthogonalized U_{ij} tensor.

	x/a	y/b	z/c	U(eq)
C1	0.06212(10)	0.04138(10)	0.96012(19)	0.0726(7)
C2	0.07366(10)	0.02773(10)	0.03576(18)	0.0727(7)
C3	0.11442(9)	0.98907(9)	0.05306(14)	0.0572(6)
C4	0.14463(8)	0.96440(7)	0.99413(11)	0.0428(5)

	x/a	y/b	z/c	U(eq)
C5	0.18727(7)	0.92085(7)	0.01108(10)	0.0389(4)
C6	0.24351(8)	0.93546(7)	0.01436(10)	0.0397(4)
C7	0.28310(7)	0.89466(8)	0.03102(10)	0.0404(5)
C8	0.26568(8)	0.83977(7)	0.04461(10)	0.0401(5)
C9	0.30773(8)	0.79587(8)	0.06156(11)	0.0428(5)
C10	0.32456(9)	0.78546(9)	0.13691(13)	0.0608(6)
C11	0.36324(10)	0.74477(11)	0.15389(16)	0.0718(7)
C12	0.38500(10)	0.71377(10)	0.09498(19)	0.0757(8)
C13	0.09214(10)	0.01766(9)	0.90143(16)	0.0655(7)
C14	0.13349(9)	0.97978(8)	0.91791(13)	0.0527(5)
C15	0.34405(7)	0.90934(8)	0.03672(12)	0.0487(5)
C16	0.35877(9)	0.96458(9)	0.00020(15)	0.0663(7)
C17	0.31898(8)	0.00855(9)	0.02202(15)	0.0618(6)
C18	0.26061(8)	0.99489(8)	0.99787(11)	0.0497(5)
C19	0.20970(8)	0.82560(7)	0.04143(10)	0.0392(4)
C20	0.19196(7)	0.76690(7)	0.05587(11)	0.0411(5)
C21	0.18073(9)	0.73096(9)	0.99573(12)	0.0557(6)
C22	0.16430(10)	0.67730(9)	0.00971(14)	0.0656(7)
C23	0.15795(9)	0.65855(9)	0.08384(14)	0.0614(6)
C24	0.16865(11)	0.69330(10)	0.14389(14)	0.0767(8)
C25	0.18591(11)	0.74702(9)	0.13039(12)	0.0671(7)
C26	0.17014(7)	0.86628(7)	0.02450(10)	0.0390(4)
C27	0.11009(8)	0.85102(7)	0.01875(11)	0.0409(5)
C28	0.07877(9)	0.83841(9)	0.08357(13)	0.0586(6)
C29	0.02354(10)	0.82376(10)	0.07661(16)	0.0697(7)
C30	0.99901(9)	0.82083(9)	0.00501(16)	0.0671(7)
C31	0.02920(9)	0.83302(9)	0.94024(16)	0.0639(6)
C32	0.08455(8)	0.84806(8)	0.94680(13)	0.0536(5)
C33	0.36853(11)	0.72284(10)	0.01985(18)	0.0796(8)
C34	0.33023(10)	0.76365(9)	0.00301(13)	0.0619(6)

Table 4. Bond lengths (Å) for TetraPhenTrap.

C1-C13	1.369(4)	C1-C2	1.372(4)
C1-H1	0.95	C2-C3	1.389(3)
C2-H6	0.95	C3-C4	1.385(3)
C3-H5	0.95	C4-C14	1.390(3)
C4-C5	1.501(3)	C5-C26	1.401(3)
C5-C6	1.405(3)	C6-C7	1.403(3)
C6-C18	1.521(3)	C7-C8	1.411(3)
C7-C15	1.517(2)	C8-C19	1.396(3)

C8-C9	1.497(3)	C9-C10	1.383(3)
C9-C34	1.385(3)	C10-C11	1.387(3)
C10-H25	0.95	C11-C12	1.366(4)
C11-H26	0.95	C12-C33	1.371(4)
C12-H2	0.95	C13-C14	1.384(3)
C13-H3	0.95	C14-H4	0.95
C15-C16	1.517(3)	C15-H14	0.99
C15-H7	0.99	C16-C17	1.481(3)
C16-H8	0.99	C16-H13	0.99
C17-C18	1.507(3)	C17-H9	0.99
C17-H10	0.99	C18-H12	0.99
C18-H11	0.99	C19-C26	1.402(3)
C19-C20	1.502(2)	C20-C25	1.378(3)
C20-C21	1.378(3)	C21-C22	1.377(3)
C21-H19	0.95	C22-C23	1.363(3)
C22-H15	0.95	C23-C24	1.357(3)
C23-H16	0.95	C24-C25	1.383(3)
C24-H18	0.95	C25-H17	0.95
C26-C27	1.500(2)	C27-C28	1.382(3)
C27-C32	1.386(3)	C28-C29	1.385(3)
C28-H24	0.95	C29-C30	1.370(3)
C29-H20	0.95	C30-C31	1.365(3)
C30-H23	0.95	C31-C32	1.390(3)
C31-H22	0.95	C32-H21	0.95
C33-C34	1.383(3)	C33-H27	0.95
C34-H28	0.95		

Table 5. Bond angles (°) for TetraPhenTrap.

C13-C1-C2	119.5(2)	C13-C1-H1	120.3
C2-C1-H1	120.3	C1-C2-C3	120.6(2)
C1-C2-H6	119.7	C3-C2-H6	119.7
C4-C3-C2	120.4(2)	C4-C3-H5	119.8
C2-C3-H5	119.8	C3-C4-C14	118.33(19)
C3-C4-C5	121.39(18)	C14-C4-C5	120.25(18)
C26-C5-C6	121.04(17)	C26-C5-C4	119.26(16)
C6-C5-C4	119.69(16)	C7-C6-C5	119.41(16)
C7-C6-C18	121.08(16)	C5-C6-C18	119.50(16)
C6-C7-C8	119.39(16)	C6-C7-C15	120.69(16)
C8-C7-C15	119.90(16)	C19-C8-C7	120.86(16)
C19-C8-C9	119.42(16)	C7-C8-C9	119.71(16)
C10-C9-C34	117.75(19)	C10-C9-C8	120.74(18)

C34-C9-C8	121.50(18)	C9-C10-C11	121.6(2)
C9-C10-H25	119.2	C11-C10-H25	119.2
C12-C11-C10	119.4(2)	C12-C11-H26	120.3
C10-C11-H26	120.3	C11-C12-C33	120.1(2)
C11-C12-H2	120.0	C33-C12-H2	120.0
C1-C13-C14	120.5(2)	C1-C13-H3	119.8
C14-C13-H3	119.8	C13-C14-C4	120.7(2)
C13-C14-H4	119.7	C4-C14-H4	119.7
C16-C15-C7	113.97(17)	C16-C15-H14	108.8
C7-C15-H14	108.8	C16-C15-H7	108.8
C7-C15-H7	108.8	H14-C15-H7	107.7
C17-C16-C15	111.92(18)	C17-C16-H8	109.2
C15-C16-H8	109.2	C17-C16-H13	109.2
C15-C16-H13	109.2	H8-C16-H13	107.9
C16-C17-C18	112.36(18)	C16-C17-H9	109.1
C18-C17-H9	109.1	C16-C17-H10	109.1
C18-C17-H10	109.1	H9-C17-H10	107.9
C17-C18-C6	114.17(17)	C17-C18-H12	108.7
C6-C18-H12	108.7	C17-C18-H11	108.7
C6-C18-H11	108.7	H12-C18-H11	107.6
C8-C19-C26	119.79(16)	C8-C19-C20	120.09(16)
C26-C19-C20	120.11(16)	C25-C20-C21	117.34(18)
C25-C20-C19	120.89(17)	C21-C20-C19	121.76(17)
C22-C21-C20	121.2(2)	C22-C21-H19	119.4
C20-C21-H19	119.4	C23-C22-C21	120.6(2)
C23-C22-H15	119.7	C21-C22-H15	119.7
C24-C23-C22	119.1(2)	C24-C23-H16	120.4
C22-C23-H16	120.4	C23-C24-C25	120.7(2)
C23-C24-H18	119.7	C25-C24-H18	119.7
C20-C25-C24	121.0(2)	C20-C25-H17	119.5
C24-C25-H17	119.5	C5-C26-C19	119.51(16)
C5-C26-C27	120.41(16)	C19-C26-C27	120.06(16)
C28-C27-C32	117.82(19)	C28-C27-C26	122.02(17)
C32-C27-C26	120.14(17)	C27-C28-C29	120.9(2)
C27-C28-H24	119.5	C29-C28-H24	119.5
C30-C29-C28	120.5(2)	C30-C29-H20	119.7
C28-C29-H20	119.7	C31-C30-C29	119.6(2)
C31-C30-H23	120.2	C29-C30-H23	120.2
C30-C31-C32	120.3(2)	C30-C31-H22	119.9
C32-C31-H22	119.9	C27-C32-C31	121.0(2)
C27-C32-H21	119.5	C31-C32-H21	119.5
C12-C33-C34	120.4(2)	C12-C33-H27	119.8
C34-C33-H27	119.8	C33-C34-C9	120.7(2)
C33-C34-H28	119.6	C9-C34-H28	119.6

Table 6. Torsion angles (°) for TetraPhenTrap.

C13-C1-C2-C3	-1.7(4)	C1-C2-C3-C4	1.1(3)
C2-C3-C4-C14	0.7(3)	C2-C3-C4-C5	-177.49(19)
C3-C4-C5-C26	80.2(2)	C14-C4-C5-C26	-97.9(2)
C3-C4-C5-C6	-98.9(2)	C14-C4-C5-C6	83.0(2)
C26-C5-C6-C7	0.3(3)	C4-C5-C6-C7	179.35(16)
C26-C5-C6-C18	178.78(17)	C4-C5-C6-C18	-2.1(3)
C5-C6-C7-C8	-0.3(3)	C18-C6-C7-C8	-178.84(17)
C5-C6-C7-C15	-178.65(16)	C18-C6-C7-C15	2.9(3)
C6-C7-C8-C19	0.2(3)	C15-C7-C8-C19	178.53(16)
C6-C7-C8-C9	179.32(17)	C15-C7-C8-C9	-2.4(3)
C19-C8-C9-C10	-92.0(2)	C7-C8-C9-C10	88.9(2)
C19-C8-C9-C34	86.7(2)	C7-C8-C9-C34	-92.4(2)
C34-C9-C10-C11	0.9(3)	C8-C9-C10-C11	179.6(2)
C9-C10-C11-C12	-0.6(4)	C10-C11-C12-C33	-0.2(4)
C2-C1-C13-C14	0.6(3)	C1-C13-C14-C4	1.1(3)
C3-C4-C14-C13	-1.8(3)	C5-C4-C14-C13	176.42(18)
C6-C7-C15-C16	-17.4(3)	C8-C7-C15-C16	164.34(18)
C7-C15-C16-C17	45.2(3)	C15-C16-C17-C18	-59.2(3)
C16-C17-C18-C6	43.8(3)	C7-C6-C18-C17	-15.8(3)
C5-C6-C18-C17	165.73(18)	C7-C8-C19-C26	0.0(3)
C9-C8-C19-C26	-179.09(17)	C7-C8-C19-C20	179.85(17)
C9-C8-C19-C20	0.7(3)	C8-C19-C20-C25	81.8(2)
C26-C19-C20-C25	-98.4(2)	C8-C19-C20-C21	-98.6(2)
C26-C19-C20-C21	81.2(2)	C25-C20-C21-C22	-0.2(3)
C19-C20-C21-C22	-179.8(2)	C20-C21-C22-C23	0.9(4)
C21-C22-C23-C24	-0.8(4)	C22-C23-C24-C25	-0.1(4)
C21-C20-C25-C24	-0.7(4)	C19-C20-C25-C24	178.9(2)
C23-C24-C25-C20	0.9(4)	C6-C5-C26-C19	0.0(3)
C4-C5-C26-C19	-179.12(16)	C6-C5-C26-C27	-178.40(16)
C4-C5-C26-C27	2.5(3)	C8-C19-C26-C5	-0.1(3)
C20-C19-C26-C5	-179.94(16)	C8-C19-C26-C27	178.26(16)
C20-C19-C26-C27	-1.6(3)	C5-C26-C27-C28	-108.7(2)

C19-C26-C27-C28	73.0(2)	C5-C26-C27-C32	72.7(2)
C19-C26-C27-C32	-105.6(2)	C32-C27-C28-C29	-0.5(3)
C26-C27-C28-C29	-179.2(2)	C27-C28-C29-C30	0.8(4)
C28-C29-C30-C31	-0.7(4)	C29-C30-C31-C32	0.3(3)
C28-C27-C32-C31	0.2(3)	C26-C27-C32-C31	178.84(18)
C30-C31-C32-C27	-0.1(3)	C11-C12-C33-C34	0.6(4)
C12-C33-C34-C9	-0.2(4)	C10-C9-C34-C33	-0.5(3)
C8-C9-C34-C33	-179.2(2)		

Table 7. Anisotropic atomic displacement parameters (Å^2) for TetraPhenTrap.

The anisotropic atomic displacement factor exponent takes the form: $-2\pi^2[h^2 a^{*2} U_{11} + ... + 2 h k a^* b^* U_{12}]$

	U_{11}	U_{22}	U_{33}	U_{23}	U_{13}	U_{12}
C1	0.0518(14)	0.0452(13)	0.121(2)	0.0062(14)	-0.0152(15)	0.0065(11)
C2	0.0585(15)	0.0558(15)	0.104(2)	-0.0118(14)	0.0136(14)	0.0097(12)
C3	0.0538(13)	0.0546(13)	0.0631(15)	-0.0042(11)	0.0037(11)	0.0031(10)
C4	0.0396(11)	0.0354(10)	0.0534(13)	0.0002(9)	-0.0050(9)	-0.0028(8)
C5	0.0409(10)	0.0383(10)	0.0375(10)	-0.0010(8)	-0.0015(8)	0.0006(8)
C6	0.0436(11)	0.0391(10)	0.0363(10)	-0.0017(8)	0.0003(8)	-0.0023(8)
C7	0.0381(10)	0.0444(11)	0.0386(11)	-0.0006(8)	-0.0011(8)	-0.0012(8)
C8	0.0408(10)	0.0410(10)	0.0385(11)	-0.0006(8)	-0.0011(8)	0.0021(8)
C9	0.0373(10)	0.0398(10)	0.0513(12)	0.0034(9)	0.0013(9)	-0.0018(8)
C10	0.0579(14)	0.0631(14)	0.0613(15)	0.0084(11)	-0.0029(11)	0.0133(11)
C11	0.0617(15)	0.0711(16)	0.0827(18)	0.0280(14)	-0.0038(13)	0.0102(12)
C12	0.0516(14)	0.0537(14)	0.122(2)	0.0287(15)	0.0141(15)	0.0124(11)
C13	0.0627(15)	0.0517(13)	0.0820(18)	0.0111(12)	-0.0224(13)	-0.0003(11)
C14	0.0541(13)	0.0460(12)	0.0580(14)	0.0039(10)	-0.0080(10)	0.0022(10)
C15	0.0385(11)	0.0498(12)	0.0579(13)	-0.0006(10)	0.0011(9)	-0.0005(9)
C16	0.0489(13)	0.0588(14)	0.0912(19)	0.0023(13)	0.0059(12)	-

	U_{11}	U_{22}	U_{33}	U_{23}	U_{13}	U_{12}
						0.0080(11)
C17	0.0488(13)	0.0466(12)	0.0898(17)	0.0028(11)	-0.0024(12)	-0.0085(10)
C18	0.0472(12)	0.0419(11)	0.0598(14)	0.0045(10)	-0.0005(10)	-0.0042(9)
C19	0.0406(10)	0.0402(10)	0.0368(10)	0.0007(8)	-0.0040(8)	-0.0016(8)
C20	0.0365(10)	0.0394(10)	0.0473(12)	0.0006(9)	-0.0050(8)	0.0004(8)
C21	0.0671(15)	0.0526(13)	0.0475(13)	-0.0039(10)	0.0004(10)	-0.0082(10)
C22	0.0770(17)	0.0509(14)	0.0689(16)	-0.0151(12)	-0.0028(13)	-0.0113(11)
C23	0.0606(14)	0.0453(12)	0.0783(17)	0.0117(12)	-0.0173(12)	-0.0094(10)
C24	0.115(2)	0.0592(15)	0.0561(15)	0.0145(12)	-0.0201(14)	-0.0290(15)
C25	0.1011(19)	0.0527(13)	0.0474(14)	0.0016(10)	-0.0116(12)	-0.0213(13)
C26	0.0383(10)	0.0419(11)	0.0370(10)	-0.0022(8)	-0.0026(8)	-0.0007(8)
C27	0.0390(10)	0.0319(9)	0.0518(12)	-0.0036(8)	-0.0029(9)	0.0006(8)
C28	0.0520(13)	0.0640(14)	0.0598(14)	-0.0050(11)	0.0048(11)	-0.0077(10)
C29	0.0530(14)	0.0687(16)	0.0874(19)	-0.0076(14)	0.0209(13)	-0.0074(12)
C30	0.0381(12)	0.0513(13)	0.112(2)	-0.0184(14)	-0.0048(13)	0.0036(10)
C31	0.0485(13)	0.0593(14)	0.0839(18)	-0.0107(12)	-0.0201(12)	0.0050(11)
C32	0.0486(12)	0.0518(12)	0.0603(14)	-0.0043(10)	-0.0085(10)	0.0017(10)
C33	0.0757(18)	0.0589(16)	0.104(2)	-0.0003(15)	0.0206(16)	0.0188(13)
C34	0.0634(15)	0.0548(14)	0.0675(16)	-0.0039(11)	0.0088(11)	0.0116(11)

Table 8. Hydrogen atomic coordinates and isotropic atomic displacement parameters (Å^2) for TetraPhenTrap.

	x/a	y/b	z/c	U(eq)
H1	0.0335	1.0671	-0.0514	0.087
H6	0.0536	1.0449	0.0767	0.087
H5	0.1216	0.9795	0.1056	0.069

	x/a	y/b	z/c	U(eq)
H25	0.3093	0.8067	0.1781	0.073
H26	0.3745	0.7385	0.2060	0.086
H2	0.4116	0.6859	0.1061	0.091
H3	0.0845	1.0273	-0.1510	0.079
H4	0.1545	0.9641	-0.1233	0.063
H14	0.3548	0.9101	0.0922	0.058
H7	0.3659	0.8799	0.0111	0.058
H8	0.3964	0.9756	0.0170	0.08
H13	0.3592	0.9606	-0.0570	0.08
H9	0.3303	1.0438	-0.0027	0.074
H10	0.3201	1.0139	0.0790	0.074
H12	0.2568	1.0020	-0.0585	0.06
H11	0.2349	1.0201	0.0253	0.06
H19	0.1844	0.7434	-0.0563	0.067
H15	0.1573	0.6531	-0.0327	0.079
H16	0.1462	0.6216	0.0933	0.074
H18	0.1642	0.6806	0.1957	0.092
H17	0.1937	0.7706	0.1732	0.08
H24	0.0953	0.8398	0.1336	0.07
H20	0.0025	0.8157	0.1218	0.084
H23	-0.0388	0.8104	0.0005	0.081
H22	0.0123	0.8312	-0.1095	0.077
H21	0.1052	0.8564	-0.0987	0.064
H27	0.3835	0.7010	-0.0209	0.096
H28	0.3192	0.7697	-0.0493	0.074

Crystal Structure Report for BisanthraToluene

A clear colourless block-like specimen of $C_{35}H_{24}$, approximate dimensions 0.140 mm x 0.160 mm x 0.310 mm, was used for the X-ray crystallographic analysis. The X-ray intensity data were measured.

The total exposure time was 15.41 hours. The frames were integrated with the Bruker SAINT software package using a narrow-frame algorithm. The integration of the data using a triclinic unit cell yielded a total of 11133 reflections to a maximum θ angle of 29.36° (0.72 Å resolution), of which 5567 were independent (average redundancy 2.000, completeness = 87.9%, R_{int} = 1.73%, R_{sig} = 2.77%) and 4223 (75.86%) were greater than $2\sigma(F^2)$. The final cell constants of a = 9.4155(7) Å, b = 11.4502(9) Å, c = 11.4893(9) Å, α = 103.4850(10)°, β = 106.1810(10)°, γ = 91.2110(10)°, volume = 1151.86(15) $Å^3$, are based upon the refinement of the XYZ-centroids of 3225 reflections above 20 σ(I) with 4.523° < 2θ < 57.77°. Data were corrected for absorption effects using the multi-scan method (SADABS). The ratio of minimum to maximum apparent transmission was 0.887. The calculated minimum and maximum transmission coefficients (based on crystal size) are 0.9780 and 0.9900.

The final anisotropic full-matrix least-squares refinement on F^2 with 317 variables converged at R1 = 5.62%, for the observed data and wR2 = 17.65% for all data. The goodness-of-fit was 1.156. The largest peak in the final difference electron density synthesis was 0.362 $e^-/Å^3$ and the largest hole was -0.175 $e^-/Å^3$ with an RMS deviation of 0.053 $e^-/Å^3$. On the basis of the final model, the calculated density was 1.282 g/cm^3 and F(000), 468 e^-.

Table 1. Sample and crystal data for BisanthraToluene.

Identification code	BisanthraToluene	
Chemical formula	$C_{35}H_{24}$	
Formula weight	444.54 g/mol	
Temperature	173(2) K	
Wavelength	0.71073 Å	
Crystal size	0.140 x 0.160 x 0.310 mm	
Crystal habit	clear colourless block	
Crystal system	triclinic	
Space group	P -1	
Unit cell dimensions	a = 9.4155(7) Å	α = 103.4850(10)°
	b = 11.4502(9) Å	β = 106.1810(10)°
	c = 11.4893(9) Å	γ = 91.2110(10)°
Volume	1151.86(15) $Å^3$	
Z	2	

Density (calculated)	1.282 g/cm^3
Absorption coefficient	0.072 mm^{-1}
F(000)	468

Table 2. Data collection and structure refinement for BisanthraToluene.

Theta range for data collection	1.84 to 29.36°	
Index ranges	-12<=h<=12, -15<=k<=15, -15<=l<=15	
Reflections collected	11133	
Independent reflections	5567 [R(int) = 0.0173]	
Coverage of independent reflections	87.9%	
Absorption correction	multi-scan	
Max. and min. transmission	0.9900 and 0.9780	
Refinement method	Full-matrix least-squares on F^2	
Refinement program	SHELXL-2014/7 (Sheldrick, 2014)	
Function minimized	$\Sigma\, w(F_o^2 - F_c^2)^2$	
Data / restraints / parameters	5567 / 0 / 317	
Goodness-of-fit on F^2	1.156	
Final R indices	4223 data; I>2σ(I)	R1 = 0.0562, wR2 = 0.1558
	all data	R1 = 0.0724, wR2 = 0.1765
Weighting scheme	$w=1/[\sigma^2(F_o^2)+(0.1000P)^2]$ where $P=(F_o^2+2F_c^2)/3$	
Largest diff. peak and hole	0.362 and -0.175 eÅ^{-3}	
R.M.S. deviation from mean	0.053 eÅ^{-3}	

Table 3. Atomic coordinates and equivalent isotropic atomic displacement parameters (Å^2) for BisanthraToluene.

U(eq) is defined as one third of the trace of the orthogonalized U_{ij} tensor.

	x/a	y/b	z/c	U(eq)
C1	0.36835(17)	0.26388(15)	0.63980(15)	0.0388(4)
C2	0.22540(17)	0.28519(13)	0.63203(13)	0.0337(3)
C3	0.13012(16)	0.31609(12)	0.52526(12)	0.0270(3)
C4	0.18967(15)	0.32623(12)	0.42503(12)	0.0268(3)

	x/a	y/b	z/c	U(eq)
C5	0.09695(15)	0.35495(12)	0.31784(12)	0.0255(3)
C6	0.15710(14)	0.36679(12)	0.21262(12)	0.0251(3)
C7	0.14571(14)	0.26663(12)	0.11171(12)	0.0251(3)
C8	0.19726(14)	0.28121(12)	0.01173(12)	0.0256(3)
C9	0.17796(15)	0.17901(12)	0.89822(12)	0.0262(3)
C10	0.03507(15)	0.14548(12)	0.81209(12)	0.0272(3)
C11	0.90954(16)	0.20925(13)	0.82496(13)	0.0337(3)
C12	0.77357(18)	0.17584(15)	0.73946(15)	0.0409(4)
C13	0.75192(19)	0.07506(16)	0.63515(15)	0.0439(4)
C14	0.5419(2)	0.99821(17)	0.82163(18)	0.0495(5)
C15	0.4032(2)	0.96085(15)	0.74483(16)	0.0432(4)
C16	0.27771(18)	0.01927(13)	0.76770(14)	0.0339(3)
C17	0.13513(18)	0.98375(13)	0.68679(13)	0.0359(4)
C18	0.01360(17)	0.04501(12)	0.70451(13)	0.0311(3)
C19	0.86805(19)	0.01225(14)	0.61862(14)	0.0389(4)
C20	0.30056(16)	0.11908(12)	0.87584(13)	0.0293(3)
C21	0.44887(16)	0.15392(14)	0.95558(14)	0.0355(3)
C22	0.56571(19)	0.09683(16)	0.92910(17)	0.0446(4)
C23	0.26182(16)	0.39316(12)	0.01575(13)	0.0305(3)
C24	0.27499(17)	0.49102(13)	0.11595(14)	0.0345(3)
C25	0.22166(16)	0.47794(12)	0.21399(13)	0.0314(3)
C26	0.07651(17)	0.14641(13)	0.11099(14)	0.0340(3)
C27	0.94608(15)	0.37070(12)	0.30742(12)	0.0270(3)
C28	0.84588(16)	0.39547(13)	0.19869(13)	0.0326(3)
C29	0.70069(17)	0.40813(14)	0.19077(15)	0.0381(4)
C30	0.64375(17)	0.39927(14)	0.29061(16)	0.0397(4)
C31	0.73455(16)	0.37640(13)	0.39558(15)	0.0346(3)
C32	0.88751(15)	0.35983(12)	0.40831(13)	0.0277(3)
C33	0.98137(16)	0.33390(12)	0.51471(13)	0.0289(3)
C34	0.42681(17)	0.27331(15)	0.54050(15)	0.0401(4)
C35	0.34045(16)	0.30354(14)	0.43699(14)	0.0337(3)

Table 4. Bond lengths (Å) for BisanthraToluene.

C1-C2	1.355(2)	C1-C34	1.422(2)
C1-H1	0.95	C2-C3	1.427(2)
C2-H18	0.95	C3-C33	1.395(2)
C3-C4	1.4400(17)	C4-C5	1.4103(19)
C4-C35	1.423(2)	C5-C27	1.4111(19)
C5-C6	1.5016(16)	C6-C25	1.3937(18)
C6-C7	1.4058(18)	C7-C8	1.4070(16)

C7-C26	1.5077(18)	C8-C23	1.3924(18)
C8-C9	1.5001(18)	C9-C20	1.4093(19)
C9-C10	1.4127(19)	C10-C11	1.427(2)
C10-C18	1.4421(19)	C11-C12	1.361(2)
C11-H6	0.95	C12-C13	1.421(2)
C12-H23	0.95	C13-C19	1.354(2)
C13-H2	0.95	C14-C15	1.351(3)
C14-C22	1.426(3)	C14-H3	0.95
C15-C16	1.427(2)	C15-H24	0.95
C16-C17	1.392(2)	C16-C20	1.440(2)
C17-C18	1.393(2)	C17-H4	0.95
C18-C19	1.430(2)	C19-H5	0.95
C20-C21	1.429(2)	C21-C22	1.362(2)
C21-H7	0.95	C22-H8	0.95
C23-C24	1.382(2)	C23-H22	0.95
C24-C25	1.3906(18)	C24-H21	0.95
C25-H9	0.95	C26-H11	0.98
C26-H12	0.98	C26-H10	0.98
C27-C28	1.4321(19)	C27-C32	1.4436(17)
C28-C29	1.358(2)	C28-H13	0.95
C29-C30	1.417(2)	C29-H14	0.95
C30-C31	1.355(2)	C30-H15	0.95
C31-C32	1.428(2)	C31-H16	0.95
C32-C33	1.393(2)	C33-H17	0.95
C34-C35	1.364(2)	C34-H20	0.95
C35-H19	0.95		

Table 5. Bond angles (°) for BisanthraToluene.

C2-C1-C34	119.87(14)	C2-C1-H1	120.1
C34-C1-H1	120.1	C1-C2-C3	121.58(13)
C1-C2-H18	119.2	C3-C2-H18	119.2
C33-C3-C2	121.85(12)	C33-C3-C4	119.64(12)
C2-C3-C4	118.50(13)	C5-C4-C35	122.32(12)
C5-C4-C3	119.47(12)	C35-C4-C3	118.18(12)
C4-C5-C27	120.31(12)	C4-C5-C6	120.33(12)
C27-C5-C6	119.35(12)	C25-C6-C7	120.01(12)
C25-C6-C5	119.84(11)	C7-C6-C5	120.13(11)
C6-C7-C8	119.07(11)	C6-C7-C26	119.82(12)
C8-C7-C26	121.10(12)	C23-C8-C7	119.69(12)
C23-C8-C9	119.39(11)	C7-C8-C9	120.87(11)
C20-C9-C10	120.30(12)	C20-C9-C8	120.79(12)

C10-C9-C8	118.89(12)	C9-C10-C11	122.60(13)
C9-C10-C18	119.63(13)	C11-C10-C18	117.75(13)
C12-C11-C10	121.28(14)	C12-C11-H6	119.4
C10-C11-H6	119.4	C11-C12-C13	120.86(15)
C11-C12-H23	119.6	C13-C12-H23	119.6
C19-C13-C12	119.95(15)	C19-C13-H2	120.0
C12-C13-H2	120.0	C15-C14-C22	120.32(15)
C15-C14-H3	119.8	C22-C14-H3	119.8
C14-C15-C16	121.29(16)	C14-C15-H24	119.4
C16-C15-H24	119.4	C17-C16-C15	121.60(14)
C17-C16-C20	119.54(13)	C15-C16-C20	118.85(15)
C16-C17-C18	121.84(13)	C16-C17-H4	119.1
C18-C17-H4	119.1	C17-C18-C19	122.08(14)
C17-C18-C10	119.14(13)	C19-C18-C10	118.78(14)
C13-C19-C18	121.35(14)	C13-C19-H5	119.3
C18-C19-H5	119.3	C9-C20-C21	122.74(13)
C9-C20-C16	119.42(13)	C21-C20-C16	117.84(13)
C22-C21-C20	121.35(15)	C22-C21-H7	119.3
C20-C21-H7	119.3	C21-C22-C14	120.34(16)
C21-C22-H8	119.8	C14-C22-H8	119.8
C24-C23-C8	121.12(12)	C24-C23-H22	119.4
C8-C23-H22	119.4	C23-C24-C25	119.53(12)
C23-C24-H21	120.2	C25-C24-H21	120.2
C24-C25-C6	120.55(12)	C24-C25-H9	119.7
C6-C25-H9	119.7	C7-C26-H11	109.5
C7-C26-H12	109.5	H11-C26-H12	109.5
C7-C26-H10	109.5	H11-C26-H10	109.5
H12-C26-H10	109.5	C5-C27-C28	122.55(12)
C5-C27-C32	119.69(12)	C28-C27-C32	117.75(12)
C29-C28-C27	121.09(13)	C29-C28-H13	119.5
C27-C28-H13	119.5	C28-C29-C30	121.14(14)
C28-C29-H14	119.4	C30-C29-H14	119.4
C31-C30-C29	119.86(14)	C31-C30-H15	120.1
C29-C30-H15	120.1	C30-C31-C32	121.55(13)
C30-C31-H16	119.2	C32-C31-H16	119.2
C33-C32-C31	122.13(12)	C33-C32-C27	119.28(12)
C31-C32-C27	118.60(13)	C32-C33-C3	121.59(12)
C32-C33-H17	119.2	C3-C33-H17	119.2
C35-C34-C1	120.72(14)	C35-C34-H20	119.6
C1-C34-H20	119.6	C34-C35-C4	121.15(13)
C34-C35-H19	119.4	C4-C35-H19	119.4

Table 6. Torsion angles (°) for

BisanthraToluene.

C34-C1-C2-C3	0.6(2)	C1-C2-C3-C33	177.66(14)
C1-C2-C3-C4	-0.9(2)	C33-C3-C4-C5	0.47(19)
C2-C3-C4-C5	179.09(12)	C33-C3-C4-C35	-177.93(12)
C2-C3-C4-C35	0.69(19)	C35-C4-C5-C27	176.77(12)
C3-C4-C5-C27	-1.56(19)	C35-C4-C5-C6	-2.1(2)
C3-C4-C5-C6	179.58(11)	C4-C5-C6-C25	-88.86(16)
C27-C5-C6-C25	92.28(16)	C4-C5-C6-C7	92.40(16)
C27-C5-C6-C7	-86.46(16)	C25-C6-C7-C8	-1.38(19)
C5-C6-C7-C8	177.35(12)	C25-C6-C7-C26	179.68(13)
C5-C6-C7-C26	-1.59(19)	C6-C7-C8-C23	1.64(19)
C26-C7-C8-C23	-179.44(13)	C6-C7-C8-C9	-175.82(12)
C26-C7-C8-C9	3.1(2)	C23-C8-C9-C20	74.45(17)
C7-C8-C9-C20	-108.08(15)	C23-C8-C9-C10	-104.01(15)
C7-C8-C9-C10	73.46(17)	C20-C9-C10-C11	-174.87(12)
C8-C9-C10-C11	3.60(19)	C20-C9-C10-C18	3.48(19)
C8-C9-C10-C18	-178.05(11)	C9-C10-C11-C12	179.06(13)
C18-C10-C11-C12	0.7(2)	C10-C11-C12-C13	0.8(2)
C11-C12-C13-C19	-1.2(2)	C22-C14-C15-C16	0.8(3)
C14-C15-C16-C17	177.90(14)	C14-C15-C16-C20	-0.7(2)
C15-C16-C17-C18	-176.06(13)	C20-C16-C17-C18	2.5(2)
C16-C17-C18-C19	177.14(13)	C16-C17-C18-C10	-2.2(2)
C9-C10-C18-C17	-0.81(19)	C11-C10-C18-C17	177.61(12)
C9-C10-C18-C19	179.82(12)	C11-C10-C18-C19	-1.76(19)
C12-C13-C19-C18	0.1(2)	C17-C18-C19-C13	-177.94(13)
C10-C18-C19-C13	1.4(2)	C10-C9-C20-C21	176.07(12)
C8-C9-C20-C21	-2.37(19)	C10-C9-C20-C16	-3.17(19)
C8-C9-C20-C16	178.39(11)	C17-C16-C20-C9	0.2(2)
C15-C16-C20-C9	178.81(12)	C17-C16-C20-C21	-179.08(12)
C15-C16-C20-C21	-0.47(19)	C9-C20-C21-C22	-177.71(13)
C16-C20-C21-C22	1.5(2)	C20-C21-C22-C14	-1.5(2)
C15-C14-C22-C21	0.3(2)	C7-C8-C23-C24	-0.7(2)
C9-C8-C23-C24	176.84(14)	C8-C23-C24-C25	-0.6(2)

C23-C24-C25-C6	0.9(2)	C7-C6-C25-C24	0.1(2)
C5-C6-C25-C24	-178.61(13)	C4-C5-C27-C28	-177.61(12)
C6-C5-C27-C28	1.25(19)	C4-C5-C27-C32	1.32(19)
C6-C5-C27-C32	-179.81(11)	C5-C27-C28-C29	178.87(13)
C32-C27-C28-C29	-0.1(2)	C27-C28-C29-C30	1.1(2)
C28-C29-C30-C31	-0.8(2)	C29-C30-C31-C32	-0.5(2)
C30-C31-C32-C33	-178.70(13)	C30-C31-C32-C27	1.4(2)
C5-C27-C32-C33	0.02(19)	C28-C27-C32-C33	179.00(12)
C5-C27-C32-C31	179.89(12)	C28-C27-C32-C31	-1.13(19)
C31-C32-C33-C3	179.01(12)	C27-C32-C33-C3	-1.1(2)
C2-C3-C33-C32	-177.68(12)	C4-C3-C33-C32	0.9(2)
C2-C1-C34-C35	-0.1(2)	C1-C34-C35-C4	-0.1(2)
C5-C4-C35-C34	-178.53(13)	C3-C4-C35-C34	-0.2(2)

Table 7. Anisotropic atomic displacement parameters (Å^2) for BisanthraToluene.

The anisotropic atomic displacement factor exponent takes the form: $-2\pi^2[h^2 a^{*2} U_{11} + ... + 2 h k a^* b^* U_{12}]$

	U_{11}	U_{22}	U_{33}	U_{23}	U_{13}	U_{12}
C1	0.0375(8)	0.0482(9)	0.0317(8)	0.0193(7)	0.0041(6)	0.0006(7)
C2	0.0408(8)	0.0374(8)	0.0246(7)	0.0109(6)	0.0099(6)	-0.0013(6)
C3	0.0350(7)	0.0252(6)	0.0212(7)	0.0046(5)	0.0099(5)	-0.0003(5)
C4	0.0319(7)	0.0266(7)	0.0227(7)	0.0044(5)	0.0106(6)	0.0013(5)
C5	0.0317(7)	0.0248(6)	0.0205(6)	0.0040(5)	0.0098(5)	0.0023(5)
C6	0.0273(6)	0.0289(7)	0.0201(6)	0.0065(5)	0.0081(5)	0.0038(5)
C7	0.0272(6)	0.0270(6)	0.0221(6)	0.0065(5)	0.0082(5)	0.0029(5)
C8	0.0274(6)	0.0283(7)	0.0221(6)	0.0064(5)	0.0090(5)	0.0036(5)
C9	0.0342(7)	0.0258(6)	0.0210(6)	0.0062(5)	0.0119(5)	0.0012(5)
C10	0.0351(7)	0.0278(7)	0.0211(6)	0.0073(5)	0.0109(6)	0.0016(5)
C11	0.0358(8)	0.0364(8)	0.0281(7)	0.0057(6)	0.0099(6)	0.0027(6)
C12	0.0363(8)	0.0479(9)	0.0371(9)	0.0112(7)	0.0079(7)	0.0054(7)
C13	0.0425(9)	0.0490(10)	0.0330(8)	0.0109(7)	-0.0001(7)	-0.0057(7)
C14	0.0530(11)	0.0522(10)	0.0604(12)	0.0226(9)	0.0354(9)	0.0237(8)
C15	0.0585(11)	0.0368(8)	0.0446(10)	0.0106(7)	0.0306(8)	0.0154(7)
C16	0.0485(9)	0.0302(7)	0.0302(8)	0.0092(6)	0.0214(7)	0.0077(6)
C17	0.0560(10)	0.0286(7)	0.0253(7)	0.0033(6)	0.0187(7)	0.0022(6)
C18	0.0436(8)	0.0278(7)	0.0234(7)	0.0073(5)	0.0118(6)	-0.0009(6)

	U_{11}	U_{22}	U_{33}	U_{23}	U_{13}	U_{12}
C19	0.0532(10)	0.0342(8)	0.0248(7)	0.0053(6)	0.0066(7)	-0.0053(7)
C20	0.0373(8)	0.0291(7)	0.0268(7)	0.0100(6)	0.0151(6)	0.0048(6)
C21	0.0374(8)	0.0387(8)	0.0345(8)	0.0130(6)	0.0139(6)	0.0058(6)
C22	0.0385(9)	0.0529(10)	0.0512(10)	0.0214(8)	0.0197(8)	0.0103(7)
C23	0.0384(8)	0.0309(7)	0.0266(7)	0.0092(6)	0.0150(6)	0.0019(6)
C24	0.0455(8)	0.0276(7)	0.0326(8)	0.0073(6)	0.0156(7)	-0.0029(6)
C25	0.0405(8)	0.0271(7)	0.0263(7)	0.0026(5)	0.0125(6)	0.0017(6)
C26	0.0449(8)	0.0295(7)	0.0309(8)	0.0060(6)	0.0179(6)	-0.0013(6)
C27	0.0315(7)	0.0242(6)	0.0257(7)	0.0047(5)	0.0101(6)	0.0019(5)
C28	0.0342(8)	0.0350(8)	0.0300(8)	0.0109(6)	0.0094(6)	0.0020(6)
C29	0.0337(8)	0.0392(8)	0.0413(9)	0.0162(7)	0.0054(7)	0.0027(6)
C30	0.0294(7)	0.0406(9)	0.0524(10)	0.0160(7)	0.0137(7)	0.0034(6)
C31	0.0334(8)	0.0350(8)	0.0397(8)	0.0089(6)	0.0178(7)	0.0018(6)
C32	0.0315(7)	0.0245(6)	0.0277(7)	0.0031(5)	0.0126(6)	0.0001(5)
C33	0.0364(8)	0.0287(7)	0.0247(7)	0.0051(5)	0.0152(6)	-0.0001(5)
C34	0.0323(8)	0.0522(10)	0.0402(9)	0.0199(7)	0.0105(7)	0.0062(7)
C35	0.0322(7)	0.0429(8)	0.0312(8)	0.0145(6)	0.0131(6)	0.0054(6)

Table 8. Hydrogen atomic coordinates and isotropic atomic displacement parameters (Å^2) for BisanthraToluene.

	x/a	y/b	z/c	U(eq)
H1	0.4294	0.2427	0.7115	0.047
H18	0.1877	0.2794	0.6993	0.04
H6	-0.0789	0.2763	-0.1055	0.04
H23	-0.3079	0.2205	-0.2503	0.049
H2	-0.3439	0.0517	-0.4230	0.053
H3	0.6239	-0.0414	-0.1960	0.059
H24	0.3889	-0.1056	-0.3258	0.052
H4	0.1203	-0.0842	-0.3825	0.043
H5	-0.1475	-0.0549	-0.4515	0.047
H7	0.4663	0.2182	0.0286	0.043
H8	0.6636	0.1228	-0.0175	0.054
H22	0.2974	0.4024	-0.0515	0.037
H21	0.3201	0.5667	0.1179	0.041
H9	0.2293	0.5453	0.2825	0.038
H11	-0.0319	0.1459	0.0848	0.051
H12	0.1097	0.1331	0.1953	0.051

	x/a	y/b	z/c	U(eq)
H10	0.1068	0.0821	0.0525	0.051
H13	-0.1184	0.4032	0.1310	0.039
H14	-0.3638	0.4232	0.1170	0.046
H15	-0.4579	0.4093	0.2840	0.048
H16	-0.3045	0.3713	0.4623	0.042
H17	-0.0568	0.3282	0.5817	0.035
H20	0.5271	0.2584	0.5463	0.048
H19	0.3817	0.3095	0.3717	0.04

Appendix C

Computational Results

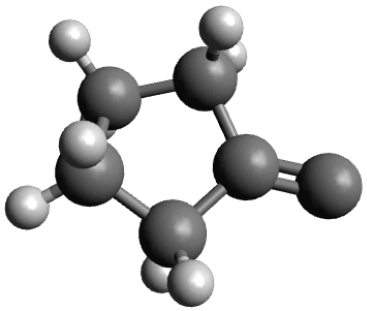

Input orientation:

Center Number	Atomic Number	Atomic Type	Coordinates (Angstroms) X	Y	Z
1	6	0	0.000000	1.259154	0.115104
2	6	0	0.000000	-1.259154	0.115104
3	6	0	-0.322451	-0.696424	-1.287276
4	6	0	0.322451	0.696424	-1.287276
5	1	0	-0.999822	1.709931	0.129056
6	1	0	0.712311	2.016288	0.454514
7	1	0	0.999822	-1.709931	0.129056
8	1	0	-0.712311	-2.016288	0.454514
9	1	0	0.051674	-1.348701	-2.084466
10	1	0	-1.409412	-0.607031	-1.412564
11	1	0	1.409412	0.607031	-1.412564
12	1	0	-0.051674	1.348701	-2.084466
13	6	0	0.000000	0.000000	2.309387
14	6	0	0.000000	0.000000	1.006111

CCSD(T) = -232.875179 a.u.
T1 Diagnostic = 0.01323064

Figure C.1. Singlet Cyclopentylidenecarbene at CCSD(T)/cc-pVTZ//B3LYP/6-31+G*.

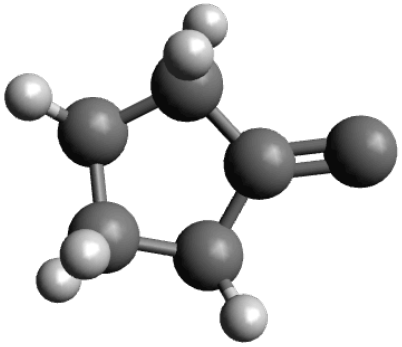

Input orientation:

Center Number	Atomic Number	Atomic Type	Coordinates (Angstroms) X	Y	Z
1	6	0	0.106507	1.223128	0.108238
2	6	0	0.106363	-1.221421	-0.129117
3	6	0	-1.313612	-0.739779	0.233734
4	6	0	-1.321959	0.736387	-0.213817
5	1	0	0.178615	1.569686	1.154021
6	1	0	0.471066	2.056281	-0.504898
7	1	0	0.151027	-1.563508	-1.178844
8	1	0	0.489622	-2.055092	0.470495
9	1	0	-2.101493	-1.336117	-0.238023
10	1	0	-1.458582	-0.804242	1.320329
11	1	0	-1.498427	0.799917	-1.295825
12	1	0	-2.097359	1.331001	0.280166
13	6	0	0.990299	0.002199	-0.025168
14	6	0	2.409992	-0.000167	0.024893

CCSD(T) = - 232.7987273 a.u.
T1 Diagnostic = 0.01587434

Figure C.2. Triplet Cyclopentylidenecarbene at CCSD(T)/cc-pVTZ//B3LYP/6-31+G*.

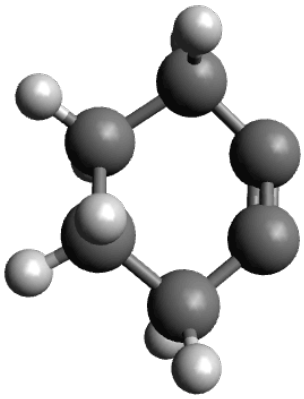

Input orientation:

Center Number	Atomic Number	Atomic Type	Coordinates (Angstroms) X	Y	Z
1	6	0	1.592781	-0.196154	0.116373
2	6	0	-1.592498	-0.199066	-0.116228
3	6	0	-0.722088	1.054182	0.282055
4	6	0	0.719678	1.055143	-0.282021
5	1	0	1.983614	-0.103140	1.137831
6	1	0	2.455737	-0.284379	-0.553368
7	1	0	-1.983577	-0.106399	-1.137644
8	1	0	-2.455279	-0.289080	0.553537
9	1	0	-1.238681	1.962338	-0.057631
10	1	0	-0.679630	1.100697	1.378289
11	1	0	0.676481	1.101133	-1.378302
12	1	0	1.234773	1.964448	0.056771
13	6	0	-0.609514	-1.302403	-0.020382
14	6	0	0.612735	-1.302638	0.020289

CCSD(T) = -232.899187 a.u.
T1 Diagnostic = 0.01166562

Figure C.3. C_1 Cyclohexyne at CCSD(T)/cc-pVTZ//B3LYP/6-31+G*.

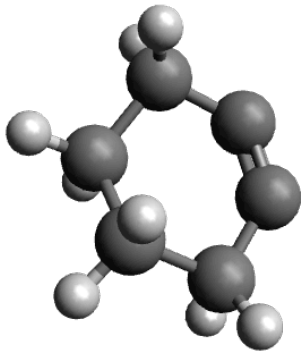

Input orientation:

Center Number	Atomic Number	Atomic Type	Coordinates (Angstroms) X	Y	Z
1	6	0	-0.556141	1.496962	-0.197701
2	6	0	0.556141	-1.496962	-0.197701
3	6	0	0.556141	-0.538134	1.054805
4	6	0	-0.556141	0.538134	1.054805
5	1	0	0.210534	2.276994	-0.104674
6	1	0	-1.524012	2.003378	-0.286500
7	1	0	-0.210534	-2.276994	-0.104674
8	1	0	1.524012	-2.003378	-0.286500
9	1	0	0.462454	-1.147939	1.963820
10	1	0	1.535088	-0.042801	1.100121
11	1	0	-1.535088	0.042801	1.100121
12	1	0	-0.462454	1.147939	1.963820
13	6	0	0.235662	-0.564355	-1.302565
14	6	0	-0.235662	0.564355	-1.302565

CCSD(T) = -232.8991907 a.u.
T1 Diagnostic = 0.01167244

Figure C.4. C_2 Cyclohexyne at CCSD(T)/cc-pVTZ//B3LYP/6-31+G*.

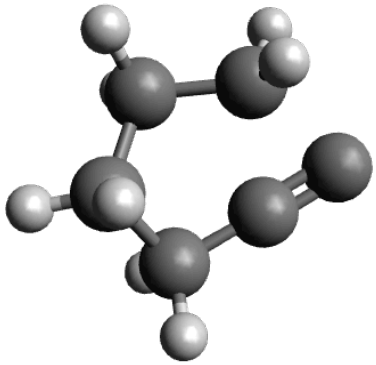

Input orientation:

Center Number	Atomic Number	Atomic Type	Coordinates (Angstroms) X	Y	Z
1	6	0	-0.723751	-1.245381	-0.122726
2	6	0	0.909270	0.976091	0.140228
3	6	0	-0.562899	1.190634	-0.282034
4	6	0	-1.444253	0.071336	0.278381
5	1	0	-0.997825	-1.546327	-1.142455
6	1	0	-0.973767	-2.073159	0.550591
7	1	0	1.071375	1.246019	1.184353
8	1	0	1.565734	1.560986	-0.501708
9	1	0	-0.880544	2.182643	0.065828
10	1	0	-0.625885	1.194072	-1.377866
11	1	0	-1.490287	0.139756	1.372426
12	1	0	-2.471143	0.103653	-0.101949
13	6	0	1.919711	-0.567613	0.021428
14	6	0	0.702312	-0.893008	-0.043480

CCSD(T) = -232.8606998 a.u.
T1 Diagnostic = 0.01183021
ν = -375.20 cm^{-1}

Figure C.5. TS from Singlet Cyclopentylidenecarbene to C_2 Cyclohexyne at CCSD(T)/cc-pVTZ//B3LYP/6-31+G*.

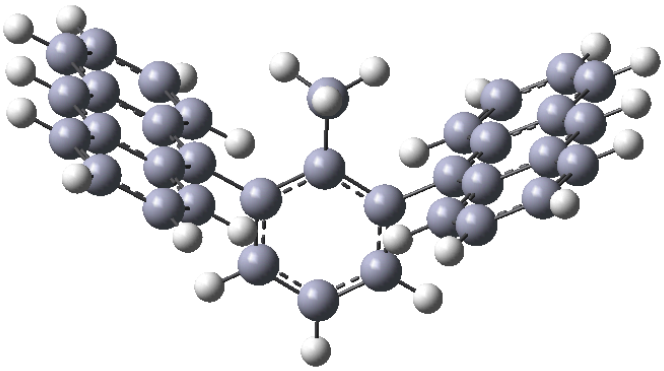

Input orientation:

Center Number	Atomic Number	Atomic Type	Coordinates (Angstroms) X	Y	Z
1	6	0	-1.202515	-0.220515	2.429309
2	6	0	0.000000	-0.281155	3.129113
3	6	0	1.202516	-0.220516	2.429308
4	6	0	1.217097	-0.099621	1.032578
5	6	0	0.000000	-0.041956	0.316077
6	6	0	-1.217097	-0.099621	1.032578
7	1	0	-2.148241	-0.265658	2.962734
8	1	0	0.000000	-0.374206	4.211792
9	1	0	2.148242	-0.265659	2.962734
10	6	0	0.000000	0.101716	-1.190449
11	1	0	-0.886896	-0.357551	-1.633669
12	1	0	-0.000003	1.159205	-1.486564
13	1	0	0.886898	-0.357545	-1.633669
14	6	0	2.545034	-0.033884	0.335439
15	6	0	3.127003	1.221227	0.042178
16	6	0	3.224149	-1.227735	-0.003519
17	6	0	2.490509	2.460698	0.374294
18	6	0	4.414974	1.279174	-0.611880
19	6	0	4.512697	-1.158977	-0.655998
20	6	0	2.681629	-2.525699	0.267709
21	6	0	3.075357	3.663938	0.077048
22	1	0	1.529591	2.432571	0.877163
23	6	0	4.989740	2.555944	-0.903238
24	6	0	5.071238	0.090062	-0.942598
25	6	0	5.186567	-2.374123	-0.994347
26	1	0	1.715233	-2.594041	0.755394
27	6	0	3.359766	-3.666433	-0.074522
28	6	0	4.342257	3.715632	-0.572174

29	1	0	2.571872	4.590338	0.340377
30	1	0	5.958975	2.583598	-1.395769
31	1	0	6.040722	0.137944	-1.434613
32	6	0	4.630592	-3.593165	-0.713723
33	1	0	6.155604	-2.305884	-1.483333
34	1	0	2.926279	-4.639138	0.142242
35	1	0	4.790906	4.678832	-0.799592
36	1	0	5.153616	-4.508507	-0.977121
37	6	0	-2.545034	-0.033884	0.335439
38	6	0	-3.224150	-1.227734	-0.003519
39	6	0	-3.127002	1.221228	0.042178
40	6	0	-2.681631	-2.525699	0.267709
41	6	0	-4.512698	-1.158975	-0.655997
42	6	0	-4.414973	1.279175	-0.611880
43	6	0	-2.490508	2.460698	0.374295
44	6	0	-3.359768	-3.666432	-0.074522
45	1	0	-1.715235	-2.594041	0.755394
46	6	0	-5.186569	-2.374121	-0.994347
47	6	0	-5.071238	0.090064	-0.942598
48	6	0	-4.989738	2.555945	-0.903238
49	1	0	-1.529590	2.432571	0.877163
50	6	0	-3.075355	3.663938	0.077049
51	6	0	-4.630594	-3.593164	-0.713722
52	1	0	-2.926282	-4.639137	0.142242
53	1	0	-6.155606	-2.305881	-1.483332
54	1	0	-6.040722	0.137947	-1.434613
55	6	0	-4.342255	3.715633	-0.572175
56	1	0	-5.958973	2.583600	-1.395770
57	1	0	-2.571869	4.590338	0.340377
58	1	0	-5.153619	-4.508505	-0.977121
59	1	0	-4.790902	4.678833	-0.799593

Shielding (ppm) of methyl protons: 30.2529, 30.5687, 30.5687

Zero-point correction = 0.477160 (Hartree/Particle)
Thermal correction to Energy = 0.503458
Thermal correction to Enthalpy = 0.504403
Thermal correction to Gibbs Free Energy = 0.418889
Sum of electronic and zero-point Energies = -1347.759013
Sum of electronic and thermal Energies = -1347.732715
Sum of electronic and thermal Enthalpies = -1347.731770
Sum of electronic and thermal Free Energies = -1347.817284

Figure C.6. Bisanthracenyltoluene at B3LYP/6-31G* and GIAO/WP04/cc-pVDZ

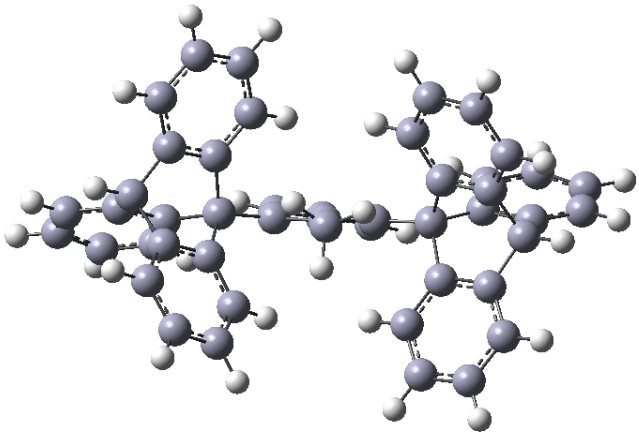

Input orientation:

Center Number	Atomic Number	Atomic Type	Coordinates (Angstroms) X	Y	Z
1	6	0	0.002860	-0.031949	3.205804
2	6	0	1.191515	0.108893	2.506115
3	6	0	1.229930	0.037562	1.106614
4	6	0	-0.008714	0.088241	0.392041
5	6	0	-1.242334	0.032130	1.120138
6	6	0	-1.191644	-0.142760	2.508088
7	1	0	0.007913	-0.065044	4.291998
8	1	0	2.102800	0.271104	3.061038
9	1	0	-2.093540	-0.363671	3.057826
10	6	0	2.431477	-2.970383	-2.044723
11	6	0	2.066273	-2.102997	-1.008940
12	6	0	2.826073	-0.963358	-0.752320
13	6	0	4.004591	-0.748717	-1.488290
14	6	0	4.363013	-1.602219	-2.525688
15	6	0	3.563823	-2.713144	-2.815776
16	6	0	4.057569	1.635299	-0.882927
17	6	0	2.873015	1.489720	-0.149105
18	6	0	2.069745	2.610610	0.062993
19	1	0	1.167694	2.532906	0.659874
20	6	0	2.430920	3.846240	-0.485600
21	6	0	3.596458	3.972486	-1.240333
22	6	0	4.420278	2.860425	-1.433891
23	1	0	1.821650	-3.846882	-2.246434
24	1	0	1.175980	-2.308702	-0.423732
25	1	0	5.276366	-1.420444	-3.087506
26	1	0	3.840271	-3.385272	-3.623628

27	1	0	1.796258	4.712101	-0.316320
28	1	0	3.871155	4.933616	-1.666710
29	1	0	5.344288	2.949477	-2.000575
30	6	0	4.877563	0.368473	-0.926872
31	1	0	5.816960	0.484368	-1.473915
32	6	0	2.612034	0.061014	0.409182
33	6	0	4.018377	-0.977905	2.462582
34	6	0	5.277875	-1.264186	3.008963
35	6	0	6.441885	-0.912468	2.335739
36	6	0	6.345035	-0.326882	1.068963
37	6	0	5.097045	-0.053018	0.525682
38	6	0	3.905313	-0.302346	1.245066
39	1	0	3.144425	-1.325324	2.996663
40	1	0	5.333098	-1.775634	3.966298
41	1	0	7.241674	-0.116581	0.490503
42	1	0	7.416054	-1.127712	2.766219
43	6	0	-5.419949	0.871034	3.053094
44	6	0	-4.132207	0.722561	2.516958
45	6	0	-3.947603	0.167124	1.249352
46	6	0	-5.103822	-0.106060	0.480380
47	6	0	-6.378105	0.032211	1.012816
48	6	0	-6.541652	0.499327	2.321768
49	6	0	-4.024547	0.808436	-1.454665
50	6	0	-2.888088	1.054536	-0.664899
51	6	0	-2.243727	2.284343	-0.774077
52	1	0	-1.423480	2.531419	-0.107025
53	6	0	-2.654522	3.207536	-1.742844
54	6	0	-3.723826	2.915156	-2.588001
55	6	0	-4.427158	1.716380	-2.427714
56	1	0	-5.530951	1.291322	4.049153
57	1	0	-3.295979	1.082763	3.100654
58	1	0	-7.246174	-0.191901	0.397131
59	1	0	-7.537198	0.607939	2.743353
60	1	0	-2.134674	4.157784	-1.830938
61	1	0	-4.034987	3.630745	-3.344251
62	1	0	-5.306318	1.509633	-3.033732
63	6	0	-4.826919	-0.403772	-0.994906
64	1	0	-5.745411	-0.544910	-1.570747
65	6	0	-2.618642	-0.033449	0.417019
66	6	0	-1.908143	-2.523170	-0.064478
67	6	0	-2.175567	-3.742018	-0.697778
68	6	0	-3.306689	-3.890606	-1.499289
69	6	0	-4.192506	-2.820695	-1.651660
70	6	0	-3.924051	-1.613016	-1.014560
71	6	0	-2.771109	-1.440013	-0.237990
72	1	0	-1.031954	-2.429678	0.566816

73	1	0	-1.495331	-4.577777	-0.556381
74	1	0	-5.093173	-2.930231	-2.251361
75	1	0	-3.508256	-4.838080	-1.991927
76	6	0	-0.019094	0.241169	-1.118726
77	1	0	-0.849884	-0.295161	-1.579961
78	1	0	-0.115878	1.291303	-1.404265
79	1	0	0.894305	-0.118138	-1.577958

Shielding (ppm) of methyl protons: 29.8016, 30.3744, 30.8468

Zero-point correction = 0.643083 (Hartree/Particle)
Thermal correction to Energy = 0.676257
Thermal correction to Enthalpy = 0.677202
Thermal correction to Gibbs Free Energy = 0.580154
Sum of electronic and zero-point Energies = -1809.604964
Sum of electronic and thermal Energies = -1809.571789
Sum of electronic and thermal Enthalpies = -1809.570845
Sum of electronic and thermal Free Energies = -1809.667892

Figure C.7. Bistriptycenyltoluene at B3LYP/6-31G* and GIAO/WP04/cc-pVDZ